

Review

# Complex Metal Borohydrides: From Laboratory Oddities to Prime Candidates in Energy Storage Applications

Cezar Comanescu <sup>1,2,3</sup> 

<sup>1</sup> National Institute of Materials Physics, 405A Atomîștilor St., 077125 Magurele, Romania; cezar.comanescu@infim.ro

<sup>2</sup> Inorganic Chemistry Department, Politehnica University of Bucharest, 1 Polizu St., 011061 Bucharest, Romania

<sup>3</sup> Faculty of Physics, University of Bucharest, 405, Atomîștilor St., 077125 Magurele, Romania

**Abstract:** Despite being the lightest element in the periodic table, hydrogen poses many risks regarding its production, storage, and transport, but it is also the one element promising pollution-free energy for the planet, energy reliability, and sustainability. Development of such novel materials conveying a hydrogen source face stringent scrutiny from both a scientific and a safety point of view: they are required to have a high hydrogen wt.% storage capacity, must store hydrogen in a safe manner (i.e., by chemically binding it), and should exhibit controlled, and preferably rapid, absorption–desorption kinetics. Even the most advanced composites today face the difficult task of overcoming the harsh re-hydrogenation conditions (elevated temperature, high hydrogen pressure). Traditionally, the most utilized materials have been RMH (reactive metal hydrides) and complex metal borohydrides  $M(\text{BH}_4)_x$  (M: main group or transition metal; x: valence of M), often along with metal amides or various additives serving as catalysts ( $\text{Pd}^{2+}$ ,  $\text{Ti}^{4+}$  etc.). Through destabilization (kinetic or thermodynamic),  $M(\text{BH}_4)_x$  can effectively lower their dehydrogenation enthalpy, providing for a faster reaction occurring at a lower temperature onset. The present review summarizes the recent scientific results on various metal borohydrides, aiming to present the current state-of-the-art on such hydrogen storage materials, while trying to analyze the pros and cons of each material regarding its thermodynamic and kinetic behavior in hydrogenation studies.

**Keywords:** energy storage; metal borohydride; recyclability; kinetic destabilization; hydrogen



**Citation:** Comanescu, C. Complex Metal Borohydrides: From Laboratory Oddities to Prime Candidates in Energy Storage Applications. *Materials* **2022**, *15*, 2286. <https://doi.org/10.3390/ma15062286>

Academic Editors: Haralampos N. Miras and Jacques Huot

Received: 31 January 2022

Accepted: 11 March 2022

Published: 19 March 2022

**Publisher's Note:** MDPI stays neutral with regard to jurisdictional claims in published maps and institutional affiliations.



**Copyright:** © 2022 by the author. Licensee MDPI, Basel, Switzerland. This article is an open access article distributed under the terms and conditions of the Creative Commons Attribution (CC BY) license (<https://creativecommons.org/licenses/by/4.0/>).

## 1. Introduction

A world with ever more scarce fossil fuels must transition to alternative energy storing materials. Fossil fuels, such as coal, gas, and oil, are finite, non-renewable resources, and a current estimation based on their ongoing burning rate points to a complete depletion by the end of 2060. While they are more reliable than currently engineered materials, they also pollute the environment and are responsible in great part for the greenhouse effect [1–9]. While the risk of running out of fossil fuels has been advocated for decades, the timeline is approaching and humanity needs to make a change. Therefore, alternative energy carriers are long sought-after; among them, metal hydrides and complex borohydrides have a special role [10–18]. Reaching or exceeding the U.S. Department of Energy (DOE) target is no easy task; the specific target for 2020 was 1.5 kWh/kg (4.5 wt.% hydrogen) and 1.0 kWh/L (0.03 Kg hydrogen/L), costing more than USD 10 /kWh (or USD 333/Kg of stored hydrogen capacity) [19,20]. A series of options have been investigated for hydrogen storage applications: cryo-compression (7–27 Kg/m<sup>3</sup>), metal hydrides (40–70 Kg/m<sup>3</sup>), chemical hydrides (50–120 Kg/m<sup>3</sup>), carbon sorption (20–50 Kg/m<sup>3</sup>), complex hydrides, and liquified dihydrogen (70 Kg/m<sup>3</sup>) (Figure 1).

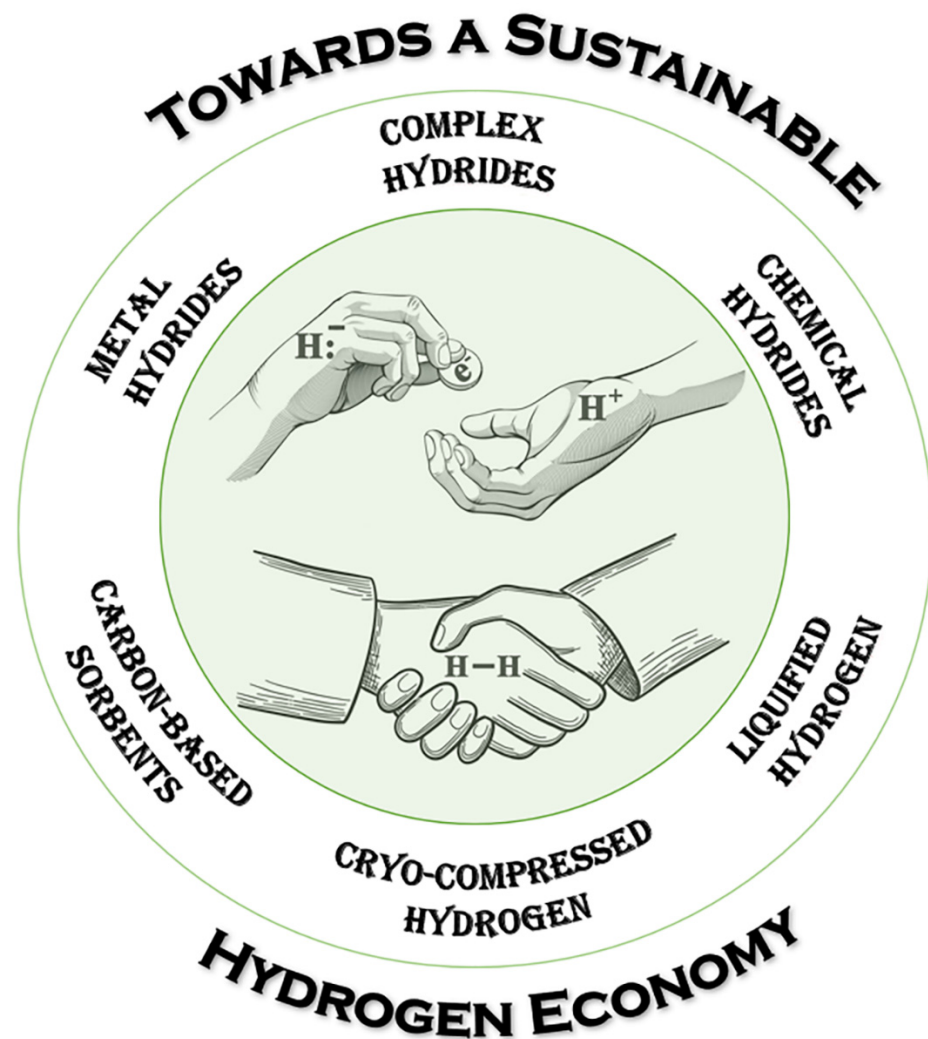


**Figure 1.** Convergence of hydrogen storage methods towards a sustainable hydrogen economy.

A special role is held by complex metal hydrides and borohydrides in particular, given their high gravimetric energy content (Figure 2).

Computing the theoretical hydrogen storage of a complex metal borohydride yields the following:

$$\text{wt.\% hydrogen in } M(\text{BH}_4)_x = \frac{4 \times}{A_M + 14.842 \times} \times 100 = \frac{400}{\frac{A_M}{x} + 14.842} \% \quad (1)$$

This relation would imply that, in order to reach a minimum storage capacity set by the DOE of 4.5 wt.%, the following relation should hold:

$$\frac{400}{\frac{A_M}{x} + 14.842} \geq 4.5 \implies \frac{A_M}{x} \leq 74.406 \quad (2)$$

One could argue that the DOE target could be met, looking at Equations (1) and (2), by any mono-valent metal having  $A_M \leq 74.406 \frac{\text{g}}{\text{mol}}$ , or a divalent metal with  $A_M \leq 148.812 \frac{\text{g}}{\text{mol}}$ , or a trivalent metal with  $A_M \leq 223.218 \frac{\text{g}}{\text{mol}}$  a.s.o. Indeed, mTHRost known borohydrides fall into this category: they afford a theoretical hydrogen storage capacity superior to that imposed by the DOE (4.5 wt.%). Equation (2) also implies that the hydrogen storage capacity will be the highest for the most lightweight borohydrides, thus corresponding to low  $A_M$  values: second, third, and fourth period metals are the borohydrides most

used to date [21–27]. A summary of known borohydrides with specific hydrogen storage capacity is presented in Figure 2, which are arranged by metal valency and atomic weight of the metal, in decreasing order of their theoretical hydrogen storage capacity (wt.%). The maximum hydrogen storage capacity (denoted herein as: H, wt.%) is computed for a series of mono-, di-, tri-, and tetravalent metals; in some cases, only hypothetical formulae were used since the actual borohydride's existence is unclear ( $\text{AuBH}_4$ ,  $\text{Ni}(\text{BH}_4)_2$ ,  $\text{Co}(\text{BH}_4)_2$ ,  $\text{Hg}(\text{BH}_4)_2$ ,  $\text{Sc}(\text{BH}_4)_3$ ,  $\text{Nb}(\text{BH}_4)_3$ ,  $\text{U}(\text{BH}_4)_3$ ,  $\text{Ge}(\text{BH}_4)_4$ ,  $\text{Sn}(\text{BH}_4)_4$ ), while for others that exist as adducts with various stabilizing solvents/ligands (like  $\text{Cr}(\text{BH}_4)_2$ ), the capacity is reported with respect to the theoretical, anhydrous form [28,29].

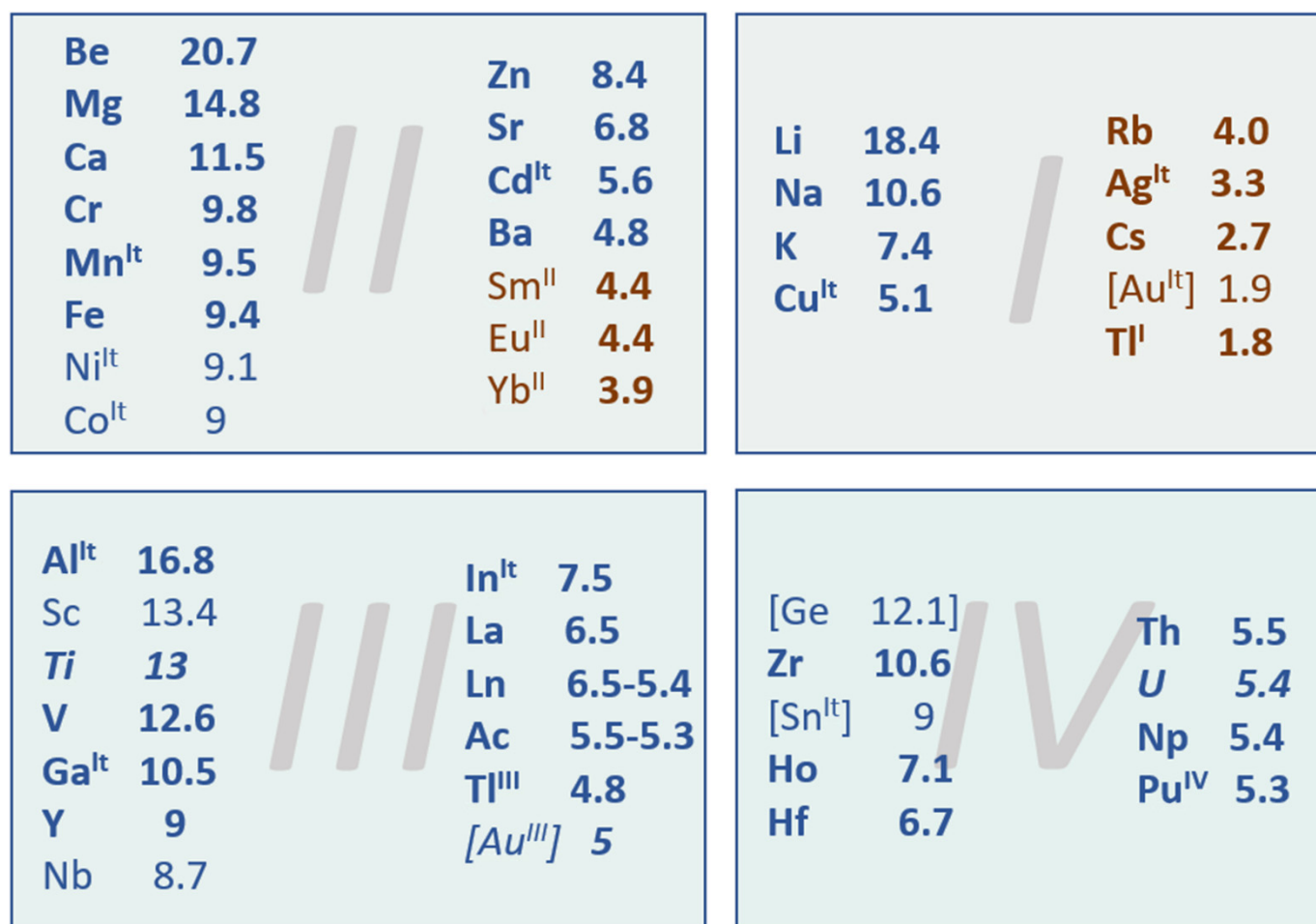


**Figure 2.** Theoretical (maximum) hydrogen storage capacity of metal borohydrides. Metal borohydrides are arranged by cation valence (I, II, III, and IV). Highlighted in blue are the borohydrides that exceed the DOE's hydrogen storage capacity set for 2020 (4.5 wt %). Ln = La, Ce, Pr, Nd, Sm(II, III), Eu(II, III), Gd, Tb, Dy, Ho, Er, Tm, Yb(II, III), Lu; Ac = Th, Pa, U, Np, Pu; <sup>lt</sup>-isolable at low temperatures; in **bold** are shown borohydrides reported by several groups (higher confidence).

Many of the formulated borohydrides from Figure 2 comply with the DOE's theoretical minimum hydrogen storage capacity (4.5 wt.%), yet very few of them can actually be used in storage materials. However, there are quite a few aspects plaguing metal borohydrides: high dehydrogenation enthalpies, high dehydrogenation temperature onset, slow dehydrogenation/rehydrogenation kinetics, and side-reactions occurring during dehydrogenation leading to boron-loss and thus incomplete/impossible rehydrogenation, but also very high temperature and H<sub>2</sub> pressures required to rehydrogenate them.

From a structural point of view, borohydrides  $\text{M}(\text{BH}_4)_x$  are ionic/covalent compounds formed by a metal center ( $\text{M}^{x+}$ ) that binds accordingly to the negatively charged borohy-

drude tetrahedra  $\text{BH}_4^-$ . The lightest member of the borohydride family is  $\text{LiBH}_4$ , depicted in Figure 3 [30–38]. Established by synchrotron XRD at RT,  $\text{LiBH}_4$  shows at normal conditions an orthorhombic symmetry ( $Pnma$ ), with the  $\text{BH}_4$  tetrahedra aligned along two orthogonal directions. The  $[\text{BH}_4]^-$  units are surrounded by four  $\text{Li}^+$  cations, and each  $\text{Li}^+$  by four  $[\text{BH}_4]^-$ .

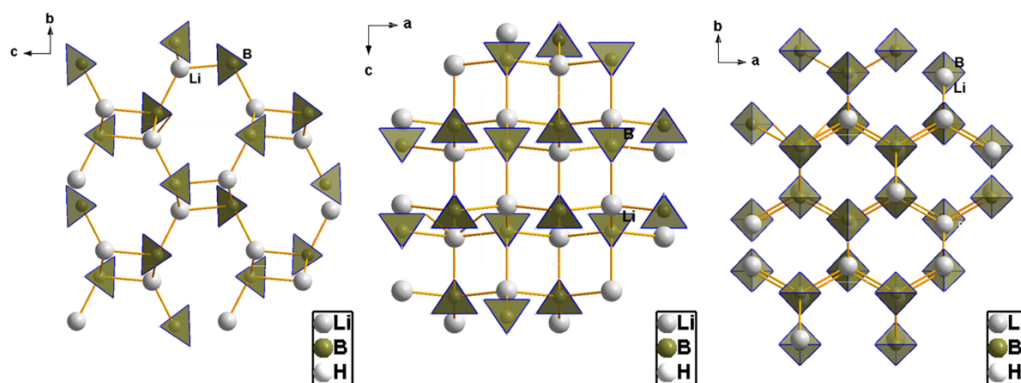


**Figure 3.** X-ray structure of lithium borohydride,  $\text{LiBH}_4$ . Projections along a-axis (left), b-axis (middle), and c-axis (right).

More important for hydrogenation studies, the B-H bond is of a covalent nature ( $r_{\text{B-H}} = 119$  pm), thus considerable energy is required to break that bond ( $E_{\text{B-H}} = 389$  kJ/mol). It follows that the dehydrogenation enthalpy  $\Delta H_{\text{dehydrogenation}}$  has a large value, an aspect that must be overcome using thermodynamical considerations. First (IA) and second group (IIA) metal borohydrides are not only known, but also commercially available. Various reviews have tackled different areas regarding complex borohydrides and hydrogen, focusing either on current technologies [1,2,6] and conceptual design of storage materials [3–5,15], or on various forms of hydrogen carriers [7,8] utilized to eventually switch the aging and depleting conventional fuel to a “green” fuel [9]. Other reviews evaluate the role of nanostructured metal hydride species for hydrogen storage [10,17], and usually focus on the potential presented by light metal borohydrides [10,16,18]. In the latter, sodium borohydride is actually presented as the fuel for the future [18] and judging by the emerging reports dating from 2021–2022 one could argue that this is true. Synthetic strategies and structure characterization [21] have been complemented by in-depth studies on hydrolysis process of light borohydrides [22,24,25,27] or by investigation on the possible intermediates that dehydrogenation could entail [12]. Destabilization strategies employed to tame the rigid behavior of tetrahydroborates during hydrogenation cycles have been reviewed [30–34], and the field of ionic conductivity has been explored with aplomb especially after the discovery of LT(low temperature)–HT(high temperature) phase transition in lithium borohydride [36–38]. The current review aims to gather most areas of interest regarding the fascinating chemistry of complex borohydrides and bring them under one umbrella, considering the historical evolution of the field, important milestones, and current and emerging trends.

## 2. Hydrogen Storage Options: Physical vs. Chemical Storage

Hydrogen storage methods can basically be divided in two groups: physical (liquid  $\text{H}_2$ , cryo-compressed and compressed gas, and physically adsorbed as in metal-organic frameworks of MOF-5 type), and chemical storage (organic liquid: BN-methyl cyclopentane; interstitial hydrides:  $\text{LaNi}_5\text{H}_6$ ; complex hydrides:  $\text{NaAlH}_4$ ; or in ammonia–borane adducts:  $\text{NH}_3 \cdot \text{BH}_3$ ) (Figure 4).

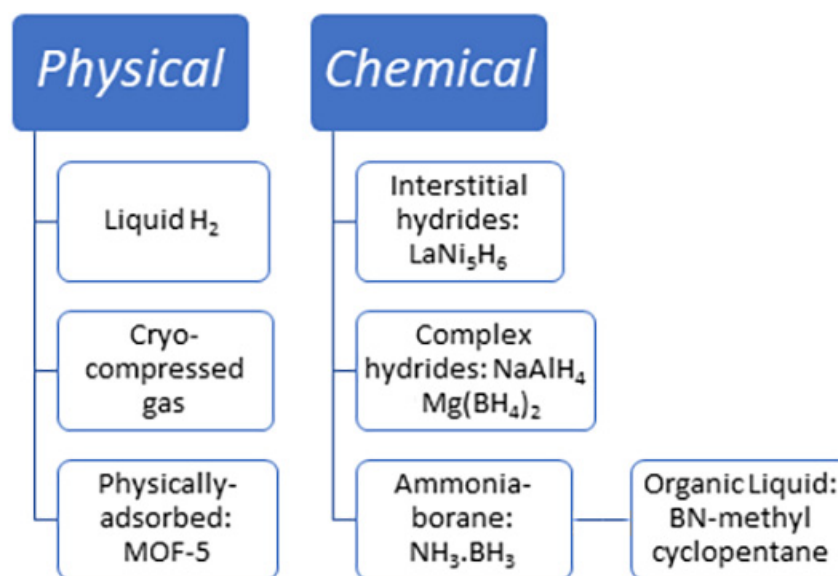


**Figure 4.** Physical vs. chemical hydrogen storage methods.

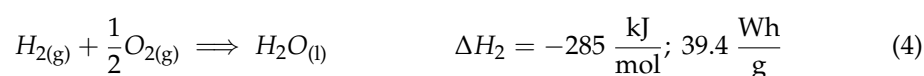
### 2.1. Physical Storage of Hydrogen

Hydrogen has an atomic weight of 1.0079 g/mol, and is thus the lightest element known. Under normal conditions (standard temperature and pressure), hydrogen is an odorless, nontoxic but combustible gas comprising two hydrogen atoms covalently bonded by a single  $\sigma$ -bond:  $H_2$ . Hydrogen ( $^1H$ , most abundant isotope called protium) has no neutrons, one proton in the nucleus and one electron in the outer shell, and a covalent radius of only 0.315 Å. The common and perhaps the most important physical properties of hydrogen related to its storage applications are the melting point (m.p. =  $-259.14$  °C) and boiling point (b.p. =  $-252.87$  °C), which, coupled with its low density (0.0898 g/L) and high diffusivity, make hydrogen storage a difficult task from an economic and technological point of view.

Hydrogen has three OS (oxidation states):  $-1$  (hydrides),  $0$  (molecular dihydrogen), and  $+1$  (typical OS for hydrogen, as found in most compounds, as for instance in hydrocarbons or the ubiquitous  $H_2O$ ); it is therefore a versatile element, as it can act as both an oxidizing and a reducing reagent. Its single valence electron makes hydrogen a very reactive element; it is therefore usually found in nature in a variety of inorganic and organic compounds.

Being a fuel and highly flammable (low ignition energy, low explosion limit in air at 4% vol.), hydrogen is regulated through a series of EU safety datasheets: S9 (containers must be kept in well-ventilated areas), S16 (no smoking allowed in its proximity, and ignition sources are forbidden nearby) and S33 (danger due to electrostatic discharge).

Combustion of hydrogen produces the highest gravimetric energy known (33.3–39.4 Wh/g), depending on the state in which water is produced—gaseous water yields the lower value (33.6 Wh/g), while combustion to liquid water produces 39.4 Wh/g:

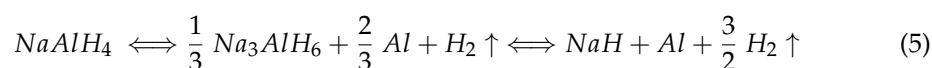


Hydrogen can be stored either as a liquid (cryogenic temperatures, due to low b.p.) or as a gas (at high pressures, in the range 350–700 atm). Physically sorbed hydrogen is also known: adsorption at surface of solids (MOF-5) or absorption (within solids).

## 2.2. Chemical Storage of Hydrogen

Facing the obvious difficulties of cryogenic temperatures and/or very high pressures, the physical storage of hydrogen has inherent safety issues that have swayed attention of researchers towards chemical storage of hydrogen. Solid-state hydrogen storage can be achieved in metal hydrides, complex metal hydrides, ammonia–borane adducts, or organic liquids (BN-methylcyclopentane) (Figure 4).

Among these, complex hydrides have gained more popularity due to their salt-like nature, high hydrogen storage wt.%, and involvement in a variety of advantageous chemical systems ( $M(\text{BH}_4)_x\text{-MH}_y$ ,  $M(\text{BH}_4)_x\text{-M}(\text{NH}_2)_y$ , etc). The general formula of a complex hydride can be written as  $A_x\text{D}_y\text{H}_z$ , with A being usually group IA and IIA elements, and D either boron or aluminum. Complex hydrides contain hydrogen covalently bonded to D, forming the complex anion  $[\text{D}_y\text{H}_z]^{r-}$ . These compounds have been known for many years, but they were revisited by Bogdanovic and Schwickard, who discovered that addition of 2 mol %  $\beta\text{-TiCl}_3$  or  $\text{Ti}(\text{O}i\text{Bu})_4$  catalyst to  $\text{NaAlH}_4$  would bring down the kinetic barrier of dehydrogenation to technologically feasible levels for hydrogenation studies. The novel material had a tentative formula  $\text{NaAlH}_{3.9}\text{Ti}_{0.02}\text{Cl}_{0.06}$  and showed a thermogravimetric curve featuring a reduction in the dehydrogenation temperature of 80–85 °C with respect to undoped  $\text{NaAlH}_4$ , while proving the reversible character of the prepared sample up to the 100th cycle. However, the dehydrogenation–rehydrogenation rate was still rather low, requiring high temperatures (>150 °C) and pressures (60–150-bar  $\text{H}_2$ ) (5) [39].



This pioneering work opened the door to further investigation of complex hydrides as new motifs for hydrogen storage materials; understanding the role of the catalyst and the exact nature of dehydrogenation and rehydrogenation reactions was the main aim. Other complex hydrides such as  $\text{Al}(\text{BH}_4)_3$  or  $\text{Mg}_2\text{FeH}_6$  have almost double volumetric hydrogen density compared to liquid hydrogen (150 kg/m<sup>3</sup> vs. 70 kg/m<sup>3</sup>), which stimulated research in this intriguing field of hydrogen storage systems.

## 3. General Synthesis Strategies for Metal Borohydrides $M(\text{BH}_4)_x$

There are many known complex metal borohydrides (Figure 2 summarizes most of them). The first known was aluminum borohydride  $\text{Al}(\text{BH}_4)_3$ , synthesized in 1939 by Schlesinger et al. by mistake, followed by discovery of  $\text{NaBH}_4$  in 1943 [40]. Out of all known borohydrides,  $\text{Be}(\text{BH}_4)_2$  remains the one providing the highest gravimetric hydrogen content (20.7 wt.%, Figure 2), but it is also very toxic, which limits its usability as hydrogen storage material. While using them as raw materials for hydrogen storage is impractical due to poor reversibility and very high (or low) decomposition temperature, the high amount of hydrogen bound to boron in complex anion  $[\text{BH}_4]^-$  or  $[\text{B}_2\text{H}_7]^-$  (the latter is identified only in solution) makes them very interesting starting points for novel energy storage systems.

The general strategies used for metal borohydride synthesis are: solid-state reactions (mechano-chemical), wet chemistry (solvent-assisted), nanoconfined hydrides, and formation of adducts of borohydrides. The mechano-chemical synthesis route is perhaps the most-used and best-known method to obtain metal borohydrides; it is also the only one able to afford mixed-cation borohydrides (like  $\text{LiZn}_2(\text{BH}_4)_5$ ) [41]. The main drawback of ball-milling / the mechano-chemical route is the impurity of the resulting borohydride with metal halides, which are by-products of the metathesis reaction [42–46]. By contrast, wet-chemistry methods can yield phase-pure metal borohydrides, and they afford far easier separation procedures.

### 3.1. Solid-State—Mechanochemical Synthesis

Ball-milling has a series of advantages: it allows for good homogenization of the sample, reduces the size of the particle, and introduces defects which are highly reactive,

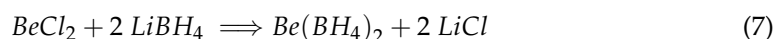
inclusive in hydrogenation studies [47]. The mechano-chemical route is a highly energetic process carried out usually in a planetary ball mill [47–49]. The milling program typically consists in 1–5 min ball-milling followed by a 1–5 min break [50], such that the chemical activation observed is not due to local temperature increase, which is estimated to remain around 60 °C [51–53], but rather due to high pressure caused by collisions between ball, powder, and vial which produce material shear stress and deformations [54]. The mechano-chemical approach can increase the reactivity of materials by size-reduction of the particles, which increases their surface area and thereby provides better interaction between particles needed for a complete reaction to occur.

A double substitution reaction (metathesis) occurs when a metal halide (such as MgCl<sub>2</sub>, or more recently MgBr<sub>2</sub>) reacts with NaBH<sub>4</sub>, producing Mg(BH<sub>4</sub>)<sub>2</sub> in its β-phase polymorph:



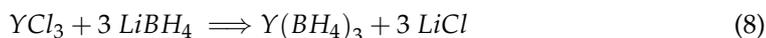
Using a bromide source rather than chloride yields the expected β-Mg(BH<sub>4</sub>)<sub>2</sub> faster (6 h), when the reactants are introduced in a near-stoichiometric ratio (MgBr<sub>2</sub>:NaBH<sub>4</sub> = 1:2 or 1:2.15). The usual workup procedure consists in Soxhlet extraction with Et<sub>2</sub>O, followed by a two-step evaporation under vacuum (150 °C, 24 h and 190 °C, 5 h) [55–59]. The observed reactivity enhancement mirrors the halide reactivity trend, which increases down the 17 group in the order Cl<sup>−</sup> < Br<sup>−</sup> < I<sup>−</sup>.

The seemingly first candidate for hydrogen storage (highest gravimetric hydrogen content, 20.7 wt.%), Be(BH<sub>4</sub>)<sub>2</sub>, was first synthesized by a metathesis reaction, at 145 °C [60]:



Schlesinger et al. made a great contribution to the development of novel metal borohydrides, after the discovery of Al(BH<sub>4</sub>)<sub>3</sub> in 1939, and studied the synthesis of borohydrides by metathetical reactions using alkali metal borohydrides [60], alternative syntheses of NaBH<sub>4</sub> and LiBH<sub>4</sub> [61], synthesis of NaBH<sub>4</sub> from NaH and borate esters [62], and synthesis of U(BH<sub>4</sub>)<sub>4</sub> [63,64]. The metathetical reaction leading to Be(BH<sub>4</sub>)<sub>2</sub> is not a proper mechano-chemical reaction since it is a solid-state reaction but performed by vigorous shaking of the reagents rather than in a planetary mill [60]. In fact, due to the requirement to continuously remove the volatile (and toxic) Be(BH<sub>4</sub>)<sub>2</sub> from the system, the reaction cannot be performed in a closed system (like the vial of a planetary mill).

The metathesis is best carried out using LiBH<sub>4</sub>, since it showed considerably faster reactivity towards MCl<sub>x</sub> than NaBH<sub>4</sub>, having also an added reaction drive due to the formation of stable alkali salt, LiCl [60]:

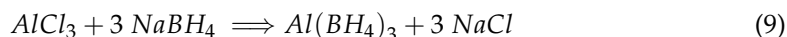


Synthesis of Y(BH<sub>4</sub>)<sub>3</sub> starts from yttrium(III) chloride and LiBH<sub>4</sub>, producing in high yield the expected borohydride of Y(III) and LiCl as by-product, in an all-solid metathesis reaction [65–75]. Yan et al. have also tried ball-milling the reagents according to Equation (8) with the aim of obtaining pure Y(BH<sub>4</sub>)<sub>3</sub>, then solvent metathesis of the grinded mixture; however, the obtained yttrium(III) borohydride was only ~85% pure (impurity: LiCl, 15 wt.%) [76]. Moreover, when the stoichiometric mixture YCl<sub>3</sub>: 3 LiBH<sub>4</sub> was employed for ball-milling at RT or cryo-ball-milling, the reaction mixture showed incomplete conversion to Y(BH<sub>4</sub>)<sub>3</sub>, while YCl<sub>3</sub>: 4 LiBH<sub>4</sub> yielded almost completely the expected borohydride [67,77–80]. Usage of LiBH<sub>4</sub> was compulsory, as Y(BH<sub>4</sub>)<sub>3</sub> was not obtained when replacing the borohydride source with NaBH<sub>4</sub> [74].

Zr(BH<sub>4</sub>)<sub>4</sub> can be prepared by a series of solid-state reactions, for instance between NaZrF<sub>5</sub> + 2 Al(BH<sub>4</sub>)<sub>3</sub>, ZrCl<sub>4</sub> + 2 Al(BH<sub>4</sub>)<sub>3</sub>, or ZrCl<sub>4</sub> + 4 LiBH<sub>4</sub> [77–80].

It has also been suggested that, in the case of mechano-chemical synthesis, the need to evacuate the volatile borohydride species (Be(BH<sub>4</sub>)<sub>2</sub> or Al(BH<sub>4</sub>)<sub>3</sub> being prime examples) advocates for an equilibrium reaction that is shifted towards products with removal of the

volatile product, in line with Le Chatelier's principle [81,82].  $\text{Al}(\text{BH}_4)_3$  has a theoretical hydrogen storage capacity of 16.8 wt.%, but is a liquid at RT (mp =  $-64\text{ }^\circ\text{C}$ ) due to weak intermolecular forces between its molecules; it is fairly unstable and begins to decompose at  $\sim 40\text{ }^\circ\text{C}$ , which is too low for use in a hydrogen production mobile tank. Its crystal structure presents  $[\text{BH}_4^-]$  units that are covalently bonded by two H-bridges to the  $\text{Al}^{3+}$  center. A ball-milling reaction of  $\text{AlCl}_3$  with  $\text{NaBH}_4$  in a stoichiometric molar ratio results in good yields of  $\text{Al}(\text{BH}_4)_3$  [60].



The solid-state  $\text{Al}(\text{BH}_4)_3$  has two polymorphs (transition temperature  $-93$  to  $-78\text{ }^\circ\text{C}$ ) [83–88]. Due to its liquid nature, toxicity, and moisture and air sensitivity,  $\text{Al}(\text{BH}_4)_3$  rather serves as a starting point for synthesis of other, more stable borohydrides, and it is not currently the focus of research on novel energy storage materials because of these limitations.

Ball-milling is also the only way to produce mixed-cation or mixed-anion borohydrides, with reaction conditions (milling time, temperature, pressure) depending ultimately on the metal electronegativity and d-electron configuration in the case of transition metal systems. For instance, mixing  $\text{ZnCl}_2$  and  $\text{KBH}_4$  in a 1:1 ratio produces a chloro-borohydride of  $\text{K}^+$  and  $\text{Zn}^{2+}$ . The complexity of the ball-milling process and its high dependence on reagent molar ratio is depicted below, showing a family of products all starting from  $\text{ZnCl}_2$  and a metal alkali borohydride source (Figure 5) [41].

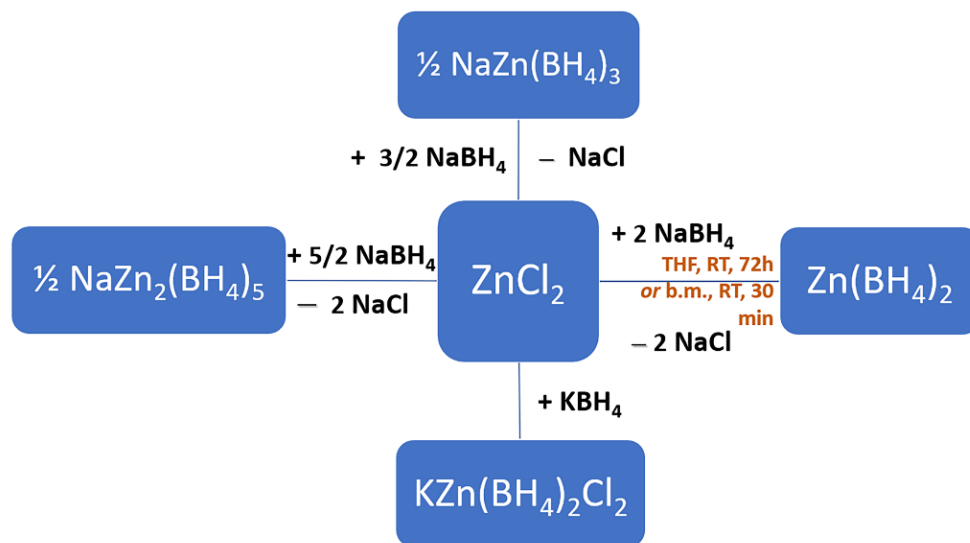


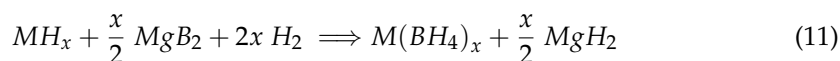
**Figure 5.** Complexity of ball-milling process, exemplified for synthesis of  $\text{Zn}(\text{BH}_4)_2$  from  $\text{ZnCl}_2$  and  $\text{MBH}_4$  ( $\text{M} = \text{Na}, \text{K}$ ) under various ratios of starting materials (1:1, 1:1.5, 1:2, and 1:2.5); THF-tetrahydrofuran, RT-room temperature, b.m - ball milling.

Besides the formation of  $\text{LiCl}$  (or  $\text{NaCl}$ ) as by-products, the metathetic route has another drawback: some amounts of this salt can dissolve in  $\text{LiBH}_4$ , yielding a solid solution of approximate formula  $\text{Li}(\text{BH}_4)_{1-p}\text{Cl}_p$  ( $p$  is an integer number,  $0 < p < 1$ ), making further purification even more difficult [89].

Synthesis of borohydrides can also be accomplished from starting elements as raw materials, but under extreme conditions caused by the very low reactivity of boron, as shown by Friedrichs et al. ( $700\text{ }^\circ\text{C}$ , 150 bar) [90,91]:



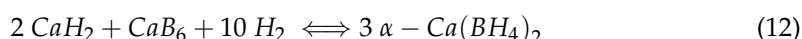
Other high-pressure reaction routes starting from solid metal hydride or metal boride have been investigated. For instance, reacting metal hydride  $MH_x$  with  $MgB_2$  and hydrogen  $H_2$  leads to corresponding  $M(BH_4)_x$  and  $MgH_2$  [92,93].



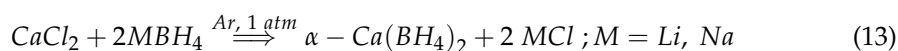
for  $x = 1$ ,  $M = Li, Na$ ; for  $x = 2$ ,  $M = Ca$

Regeneration of  $Ca(BH_4)_2$  during hydrogenation studies was shown to proceed at 350 °C and 150-bar  $H_2$ , with a faster dehydrogenation/rehydrogenation kinetics when a Ti-catalyst was employed [94].

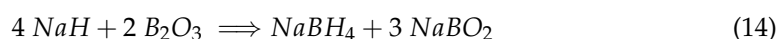
$Ca(BH_4)_2$  can be obtained in good yield (60%) by rehydrogenation of calcium hexaboride  $CaB_6$  and  $CaH_2$  under harsh conditions (690–700-bar  $H_2$ , 400–460 °C) [95]:



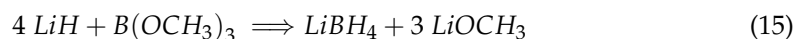
Interesting to note in Equation (12) is the formation of  $\alpha$ - $Ca(BH_4)_2$  at temperatures above 400 °C; typically, when synthesized at lower temperature,  $\alpha$ - $Ca(BH_4)_2$  undergoes an irreversible phase transformation to  $\beta$ - $Ca(BH_4)_2$  when heated above 180 °C; this synthesis route thus has a main advantage in affording the  $\alpha$ -phase at high temperatures (Equation (32)). The overall hydrogenation capacity of  $Ca(BH_4)_2$  based on Equation (12) is 9.6 wt.%. Formation of  $CaB_6$  instead of the unreactive B or high boranes like  $CaB_{12}H_{12}$  in the dehydrogenation process confers to the reaction a real potential for reversibility [96–99]. The formation of  $Ca(BH_4)_2$  can also take place in modest yields (~20%) by ball-milling at RT for 24 h and under 140-bar  $H_2$ , when using  $TiF_3$  as catalyst; in fact, many rehydrogenation reactions benefit from using Ti-based catalysts [100]. Ball-milling under Ar backpressure (1 atm) between  $CaCl_2$  and  $MBH_4$  ( $M = Li, Na$ ) was reported to also produce  $Ca(BH_4)_2$ , albeit made impure with chloride by-products (Equation (13)) [101].



Reaction between sodium hydride  $NaH$  and boric oxide have produced sodium borohydride in good yield (60%) after ball-milling at 330–350 °C for 20–48 h [62]:



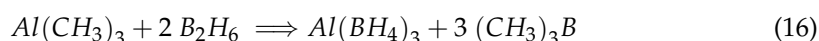
In a similar fashion, but using methyl borate  $B(OCH_3)_3$  instead of boric oxide,  $LiBH_4$  was obtained with an overall yield of about 70% [62]:

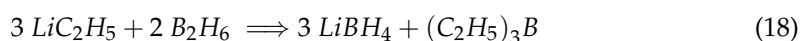


However, the economical aspect of using mechano-chemical synthesis may tip the balance, because large-scale facilities for grinding are known and operable, so that cost-effectiveness is insured for the preparation of light complex hydrides via the ball-milling technique.

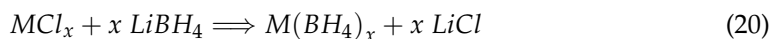
### 3.2. Wet Chemistry—Solvent-Assisted Synthesis

The first borohydride,  $Al(BH_4)_3$ , was synthesized by Schlesinger by accident in 1939 [40] (Equation (16)). He was hoping to obtain  $AlH_3$  by mixing  $Al(CH_3)_3$  and  $B_2H_6$ , when the following reaction actually occurred, which has further been expanded to the synthesis of  $Be(BH_4)_2$  (Equation (17)) and  $LiBH_4$  (using an alkyl-lithium in the latter case).  $LiBH_4$  is the second most used borohydride today, but it was first synthesized also in the 1940s by Schlesinger et al. according to Equation (18) [102].





At present, the usual procedure for the synthesis of  $\text{M}(\text{BH}_4)_x$  follows the general reactivity scheme (19) and (20), and it can be successfully applied for divalent borohydride synthesis ( $\text{M} = \text{Be}, \text{Mg}, \text{Ca}, \text{Sr}, \text{Ba}$ ) or trivalent borohydrides ( $\text{M} = \text{Al}$ ):

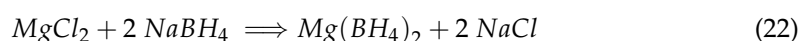


$\text{Al}(\text{BH}_4)_3$  was obtained by Kollonitsch and Fuchs and reported back in 1955, by reacting  $\text{AlCl}_3$  with  $\text{Ca}(\text{BH}_4)_2$  in a 2:3 molar ratio [103].



Synthesis of  $\text{LiBH}_4$  according to Equation (19) takes place in NaH-dried isopropylamine  $i\text{PrNH}_2$  [60,104], and usage of toxic diborane  $\text{B}_2\text{H}_6$  is now avoided as in its first synthesis by Schlesinger and Brown [102]. The metathesis reactions (19) and (20) are well-documented, and proceed with a reasonable rate for  $\text{LiBH}_4$  compared to slower alkali borohydride starting materials (i.e.,  $\text{NaBH}_4$ , and ever slower with  $\text{KBH}_4$ ) [60], and afford the complex borohydride  $\text{M}(\text{BH}_4)_x$  in near-quantitative yield.  $\text{NaBH}_4$  remains the most wide-spread borohydride in terms of synthesis methods and uses, including but not limited to organic synthesis, reduction reactions, and metathesis [105].

$\text{Mg}(\text{BH}_4)_2$  could be synthesized according to Equation (20), using diethyl ether  $\text{Et}_2\text{O}$  as solvent for the  $\text{LiBH}_4$ , but the product obtained contains impurities of Li and  $\text{Cl}^-$  [106–108]. At modest temperatures (34–60 °C), reaction (22) yields some  $\text{Mg}(\text{BH}_4)_2$  (overall yield: 0–11.5%); different conditions must therefore be used if  $\text{NaBH}_4$  is used as borohydride source [107,108]. Even when conducted in recommended solvent  $i\text{PrNH}_2$ , the final mixture could not surpass 40 wt.% of  $\text{Mg}(\text{BH}_4)_2$ , with the impurities being mainly represented by unreacted  $\text{NaBH}_4$ ; this aspect could be proof of an equilibrium reaction being reached under those specific reaction conditions, but it could also originate from poor solubility of the intermediate magnesium amine complex formed in the reaction mixture [106]. Phase-pure  $\beta\text{-Mg}(\text{BH}_4)_2$  was obtained by replacing highly reactive  $\text{LiBH}_4$  with  $\text{NaBH}_4$ , using a combined mechano-chemical (2 h) double exchange reaction (60 h, refluxing  $\text{Et}_2\text{O}$  solvent), followed by drying at 240 °C [109].



Organometallic compounds can also be used to synthesize metal borohydrides; reaction of *n*-butyl-magnesium with  $\text{Al}(\text{BH}_4)_3$  in non-coordinating solvent (toluene) yields a solvent-free  $\text{Mg}(\text{BH}_4)_2$  in very good yield (85%) (Equation (23)) [110].



Reaction of  $\text{CaH}_2$  or  $\text{Ca}(\text{OC}_2\text{H}_5)_2$  with diborane  $\text{B}_2\text{H}_6$  in THF also affords the adduct of  $\text{Ca}(\text{BH}_4)_2$  in good yield [111–117]. The reaction of ball-milled activated  $\text{CaH}_2$  (1 h, under Ar, 600 rpm) and triethylamine borazane complex  $\text{Et}_3\text{N}\cdot\text{BH}_3$  produces  $\text{Ca}(\text{BH}_4)_2$  in 85% yield (unreacted  $\text{CaH}_2$  as main impurity). The reaction is carried out at 140 °C for 5–6 h and the subsequent workup consists in *n*-hexane washing, filtering, and drying at 200 °C for 12 h [118].

$\text{Zn}(\text{BH}_4)_2$  could also be prepared by wet-chemistry at room temperature (RT), using tetrahydrofuran (THF) as solvent and  $\text{ZnCl}_2$  and  $\text{NaBH}_4$  as starting materials (Figure 5) [119–122]. With a hydrogen storage capacity of 8.5 wt.%,  $\text{Zn}(\text{BH}_4)_2$  starts to decompose at ~85 °C and eliminates up to 140 °C hydrogen and diborane  $\text{B}_2\text{H}_6$ , making it for the time being too unstable for vehicular applications. On the other hand, formation of toxic  $\text{B}_2\text{H}_6(\text{g})$  should urge researchers to look for alternative decomposition pathways that

avoid diborane as by-product, since current dehydrogenation will not be reversible in the absence of the boron source [119–122].

Potassium borohydride  $\text{KBH}_4$  (also  $\text{RbBH}_4$  and  $\text{CsBH}_4$ ) could be synthesized by a precipitation reaction of  $\text{NaBH}_4$  with a concentrated solution of a strong base,  $\text{KOH}$ ; the reaction could be carried out in aqueous or  $\text{CH}_3\text{OH}$  media, with an overall yield of 75.5% (Equation (24)). The reagents are independently dissolved in  $\text{MeOH}$ , cooled, and then mixed, when the borohydride of interest precipitates and is obtained in pure form after a subsequent vacuum drying step [123,124].



$\text{LiBH}_4$  can also be produced by reacting  $\text{LiH}$  with diborane at mild temperatures ( $120^\circ\text{C}$ ) [125]. However, no reaction takes place between  $\text{LiH}$  and  $\text{CaB}_2$ ;  $\text{Ca}(\text{BH}_4)_2$  therefore cannot be obtained via this route (Equation (25)) [92].



A similar reaction between the metal hydride  $\text{MH}_x$  ( $M = \text{Li, Mg, Ca}$ ) and  $\text{B}_2\text{H}_6$  in a solid–gas mechanochemical process was proposed by Friedrichs et al., who obtained borohydride products in good-to-high yield, but containing some impurities (unreacted starting metal hydride and Fe–Ni phases from vial abrasion during milling):  $\text{LiBH}_4$  ( $\eta = 94\%$ ),  $\text{Mg}(\text{BH}_4)_2$  ( $\eta = 91\%$ ) and  $\text{Ca}(\text{BH}_4)_2$  ( $\eta = 73\%$ ). Diborane  $\text{B}_2\text{H}_6$  was also proposed as a key intermediate in hydrogenation studies under moderate conditions [93].

Neutron diffraction studies have been facilitated by a hydrogen–deuterium H–D exchange reaction taking place at increasing temperatures for Li, Na, and K ( $200^\circ\text{C}$ ,  $350^\circ\text{C}$ , and  $500^\circ\text{C}$ , respectively) (Equation (26)) [126].



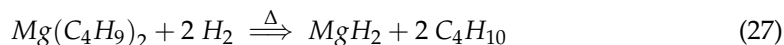
### 3.3. Nanoconfined Hydrides

The ball-milling technique is usually the go-to process for obtaining nanosized powders of metal hydrides, to sizes often less than 100 nm [127]. Ball-milling implies milling in a vial using balls of special alloys; however, the milling process could induce impurities in the sample from the materials of the vial and balls. However, these nanoparticles could also sinter into larger particles during hydrogenation–dehydrogenation cycles, which negatively impacts gravimetric hydrogen uptake and release [128–131]. Using specially engineered nano-scaffolds, complex hydrides can be obtained in the nanometer range, far below the average sizes afforded by the mechano-chemical approach.

Among nanoconfinement methods, the most widely used are the direct synthesis of nanoconfined complex metal (boro)hydride, and infiltration methods (melt-infiltration and wet-infiltration) [132].

Nanoconfinement of metal hydrides synthesized in situ has been extensively studied for magnesium hydrides in carbon aerogels produced by the resorcinol–formaldehyde reaction (RF-CA), using a 1 M solution of  $\text{Mg}(\text{C}_4\text{H}_9)_2$  in n-heptane [133,134]. Nielsen et al. synthesized by this method  $\text{MgH}_2@$ RF-CA of pore sizes 7 and 22 nm [133]. This is a typical case of soft-nanocasting, as the initial porous support is not removed from the final composite material (Figure 6).

The excess n-butyl magnesium can be removed manually after the reaction from the surface of RF-CA (Equation (27)).



Melt infiltration requires a very inert scaffold, with a melting point higher than that of the respective metal hydride used. The driving force of this method is the lower interfacial energy metal hydride/scaffold, as reviewed by de Gennes [135,136]. This method has

the advantage of completely removing the necessity of a solvent, therefore avoiding post-synthesis steps of the hydride@scaffold composite. In addition, the melting point of the hydride must not coincide with the onset of decomposition of the said material. However, sodium tetrahydroaluminate  $\text{NaAlH}_4$  ( $\text{mp} = 183\text{ }^\circ\text{C}$ ) has been utilized for melt infiltration, despite decomposition onset into Al and  $\text{Na}_3\text{AlH}_6$  upon melting [137].

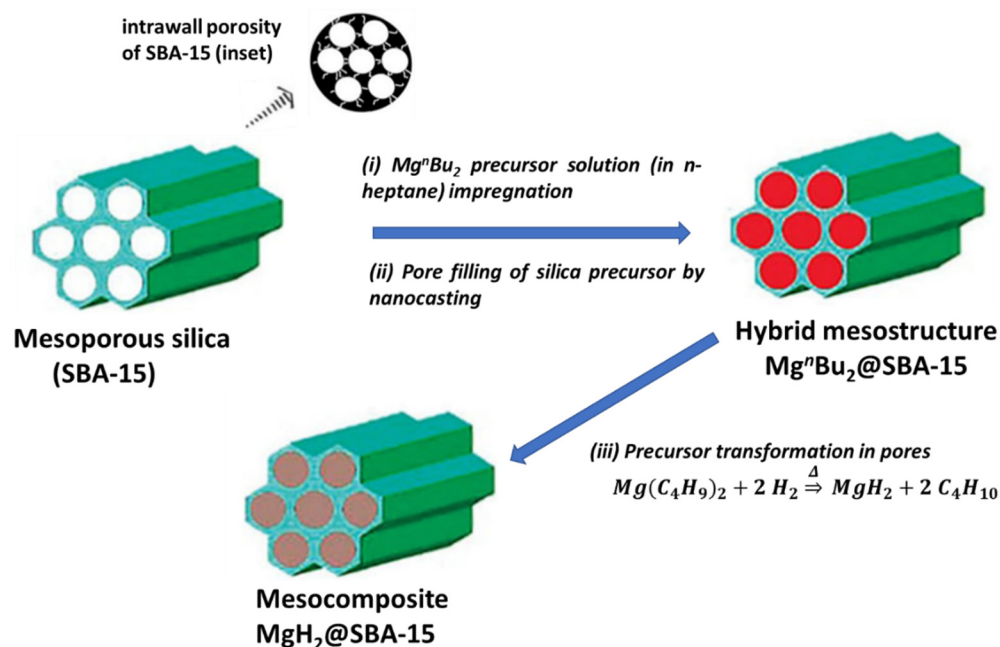
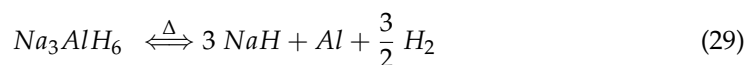
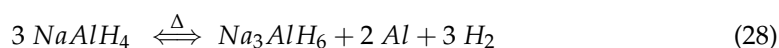


**Figure 6.** Soft nanocasting showing infiltration of  $\text{Mg}^n\text{Bu}_2$  solution into SBA-15 mesoporous silica template to yield finally porous  $\text{MgH}_2$  nanoconfined inside SBA-15 pores ( $D_p \sim 7.5\text{ nm}$ ).

The decomposition of  $\text{NaAlH}_4$  must be considered a partial equilibrium (Equations (28) and (29)), because when working around the borohydride melting point and using high  $\text{H}_2$  pressure (160–190 bar), the decomposition is avoided and melt infiltration has been successful [137–142].



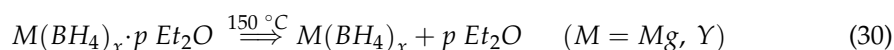
Solvent infiltration requires a suitable solvent that affords complete metal hydride dissolution in order to be successful. A series of physical properties of metal borohydrides (including knowledge of select solubility data) are a prerequisite, as limited solubility in commonly used solvents is the main limitation of this method. Sometimes even weakly coordinating solvents could be used, but these solvents should be removed under moderate conditions ( $T, p$ ). Following the rather poor solubility of complex metal hydrides, consequent steps of impregnation–evaporation may be required to reach full (or the desired degree of) scaffold pore filling [132]. This technique—incipient wetness method—can be advantageous as it avoids crystallization of active hydride species outside of mesopores; complex metal borohydrides like  $\text{Ca}(\text{BH}_4)_2$  have been infiltrated in chemically activated micro-mesoporous carbons of very high surface area to produce composites exhibiting reversible hydrogen storage under more modest conditions [143].

Various scaffolds can be used; inert, mesoporous silica of 2D-ordered type (SBA-15) could serve such a purpose. Computational studies have shown that molecules of  $\text{NH}_x\text{BH}_x$  type ( $x = 1\text{--}4$ ) display thermodynamically accessible dehydrogenation steps of less than 40 kJ/mol, and relatively low dehydrogenation temperature onset (100–150  $^\circ\text{C}$ ); they can thus be considered candidates for hydrogen storage reactions [144]. When a 5.4 M solution

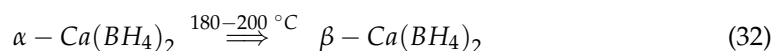
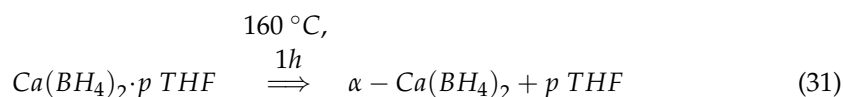
of ammonia–borane  $\text{NH}_3\cdot\text{BH}_3$  in  $\text{CH}_3\text{OH}$  infiltrated the  $\sim 7.5$  nm pores of SBA-15 silica, a total loading of roughly 50 wt.%  $\text{NH}_3\text{BH}_3$ @SBA-15 was obtained after solvent evaporation [145]. A clear advantage of solvent-mediated impregnation is that the experimental procedure requires less energy, since it can be carried out even at room temperature.

### 3.4. Derivatives—Formation of Adducts of $M(\text{BH}_4)_x$

Solvent metathesis reactions often lead to the formation of desired borohydrides as solvates:  $M(\text{BH}_4)_x \cdot p \text{Et}_2\text{O}$  ( $p$  is an integer number), as is the actual case for  $M = \text{Mg}$  and  $\text{Y}$ . Both  $\text{Mg}(\text{BH}_4)_2 \cdot p \text{Et}_2\text{O}$  [106–108] and  $\text{Y}(\text{BH}_4)_3 \cdot p \text{Et}_2\text{O}$  [76] could be obtained as pure, unsolvated solids after heating at  $150^\circ\text{C}$ , as shown by IR and TG data (Equation (30)).

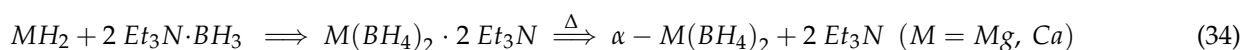


Other borohydrides are obtained as tetrahydrofuran adducts, such as  $\text{Ca}(\text{BH}_4)_2 \cdot p \text{THF}$ , which is also commercially available. Heating this adduct at  $160^\circ\text{C}$  for 1 h leads to phase-pure,  $\alpha$ - $\text{Ca}(\text{BH}_4)_2$  (Equation (31)) [146–151]. Careful control of the temperature profile is advised, as from  $180^\circ\text{C}$  the conversion to  $\beta$ - $\text{Ca}(\text{BH}_4)_2$  occurs (Equation (32)).

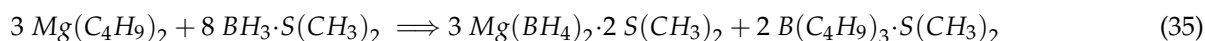


As is typical with organometallic synthesis, purification of metal borohydrides can be achieved using recrystallization from a concentrated solution (usually the synthesis solvent:  ${}^i\text{PrNH}_2$ ,  $\text{MeOH}$  or even  $\text{H}_2\text{O}$ ).  $\text{NaBH}_4$  could be recrystallized from  ${}^i\text{PrNH}_2$  [152] or  $\text{H}_2\text{O}$  [153]. In the latter case, single crystals could be obtained corresponding to dihydrate sodium borohydride,  $\text{NaBH}_4 \cdot 2\text{H}_2\text{O}$ .

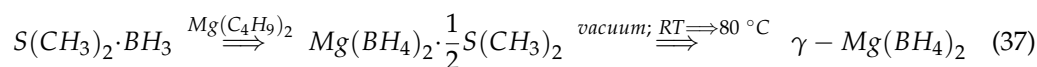
Triethylamine ( $\text{Et}_3\text{N}$ )-solvated metal borohydrides:  $\text{NaBH}_4$  or partially deuterated  $\text{NaBD}_3\text{H}$  [154,155],  $\text{Mg}(\text{BH}_4)_2$  [156], and  $\text{Ca}(\text{BH}_4)_2$  [157], could be obtained by reacting the corresponding premilled (and thus highly reactive) metal hydride with an excess of aminoborane (Equations (33) and (34)).



Dimethyl sulfide  $\text{S}(\text{CH}_3)_2$ -stabilized magnesium borohydride can also be obtained, provided that a large excess of the tioborane is used. Solvent-free  $\text{Mg}(\text{BH}_4)_2$  can be obtained by working up the reaction mixture at low pressures ( $10^{-1}$ – $10^{-5}$  mbar, for 19 h in total), a step which removes coordinating solvent  $\text{S}(\text{CH}_3)_2$  (Equations (35) and (36)) [110].



Desolvation from a dimethylsulfide borane complex solvate led instead to a new, nanoporous polymorph,  $\gamma$ - $\text{Mg}(\text{BH}_4)_2$  (Equation (37)) [158].



The structural variety of polymorphs obtained in the case of magnesium borohydride (six in total) (Equations (35)–(37)) suggests that novel, nanoporous metal hydrides could be potentially accessible via this desolvation route.

Thermal analysis coupled with IR spectroscopy data has pointed out two possible formulations of solvated complexes of closely related tetrahydroaluminates, when coordinated to a tertiary amine “L” (Figure 7). If a weak coordination is expected, then structural formula I is favorable, and it should resemble that of an uncoordinated complex metal hydride, as pointed out by Schlesinger and Brown. The complex should exhibit high thermal stability—which is actually the case for I:  $L \Rightarrow M^+ [AlH_4]^-$ , due to the increased size of the cation and the reduced distortion of the  $AlH_4^-$  tetrahedron by alkali metal interaction [102]. By contrast, formula II:  $H-M \dots AlH_3L$  is expected to have a lower thermal stability, resulting in a complex mixture of products upon decomposition due to the complex bond amine-alanate  $R_3N: \Rightarrow AlH_3$  [159].

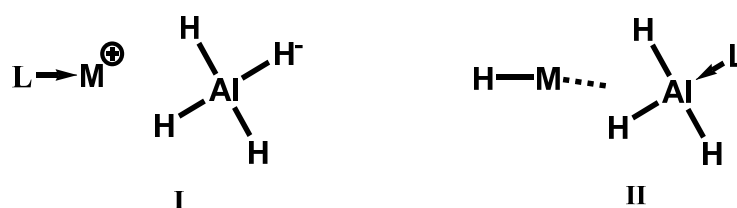
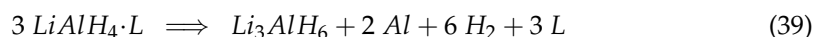
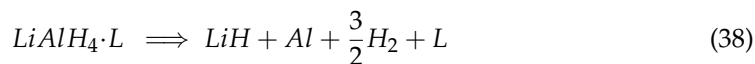


**Figure 7.** Two formulations (I [102] and II [159]) of possible solvate structures for ligand-coordinated metal alanates of select alkali metals (M: Li, Na).

Full decomposition of solvate  $LiBH_4 \cdot L$  could proceed through either pathway (38) or (39) as evidenced by the ambiguous DTA-TGA curve, with both leading to loss of coordinating molecule L:



$Mg(BH_4)_2 \cdot THF$  adducts decompose violently [160] due to the formation of alkoxy species by the THF ring-opening reaction, as is the case with aluminum hydride-THF adducts [161]. However,  $Ca(BH_4)_2 \cdot THF$  can be desolvated with relative ease, without such strong exothermic effects, as evidenced by Equation (31) [146–151,162].

A metathesis reaction is currently the preferred method of synthesis for metal borohydrides because they can be obtained in pure form. There are recent reports expanding the recognized reducing character of metal borohydrides. For instance,  $Ca(BH_4)_2$  can be successfully used in advanced organic synthesis, such as polymerization of  $\epsilon$ -caprolactine and L-lactide [163].

#### 4. Structural Considerations of $M(BH_4)_x$

There is an intricate connection between structure and solid-state chemistry related to borohydride materials. Among most important physical properties affected by lattice structure are the thermal stability and the accessible decomposition pathways.

##### 4.1. Framework and Crystal Structure

Metal borohydrides are typically ionic compounds, but covalent borohydrides are also known. Table 1 summarizes some of the novel metal borohydrides and mixed-cation borohydrides and their structural architecture; many present multiple polymorphism (LT, HT, metastable).

**Table 1.** Selected metal borohydrides with corresponding space group, decomposition temperature (and rehydrogenation temperature, where available) (°C), and crystal system.

Metal Borohydride	Decomposition Temperature (°C)	Rehydrogenation Temperature (°C)	Space Group	Crystal System	Reference
o-LiBH <sub>4</sub>	(mp = 277);	600	<i>Pnma</i>	Orthorhombic	[30–38,164]
h-LiBH <sub>4</sub>	(107)	600	<i>P6<sub>3</sub>mc</i>	Hexagonal	[30–38]
α-NaBH <sub>4</sub>	535	270–400 (2NaH/ MgH <sub>2</sub> )	<i>Fm<math>\bar{3}</math>m</i>	Cubic	[165–169]
Be(BH <sub>4</sub> ) <sub>2</sub>	(mp = 91.3) t <sub>d</sub> = 123	Explosive decomp. in air/moisture	<i>I4<sub>1</sub>/cd</i>	Tetragonal; helical polymeric chains BeH <sub>2</sub> BH <sub>2</sub> BeH <sub>2</sub> BH <sub>2</sub> and terminal bidentate BH <sub>4</sub> groups	[170]
α-Mg(BH <sub>4</sub> ) <sub>2</sub> (6 known polymorphs)	~300	(390 °C, 90-bar H <sub>2</sub> , 72 h) (400 °C, 80-bar D <sub>2</sub> ) RT stable	<i>P6<sub>1</sub>22</i>	Hexagonal	[106,171]
β-Mg(BH <sub>4</sub> ) <sub>2</sub>	~300	HT polymorph; RT metastable	<i>Fddd</i>	Orthorhombic	[172,173]
γ-Mg(BH <sub>4</sub> ) <sub>2</sub>	~300	RT metastable	<i>Ia<math>\bar{3}</math>d</i>	Cubic; 3D network of interpenetrated channels (1st borohydride with permanent porosity, S = 1505 m <sup>2</sup> /g)	[158]
α-Ca(BH <sub>4</sub> ) <sub>2</sub> (4 known polymorphs)	347–387 °C, 397–497 °C (2-step process)	RT stable	<i>F2dd</i>	Orthorhombic	[146–151]
β-Ca(BH <sub>4</sub> ) <sub>2</sub>	α – Ca(BH <sub>4</sub> ) <sub>2</sub> $\xrightleftharpoons{167\text{ °C}}$ β-Ca(BH <sub>4</sub> ) <sub>2</sub>	RT, metastable, HT polymorph	<i>P<math>\bar{4}</math></i>	Tetragonal	[146–151,157]
α-Al(BH <sub>4</sub> ) <sub>3</sub>	<100	–123	<i>C2/c</i>	Monoclinic	[83–88]
β-Al(BH <sub>4</sub> ) <sub>3</sub>	<100	–78	<i>Pna2<sub>1</sub></i>	Orthorhombic	[83–88]
α-Y(BH <sub>4</sub> ) <sub>3</sub> (β-Y(BH <sub>4</sub> ) <sub>3</sub> is the HT polymorph)	190, 270	180 °C (α-to-β phase transition)	<i>Pa<math>\bar{3}</math></i>	Cubic	[67–73]
α-Mn(BH <sub>4</sub> ) <sub>2</sub> (4 known polymorphs)	130	RT stable	<i>P3<sub>1</sub>12</i>	Hexagonal	[174–180]
LiSc(BH <sub>4</sub> ) <sub>4</sub>	400	(400), irreversible hydrogen storage in Li-Sc-B-H system	<i>P<math>\bar{4}</math>2c</i>	Tetragonal	[181–183]
NaZn(BH <sub>4</sub> ) <sub>3</sub>	>85 °C (at 110 °C NaBH <sub>4</sub> reacts with Na <sub>2</sub> ZnCl <sub>4</sub> to form Zn and NaCl)	stable RT	<i>P2<sub>1</sub>c</i>	Monoclinic	[41,184]
NaZn <sub>2</sub> (BH <sub>4</sub> ) <sub>5</sub>	unstable, converts at low temp. to NaZn(BH <sub>4</sub> ) <sub>3</sub>	unstable at RT or –32 °C	<i>P2<sub>1</sub>c</i>	Monoclinic	[41,184]

The structural diversity of metal borohydrides is stunning, and a glimpse of such diversity is provided in Figure 8, with a few representative examples. For instance,  $\text{CsSr}(\text{BH}_4)_3$  exhibits a structure similar to that of perovskite, which on the one hand explains its high stability with a decomposition onset at  $398\text{ }^\circ\text{C}$  [185]. Potassium octahydridotriborate  $\beta\text{-KB}_3\text{H}_8$ , on the other hand, exhibits discrete units implying a high mobility of boron tetrahedra during chemical transformations [186].

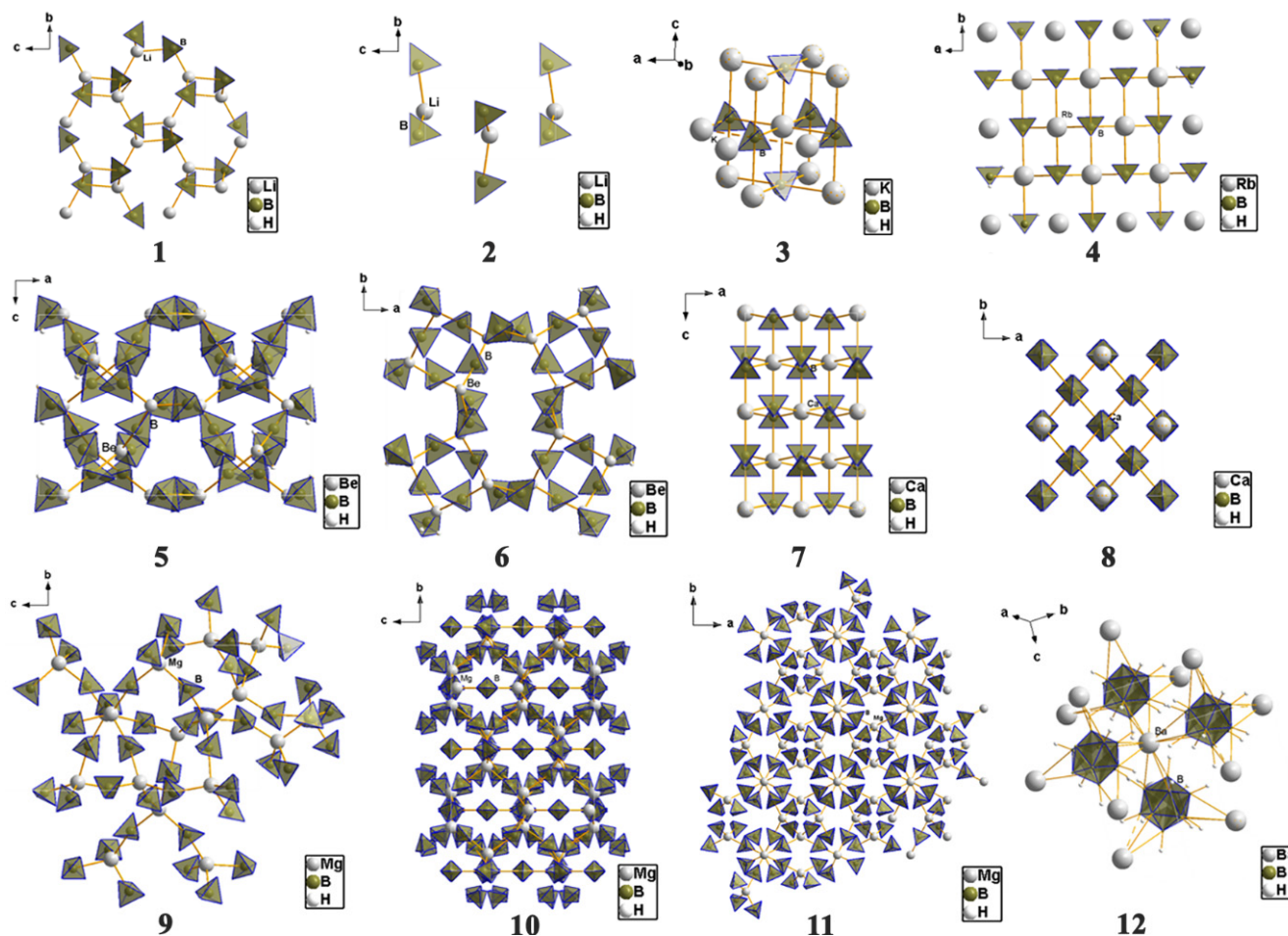


**Figure 8.** Structural diversity exhibited by known and characterized main group (alkali and alkali-earth) metal borohydrides. Crystal system for various borohydrides depicted as projections along “a” crystallographic axis. 1— $\text{LiBH}_4$  ( $\alpha$ -, LT polymorph, a-axis view); 2— $\text{LiBH}_4$  ( $\alpha$ -, HT polymorph, a-axis view); 3— $\text{KBH}_4$ ; 4— $\text{RbBH}_4$ ; 5— $\text{Be}(\text{BH}_4)_2$  (b-axis view); 6— $\text{Be}(\text{BH}_4)_2$  (c-axis view); 7— $\alpha\text{-Ca}(\text{BH}_4)_2$  (b-axis view); 8— $\alpha\text{-Ca}(\text{BH}_4)_2$  (c-axis view); 9— $\alpha\text{-Mg}(\text{BH}_4)_2$  (a-axis view); 10— $\beta\text{-Mg}(\text{BH}_4)_2$  (a-axis view); 11— $\gamma\text{-Mg}(\text{BH}_4)_2$  (c-axis view); 12— $\text{BaB}_{12}\text{H}_{12}$ .

Perhaps one of the most studied metal borohydrides of the main groups,  $\text{LiBH}_4$ , (1 in Figure 8) crystallizes in the orthorhombic  $Pnma$  space group, with cell dimensions  $a = 7.1785\text{ }\text{\AA}$ ,  $b = 4.4368\text{ }\text{\AA}$ ,  $c = 6.8032\text{ }\text{\AA}$ , and  $V = 216.685(3)\text{ }\text{\AA}^3$  at  $20\text{ }^\circ\text{C}$ . While early diffraction data of lower resolution suggesting strong distortion of the  $\text{BH}_4$  tetrahedra, more recent determinations show that B-H bonds and H-B-H angles practically describe perfect tetrahedrons [30–38]. Each  $\text{Li}^+$  cation coordinates four  $[\text{BH}_4]^-$  tetrahedra, and each  $[\text{BH}_4]^-$  tetrahedron coordinates four  $\text{Li}^+$  cations. The LT polymorph of  $\text{LiBH}_4$  shows the  $\text{Li}^+$  cation in four-coordinate tetrahedral sites between anionic layers of  $[\text{BH}_4]^-$  that are hexagonally stacked. When heated to  $\sim 110\text{ }^\circ\text{C}$ , the LT- $\text{LiBH}_4$  (o- $\text{LiBH}_4$ ) undergoes a phase transition to a hexagonal polymorph, HT- $\text{LiBH}_4$  (h- $\text{LiBH}_4$ ), which crystallizes in hexagonal space group  $P6_3mc$  resembling the wurtzite ( $\text{ZnS}$ ) structure, with the following unit cell parameters:  $a = 4.2763\text{ }\text{\AA}$ ,  $c = 6.9484\text{ }\text{\AA}$ , and  $V = 110.041(4)\text{ }\text{\AA}^3$  at  $135\text{ }^\circ\text{C}$  (2—in Figure 8).

The *o*-LiBH<sub>4</sub> to *h*-LiBH<sub>4</sub> polymorphic transformation taking place at ~110 °C can be seen as a contraction along orthorhombic axis *a* (hexagonal axis *c*) and an expansion of the [*b*\**c*] orthorhombic plane, and it is accompanied by a slight endothermic enthalpy of transition (4.18 J/mol).

KBH<sub>4</sub> (**3** in Figure 8) in its  $\beta$ -polymorph, crystallizes in the tetragonal  $P4_2/nmc$  space group. The 3D structure shows a 12-coordinate geometry around the alkali metal, in an equivalent H-surrounding. The K-H bond lengths average 2.815 Å, while the B-H bonds in the [BH<sub>4</sub>]<sup>−</sup> unit measure 1.23 Å. The structure of  $\beta$ -KBH<sub>4</sub> bears structural similarities to tetragonal NaBH<sub>4</sub>, but it is refined to a higher symmetry group  $P4_2/nmc$ . As the size of the cation increases in the alkali group (from Li to Rb), the cubic MBH<sub>4</sub> (M = alkali metal) unit cell expands and the [BH<sub>4</sub>]<sup>−</sup> . . [BH<sub>4</sub>]<sup>−</sup> repulsions are reduced, such that the cubic-to-tetragonal transition temperature is reduced in heavier alkali metal borohydrides.

RbBH<sub>4</sub> (**4** in Figure 8) crystallizes in the cubic  $Fm\bar{3}m$  space group (*a* = 6.9633 Å at 0.5 GPa). The Rb<sup>+</sup> cations and BH<sub>4</sub><sup>−</sup> anions have a NaCl structural prototype and this room-temperature polymorph is isostructural to NaBH<sub>4</sub>, with the BH<sub>4</sub> groups orientationally disordered over the two positions around the inversion center, similar to the sodium tetrahydroborate case.

Be(BH<sub>4</sub>)<sub>2</sub> (**5** in Figure 8) presents only one structurally characterized form which crystallizes in the tetragonal  $I4_1/cd$  space group. It contains helical polymeric chains with the independent Be<sup>2+</sup> coordinated in a trigonal-planar geometry to two bridging [BH<sub>4</sub>] tetrahedra via face coordination (Be-B bond distance 2.00 Å) and one terminal [BH<sub>4</sub>] tetrahedron via the tetrahedral edge (Be-B bond distance 1.92 Å). This originates presumably from the repulsive [BH<sub>4</sub>]<sup>−</sup> . . [BH<sub>4</sub>]<sup>−</sup> forces due to very short H . . H distances (ranging from 2.24 Å to 2.31 Å). The bridging [BH<sub>4</sub>] group shows a linear coordination to the two Be<sup>2+</sup> cations (Be-B-Be angle close to 180°), leading to a 1D polymeric structure.

$\alpha$ -Ca(BH<sub>4</sub>)<sub>2</sub> (**7** in Figure 8) can be obtained by desolvation of the THF adduct, and crystallizes in the orthorhombic  $Fddd$  space group, being one of the four possible polymorphs ( $\alpha$ ,  $\alpha'$ ,  $\beta$  and  $\gamma$ ) and bearing structural similarities to TiO<sub>2</sub> polymorphs [187,188]. The orthorhombic structure has been further amended to better be represented by a lower symmetry ( $F2dd$  or  $Fdd2$ ). All four polymorphs show Ca<sup>2+</sup> octahedrally coordinated to six equivalent [BH<sub>4</sub>] tetrahedra, with the Ca-B bond distances falling in the range 2.82–2.97 Å. The divalent calcium cations form in  $\alpha$ -Ca(BH<sub>4</sub>)<sub>2</sub> a close-packed, diamond-type structure where the tetrahydroborate groups exhibit T-shape coordination [188].

Three polymorphs of Mg(BH<sub>4</sub>)<sub>2</sub> are depicted (**9**:  $\alpha$ -, **10**:  $\beta$ -, **11**:  $\gamma$ -), showing increased structural complexity, but also polymeric properties [106,158,171–173,189–195]. The  $\alpha$ -Mg(BH<sub>4</sub>)<sub>2</sub> represents the most stable polymorph and its structure determination was a result of combined synchrotron (most information data) and neutron powder diffraction data (orientation of BH<sub>4</sub> tetrahedra). Single crystal diffraction data collected at 100 K established the space group to be the hexagonal  $P6_122$ , containing three symmetry-independent Mg<sup>2+</sup> ions and six independent [BH<sub>4</sub>]<sup>−</sup> units. In this novel 3D arrangement, the Mg-Mg distances lie in the range 4.6–4.9 Å, while the Mg<sup>2+</sup> center is tetrahedrally coordinating four [BH<sub>4</sub>]<sup>−</sup> tetrahedra. The Mg-B bond lengths are in the range 2.432(a)–2.434(4) Å, and there is a dispersity of B-Mg-B angles of 92.1(2)–108.80(13)° accounting for a distorted tetrahedral coordination around the metal center. The porous  $\gamma$ -Mg(BH<sub>4</sub>)<sub>2</sub> has a cubic lattice with inherited porous nature (33% open space), high surface area (in excess of 1100 m<sup>2</sup>/g as deduced from N<sub>2</sub> sorption isotherms by BET method) and a partially covalent framework. The stability of Mg(BH<sub>4</sub>)<sub>2</sub> can be related to the Mg-BH<sub>4</sub>-Mg linear units, with BH<sub>4</sub> acting as directional ligands, and stable MgH<sub>8</sub> polyhedra. This complex structural behavior resembles that of coordination polymers like MOFs. The  $\gamma$ -polymorph is particularly interesting due to large empty spaces available for gas entrapment [158].

One of the main dehydrogenation borohydride species found during hydrogen desorption studies is the [B<sub>12</sub>H<sub>12</sub>]<sup>2−</sup> anion, as found for instance in BaB<sub>12</sub>H<sub>12</sub> (**12** in Figure 8). These dodecahydro-*closo*-dodecaborate anions [B<sub>12</sub>H<sub>12</sub>]<sup>2−</sup> have a role in the poor recyclability of metal tetrahydroborates from hydrogenation studies; their formation and possible side-

reactions are therefore of clear importance. Moreover, it has been hypothesized that these species appear amorphous in XRD diffraction data, and only show short-range ordering.  $\text{BaB}_{12}\text{H}_{12}$  crystallizes in the  $P31c$  space group (trigonal symmetry) of wurtzite structural type, and shows  $\text{Ba}^{2+}$  cation surrounded by four  $[\text{B}_{12}\text{H}_{12}]^{2-}$  anions. Each *closo*-borate  $[\text{B}_{12}\text{H}_{12}]^{2-}$  anion is tetrahedrally surrounded by four  $\text{Ba}^{2+}$  cations (mutual tetrahedral arrangement of cations and anions), with distances from the center of the anion to the  $\text{Ba}^{2+}$  of 4.40 and 4.54 Å at 295 K. Since each of the four  $[\text{B}_{12}\text{H}_{12}]^{2-}$  anions is facing the  $\text{Ba}^{2+}$  metal center with three H atoms, the cation is surrounded overall by twelve H atoms (Ba–H bond distances range from 2.77–3.02 Å). The rich boron–hydrogen speciation, open channels, and convenient molecular size (5.8 Å) have made *closo*-borate salts very interesting candidates for ionic conductivity studies.

$\text{Al}(\text{BH}_4)_3$  (1 in Figure 9) is a liquid under normal conditions, but low temperature single-crystal XRD data shows two possible polymorphs with a transition temperature at ~190 K [83]. Single-crystal diffraction data by Aldridge et al. from 1997 shows that  $\text{Al}(\text{BH}_4)_3$  crystallizes at 195 K in the orthorhombic  $Pna2_1$  space group with the following unit cell parameters:  $a = 18.021(3)$  Å,  $b = 6.138(2)$  Å, and  $c = 6.199(1)$  Å. It consists of discrete  $\text{Al}(\text{BH}_4)_3$  units, with a trigonal-planar geometry around the  $\text{Al}^{3+}$  center which coordinates the  $[\text{BH}_4]$  tetrahedra via the tetrahedral edges. The Al–B bond lengths are in the range of 2.10(2)–2.14(2) Å, while the longer B–H distances for the B–H...Al bridges of 1.12(3)–1.14(4) Å are consistent with Al–H coordination [83].

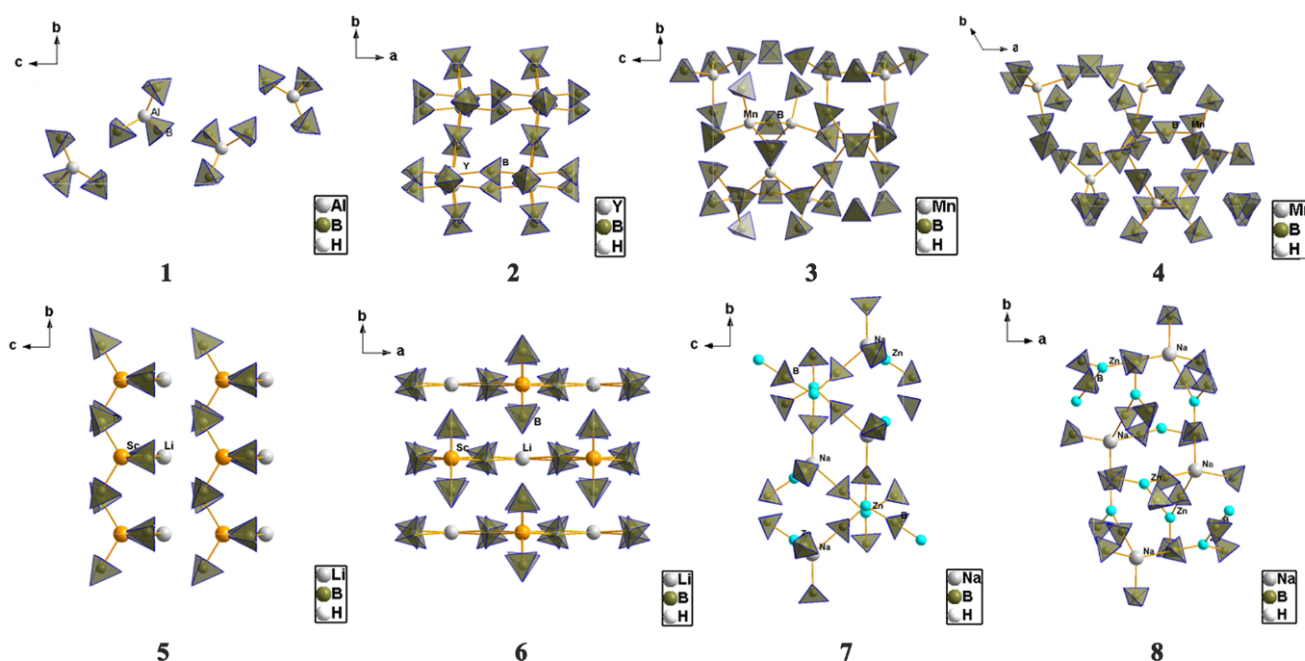


**Figure 9.** Selected examples of trivalent-, TM- (transition metal) and mixed-cation borohydrides. 1— $\text{Al}(\text{BH}_4)_3$  (a-axis view); 2— $\text{Y}(\text{BH}_4)_3$  (c-axis view); 3— $\text{Mn}(\text{BH}_4)_2$  (a-axis view); 4— $\text{Mn}(\text{BH}_4)_2$  (c-axis view); 5— $\text{LiSc}(\text{BH}_4)_4$  (a-axis view); 6— $\text{LiSc}(\text{BH}_4)_4$  (c-axis view); 7— $\text{NaZn}_2(\text{BH}_4)_5$  (a-axis view); 8— $\text{NaZn}_2(\text{BH}_4)_5$  (c-axis view). Color code: Sc—orange; Zn—blue.

$\alpha\text{-Y}(\text{BH}_4)_3$ , one of the most promising hydrogen storage candidates among transition metal borohydrides (2 in Figure 9) was synthesized by cryo-milling of  $\text{LiBH}_4$  and  $\text{YCl}_3$ . It crystallizes in the cubic  $Pa\bar{3}$  space group with a lattice constant  $a = 10.8522(7)$  Å [65,68–73]. The structure has a  $\text{Y}^{3+}$  center in a highly distorted octahedral geometry being surrounded by six  $[\text{BD}_4]^-$  tetrahedra (B–Y–B angles in the range 78.6(2)–160.9(1)°). The  $\alpha\text{-Y}(\text{BH}_4)_3$  converts at 10 MPa  $\text{D}_2$  and 475 K to the *fcc*  $\beta\text{-Y}(\text{BH}_4)_3$  polymorph in the  $Fm\bar{3}c$  space group.

$\alpha\text{-Mn}(\text{BH}_4)_2$  (3 in Figure 9) crystallizes in the  $P3_112$  space group and is isostructural with  $\zeta\text{-Mg}(\text{BH}_4)_2$ , having the unit cell parameters  $a = 10.435(1)$  Å and  $c = 10.835(2)$  Å [189–195].

This represents the first crystal structure of a 3d-metal tetrahydroborate. The  $\alpha$ -Mn(BH<sub>4</sub>)<sub>2</sub> polymorph has a stability range between 90 to 450 K. The structure bears structural similarities to Mg(BH<sub>4</sub>)<sub>2</sub>; the two independent Mn<sup>2+</sup> centers are each tetrahedrally surrounded by four [BH<sub>4</sub>] units with Mn-B distances of 2.39–2.52 Å.

LiSc(BH<sub>4</sub>)<sub>4</sub> can best be described as a Li<sup>+</sup> salt of complex anion [Sc(BH<sub>4</sub>)<sub>4</sub>]<sup>−</sup> that was evidenced by vibrational spectroscopy studies. It crystallizes in the tetragonal *P42c* space group, with a CuAlCl<sub>4</sub> structural prototype and the following unit cell parameters:  $a = 6.076$  Å and  $c = 12.034$  Å (5 in Figure 9). More specifically, it was obtained by Hageman et al. in 2008 by ball-milling processing of a 4:1 molar ratio LiBH<sub>4</sub> and ScCl<sub>3</sub> [181]. The central cation Sc<sup>3+</sup> of the complex anion [Sc(BH<sub>4</sub>)<sub>4</sub>]<sup>−</sup> is surrounded by four BH<sub>4</sub> tetrahedra in a distorted tetrahedral coordination, with a Sc-B bond distance of 2.28(1) Å, which compares favorably to the DFT value predictions of 2.33 Å. The B-Sc-B angle has a spread distribution between 96.5(5)° and 124.4(5)°, suggestive of the deformed tetrahedral coordination. Each of the four [BH<sub>4</sub>] tetrahedra has three H atoms oriented towards the Sc center, so that the global coordination is 8 + 4: 8 Sc-H distances in the range 2.11–2.15 Å and 4 Sc-H distances of 2.31 Å, while the remaining B-H bond pointing outwards is responsible for the high B-H stretching frequencies of 2485–2498 cm<sup>−1</sup>. Moreover, the crystal structure contains disordered Li<sup>+</sup> cations along the z-axis of the tetragonal cell, which in turn could make this mixed borohydride a suitable candidate for ionic conductivity applications [181].

NaZn<sub>2</sub>(BH<sub>4</sub>)<sub>5</sub> (7 in Figure 9) crystallizes in the monoclinic *P2<sub>1</sub>/c* space group, similar to the Li<sup>+</sup> counterpart LiZn<sub>2</sub>(BH<sub>4</sub>)<sub>5</sub>, and it has no analogues to known inorganic structures. The unit cell parameters are:  $a = 9.397(2)$  Å,  $b = 16.635(3)$  Å,  $c = 9.136(2)$  Å, and  $\beta = 112.66(2)^\circ$  [41]. The structure consists of two independent Zn<sup>2+</sup> cations that have almost a trigonal-planar coordination to three [BH<sub>4</sub>] tetrahedra (coordination number of Zn is 3), while the Na<sup>+</sup> cation has a new, saddle-like coordination (coordination number of Na is 4) [41]. Interestingly, NaZn<sub>2</sub>(BH<sub>4</sub>)<sub>5</sub> consists of two doubly penetrating 3D frameworks, with no covalent bonds between them—a structural motif found in coordination polymers. All [BH<sub>4</sub>] units are nearly linearly coordinated by two metal atoms, and the coordination occurs via the two opposite tetrahedral edges bridging two Zn<sup>2+</sup> cations, or a Zn<sup>2+</sup> and a Na<sup>+</sup> cation.

The hexagonal structure observed for many metal borohydrides can be attributed in part to an entropic term brought about by the vibrational amplitudes in BH<sub>4</sub> units and the shortening of B-H bonds from 1.22 to under 1.1 Å [196,197]. Mixed-cation borohydrides give rise to a fascinating family of crystal structures, and have many times exhibited promising results regarding hydrogen release and reversible hydrogen uptake.

#### 4.2. Stability of MBH

The most ionic and stable borohydrides have been studied since the 1940s, namely NaBH<sub>4</sub>, KBH<sub>4</sub>, RbBH<sub>4</sub>, and CsBH<sub>4</sub>; they are often stable in basic aqueous solution [165–169,198]. Closo-boranes are stable under neutral and acidic solutions. Being typically air- and moisture-sensitive compounds, their synthesis should be performed using Schlenk techniques or in the glove box, under inert (N<sub>2</sub>, Ar) atmosphere. Metal borohydrides are prone to adsorbing water, with which they react upon heating to release hydrogen. Some borohydrides of low electronegative elements are stable at RT, and even more so in the form of their hydrates. High electronegative metals forming metal borohydrides are highly reactive even below RT, and produce a highly exothermic reaction with water (some even explode upon contact with moisture). The layered structure of LiBH<sub>4</sub> is non-trivial and shows local distortion of the polymorphs, which defines their stability and plays a role in corresponding phase transitions [199]. Theoretical computations based on first-principles study shed new light on the stability of the family of possible borohydride intermediates from LiBH<sub>4</sub>, namely Li<sub>2</sub>B<sub>*n*</sub>H<sub>*n*</sub> ( $n = 5$ –12) [200].

Transition-metal borohydrides prepared by mechano-chemical methods are only stable when the ion itself is stable (d<sup>0</sup>, d<sup>5</sup> and d<sup>10</sup>), that is, when it has no electrons in the d-orbital, at half-occupation, or when the d-shell is completely occupied [201]. However, lowering

synthesis temperature to below  $-30\text{ }^{\circ}\text{C}$  and using ammonia as stabilizing ligand, stable  $\text{M}(\text{BH}_4)_2(\text{NH}_3)_6$  have been prepared in the case of  $\text{M} = \text{Cr}^{2+}$  ( $d^4$ ),  $\text{Fe}^{2+}$  ( $d^6$ ), and  $\text{Co}^{2+}$  ( $d^7$ ). These borohydrides are only stable in solution at low temperature, and they have not been isolated in pure, solid form, with a  $d^1$  exception to the rule coming from a molecular borohydride of  $\text{Ti}(\text{BH}_4)_3$ , which has limited stability below  $0\text{ }^{\circ}\text{C}$  [202]. Some borohydrides like  $\text{Zr}(\text{BH}_4)_4$  (sublimes at  $29\text{ }^{\circ}\text{C}$ ) form quality single-crystals by CVD when stored in a closed vessel, due to its molecular structure [203–210].

Bi- or tri-metallic borohydrides can usually be prepared by a mechano-chemical route; however, some diethyl ether  $\text{Et}_2\text{O}$  solvates have been prepared and are stable in solvated form, such as  $\text{NaMn}(\text{BH}_4)_3 \cdot 0.5 \text{Et}_2\text{O}$  [211]. Dimethyl sulfide  $\text{S}(\text{CH}_3)_2$  has recently been used as a weak-coordinating solvent which eases borohydride removal from the products, avoiding formation of ternary chlorides/bimetallic borohydrides. This strategy allowed for the synthesis and stabilization of some rare earth metal borohydrides  $\text{M}(\text{BH}_4)_3 \cdot \text{S}(\text{CH}_3)_2$ , where M is Y, La, Ce, or Gd [72,212–215]. Formation of ternary chlorides leads to incomplete reaction in mechanochemical synthesis; for instance, if  $\text{Zn}(\text{BH}_4)_2$  is targeted, a mixture of  $\text{NaBH}_4$  and  $\text{ZnCl}_2$  used as reagents can often lead to the formation of  $\text{Na}_2\text{ZnCl}_4$  by-product, which blocks  $\text{Zn}^{2+}$  cation availability for the metathesis reaction (Equation (40)).



Other approaches utilize bulky-cation-stabilized precursors like  $[\text{t}^n\text{Bu}_4\text{N}][\text{Y}(\text{BH}_4)_4]$  to produce less-stable borohydrides like  $\text{LiZn}_2(\text{BH}_4)_5$  [216,217].

#### 4.3. Multi-Cationic Borohydrides

The first reported mixed alkali metal borohydride,  $\text{LiK}(\text{BH}_4)_2$ , was observed to form when a mixture of  $\text{LiBH}_4$  and  $\text{KBH}_4$  was mixed and heated to  $125\text{ }^{\circ}\text{C}$  [218]. This intermediate compound was fully characterized, including by crystal structure determination:  $\text{Li}^+$  coordinates to four  $[\text{BH}_4]$  units, while  $\text{K}^+$  coordinates seven  $[\text{BH}_4]$  tetrahedral unit. The decomposition temperature of  $\text{LiK}(\text{BH}_4)_2$  is almost half of that of individual parent alkali-metal borohydrides.

Other mixed cation borohydrides are metastable, such as  $\text{NaK}(\text{BH}_4)_2$ ; upon cooling to RT, the mixed metal borohydride separates into the monomeric borohydrides within one day [219]. The certainty of its formation by heating the system  $\text{NaBH}_4\text{--KBH}_4$  was confirmed by an increase in the lattice parameter  $a$ , and the higher potassium content [220]. However, it was later proved that the mixed borohydride  $\text{NaK}(\text{BH}_4)_2$  is not stoichiometric, but a solid solution of approximate formula  $\text{Na}_p\text{K}_{1-p}\text{BH}_4$  ( $0 < p < 1$ ), and only stable at elevated temperatures ( $200\text{--}450\text{ }^{\circ}\text{C}$ ) [221].

Recently, a series of bimetallic borohydrides of alkali metal with alkaline earth,  $d$ - or  $f$ -block metals has been reported, containing the more electropositive alkali metal with a countercharge brought about by the complex anion [21–27,222,223].  $\text{K}_2\text{Mg}(\text{BH}_4)_4$  and  $\text{K}_3\text{Mg}(\text{BH}_4)_5$  have isolated  $[\text{Mg}(\text{BH}_4)_4]^{2-}$  tetrahedra serving as complex anions, while the metal alkali  $\text{K}^+$  ensures the charge neutrality of the framework [224].  $\text{M}^{\text{I}}\text{M}^{\text{II}}(\text{BH}_4)_3$  ( $\text{M}^{\text{I}} = \text{K, Rb, Cs}$ ;  $\text{M}^{\text{II}} = \text{Ca, Sr, Sm}$ ) of perovskite-type 3D-networks have the divalent metal in octahedral coordination via  $\kappa^2$ -bridging  $\text{BH}_4$  units, with the alkali metal cuboctahedrally surrounded by twelve  $\text{BH}_4$  units [185,225–227]. This perovskite-type structure is best stabilized by alkali-earth metals of smaller radii ( $\text{Ca}^{2+}$ ,  $1.14\text{ \AA}$ ) than heavier analogues ( $\text{Sr}^{2+}$ ,  $1.32\text{ \AA}$ ), a trend which is more apparent during heating [21–27,225,226].

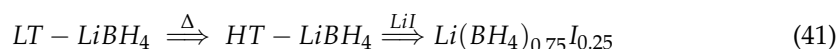
Given the size-match between ammonium cation  $\text{NH}_4^+$  ( $1.48\text{ \AA}$ ) and alkaline metals ionic radii  $\text{K}^+$  ( $1.38\text{ \AA}$ ) and  $\text{Rb}$  ( $1.52\text{ \AA}$ ), a family of bi-cationic borohydrides  $(\text{NH}_4)_x\text{M}(\text{BH}_4)_y$  was produced when  $\text{NH}_4\text{BH}_4$  was mixed with  $\text{M}(\text{BH}_4)_p$  ( $\text{M} = \text{Li, Na, Mg, Al, Y, Mn, Gd}$ ). These novel borohydrides exhibit high energy densities of up to 24.5 wt.% hydrogen [222].

#### 4.4. Anion Substitution of MBH: From Light to Heavy Halides and Pseudo-Halide Substitution

Substitution of  $\text{BH}_4^-$  was reported for  $\text{LiBH}_4\text{--LiCl}$  [228], with this mixture actually forming a partial solid solution of anticipated formula  $\text{Li}(\text{BH}_4)_{1-p}\text{Cl}_p$  ( $0 < p < 1$ ), an as-

pect which hindered further purification of the borohydride. The superionic HT-LiBH<sub>4</sub> is formed at ~110 °C (108 °C), but this phase transition could occur at even lower temperatures possibly due to the formation of Li(BH<sub>4</sub>)<sub>1-p</sub>Cl<sub>p</sub> during ball-milling [89,228]. Easier substitution has been confirmed for halide anions (F<sup>-</sup>, Cl<sup>-</sup>, Br<sup>-</sup>, I<sup>-</sup>) and it allowed for fine-tuning of the unit cell parameters and eventually to physical properties related to the crystallographic system and strain [229]. The shrinkage or enlargement of the unit cell volume mirrors the size of the anions: F<sup>-</sup> (1.33 Å) < Cl<sup>-</sup> (1.81 Å) < Br<sup>-</sup> (1.96 Å) < BH<sub>4</sub><sup>-</sup> (2.05 Å) < I<sup>-</sup> (2.20 Å) [153,230].

Depending on the crystallographic system and local environment, some polymorphs undergo anion substitution more easily than others, as shown by HT-LiBH<sub>4</sub> and β-Mg(BH<sub>4</sub>)<sub>2</sub> [231,232]. If both components of the system MBH<sub>4</sub>-MX (M-alkali metal, X- halide) are isostructural, anion substitution may occur both ways, such that two solid solutions can form: LiBH<sub>4</sub>-LiBr, LiBH<sub>4</sub>-LiI, or NaBH<sub>4</sub>-NaCl. While heavier halides (Br<sup>-</sup>, I<sup>-</sup>) stabilize the hydride, hindering hydrogen release at lower temperature, they lower the energy of hydrogen uptake during rehydrogenation [233–236]. While o-LiBH<sub>4</sub> (orthorhombic) shows no conduction at RT, its HT-polymorph, HT-LiBH<sub>4</sub> (hexagonal, stable at *t* > 110 °C), exhibits fast lithium-ion conductivity that is enhanced upon iodide anion I<sup>-</sup> substitution of 25% with respect to starting BH<sub>4</sub><sup>-</sup> units, in Li[BH<sub>4</sub>]<sub>0.75</sub>I<sub>0.25</sub> (Equation (41)) [237,238]. J. Rude et al. showed through usage of synchrotron radiation powder X-ray diffraction (SR-PXD) and attenuated total reflectance infrared spectroscopy (ATR-IR) that two solid solutions of hexagonal structure (just like HT-LiBH<sub>4</sub> and β-LiI) form in the system LiBH<sub>4</sub>-LiI, which combine into one upon heating. The solid solutions of composition Li(BH<sub>4</sub>)<sub>1-p</sub>I<sub>p</sub> (0 < *p* < 0.62) have been found to be stable over a 300-degree temperature range, and after four hydrogen release/uptake cycles they retained 68% of expected hydrogen capacity, in contrast to only 25% retained by pristine LiBH<sub>4</sub>.



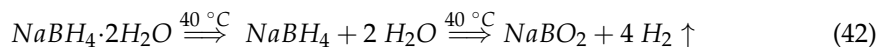
Anion substitution has also been expanded to include amide -NH<sub>2</sub>- anions, and these boron–nitrogen species are promising from a hydrogen storage viewpoint and for properties of fast ion conductivities, as seen above in the case of halide substitution.

#### 4.5. Stabilization of M(BH<sub>4</sub>)<sub>x</sub> by Coordination of Neutral Molecules (NH<sub>3</sub>, N<sub>2</sub>H<sub>4</sub>, H<sub>2</sub>O, (CH<sub>3</sub>)<sub>2</sub>S)

While exhibiting a rich and fascinating structural diversity akin to that of metal organic frameworks (MOF), the metal borohydrides do often run into stability problems: they can be obtained solely by mechano-chemical synthesis, are stable only at low temperature, are only stable in solution or as solid solutions. These shortcomings can be overcome by neutral molecule coordination, enhancing their stability. Among these, N-containing ligands are particularly interesting because they can bind hydrogen, and could interact with the Lewis acidic boron through a frustrated Lewis pair (FLP)-type interaction: B-H<sup>γ</sup>...<sup>γ</sup>+H-N. In fact, the shortest distance of 1.85 Å has been reported for Y(BH<sub>4</sub>)<sub>3</sub>·7NH<sub>3</sub>, between the complex cation [Y(NH<sub>3</sub>)<sub>7</sub>]<sup>3+</sup> and the borohydride anion BH<sub>4</sub><sup>-</sup>. These interactions facilitate heterolytic E-H bond cleavage (E = B, N) to produce molecular H<sub>2</sub>, thus becoming attractive options for hydrogenation studies. Moreover, this inherent instability caused by H...H interactions gives rise to structural flexibility and variability. The solvent should behave as a Lewis base, containing highly electronegative atoms: N, O, S. In this regard, the most studied ligands are N-based ligands, such as ammonia NH<sub>3</sub>, hydrazine H<sub>2</sub>N-NH<sub>2</sub>, and ammonia–borane NH<sub>3</sub>BH<sub>3</sub>. S-based ligands (such as S(CH<sub>3</sub>)<sub>2</sub>, dimethyl sulfide) are more desirable than O-based ones (diethyl ether (C<sub>2</sub>H<sub>5</sub>)<sub>2</sub>O, tetrahydrofuran C<sub>4</sub>H<sub>8</sub>O, and water H<sub>2</sub>O), because M-S bonds are longer than M-O bonds and thus the S-ligand could potentially be easier to remove.

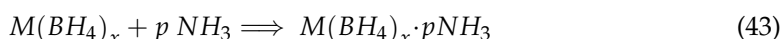
A dihydrate adduct has been isolated in the case of NaBH<sub>4</sub>·2H<sub>2</sub>O crystalline hydrate, where Na<sup>+</sup> has octahedral coordination to four [BH<sub>4</sub>]<sup>-</sup> units and two H<sub>2</sub>O molecules bridging two Na<sup>+</sup> (space group: orthorhombic, *Pbca*) [153,239]. NaBH<sub>4</sub>·2H<sub>2</sub>O loses the two wa-

ter molecules upon mild heating at 40 °C, and then slowly starts to release hydrogen (Equation (42)).



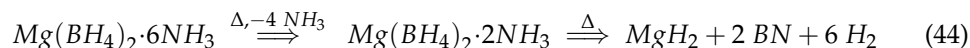
Monohydrates of lithium and calcium borohydrides have also been reported:  $\text{LiBH}_4 \cdot \text{H}_2\text{O}$  and  $\text{Ca}(\text{BH}_4)_2 \cdot \text{H}_2\text{O}$  [240].

A large class of ammine single-metal borohydrides  $\text{M}(\text{BH}_4)_x \cdot p\text{NH}_3$  and ammine bimetallic borohydrides  $\text{M}^{\text{I}}\text{M}^{\text{II}}(\text{BH}_4)_3 \cdot p\text{NH}_3$  have been synthesized and structurally characterized, containing variable solvent molecules, in the range  $p = 1\text{--}8$  (Equation (43)) [202,241,242].



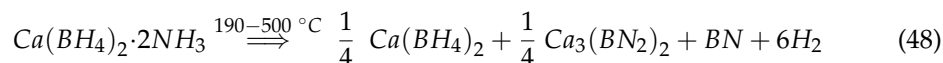
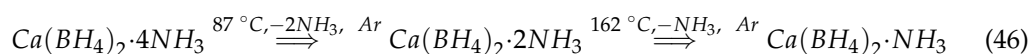
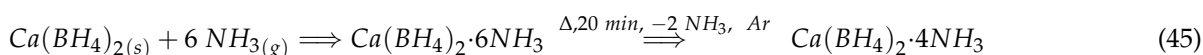
For instance,  $\text{LiBH}_4 \cdot \text{NH}_3$ , the only alkali metal borohydride stable at RT as an ammine complex [243],  $\text{Mg}(\text{BH}_4)_2 \cdot p\text{NH}_3$  with  $p = 1, 2, 3$ , and 6 [244–246], as well as octa-ammine complex  $\text{Zr}(\text{BH}_4)_2 \cdot 8\text{NH}_3$  [247], have been prepared and studied. For instance, the di-solvate  $\text{Mg}(\text{BH}_4)_2 \cdot 2\text{NH}_3$  can be written in its molecular formula  $[\text{Mg}(\text{BH}_4)_2(\text{NH}_3)_2]$ , with  $\text{Mg}^{2+}$  coordinating in a tetrahedral fashion two  $\text{BH}_4^-$  units and two ammonia molecules [245]. Moreover, whereas only ions with electron configuration  $d^0$ ,  $d^5$ , and  $d^{10}$  (with very few exceptions) could be obtained via the ball-milling technique, various other TM borohydride configurations (TM = transition metal) could be obtained as adducts due to enhanced stability brought about by  $\text{NH}_3$  coordination:  $d^1$  ( $\text{Ti}^{2+}$ ),  $d^2$  ( $\text{V}^{3+}$ ),  $d^6$  ( $\text{Fe}^{2+}$ ), or  $d^7$  ( $\text{Co}^{2+}$ ) [202].

Depending on the number of coordinating ligands, the thermal decomposition of ammine metal borohydrides can follow different pathways, as shown in Equation (44) [245].



The hexaammine complex  $\text{Mg}(\text{BH}_4)_2 \cdot 6\text{NH}_3$  produces by thermal decomposition  $\text{Mg}(\text{BH}_4)_2 \cdot 2\text{NH}_3$ , which upon further heating releases irreversibly  $\text{H}_2$  and produces traces of BN as the sole crystalline phase. Rehydrogenation attempts at 250 °C for 60 h led to no amounts of  $\text{Mg}(\text{BH}_4)_2$  [248].

A similar hexaammine complex  $\text{Ca}(\text{BH}_4)_2 \cdot 6\text{NH}_3$  was produced by solid–gas reaction between  $\text{Ca}(\text{BH}_4)_2$  and  $\text{NH}_3(\text{g})$  [249], and it is different from the solution synthesis used to prepare  $\text{Mg}(\text{BH}_4)_2 \cdot 6\text{NH}_3$  (Equations (45)–(48)) [245].



Reactions (45)–(47) were performed under Ar flow, when  $\text{NH}_3$  was released. Running the reaction in a closed vessel, no  $\text{NH}_3$  evolution was detected and instead a sudden dehydrogenation reaction with onset at 190 °C took place (Equation (48)). The final dehydrogenated species was assigned based on  $^{11}\text{B}$  NMR spectra, consistent with an overall hydrogen storage capacity of  $\text{Ca}(\text{BH}_4)_2 \cdot 2\text{NH}_3$  of 12.3 wt.%. This diammoniate system was not reversible, as no rehydrogenation occurred during attempts at 50-bar  $\text{H}_2$  and 20–300 °C [249].

Coordination of  $\text{H}_2\text{N-NH}_2$  (hydrazine) to metal borohydrides produces  $\text{M}(\text{BH}_4)_x \cdot n\text{N}_2\text{H}_4$  ( $\text{M} = \text{Li}, \text{Na}, \text{Mg}$ ), out of which the  $\text{LiBH}_4 \cdot \text{N}_2\text{H}_4$  shows a remarkably high 13 wt.%  $\text{H}_2$  released at 140 °C when using Fe-B catalyst [250,251].

$\text{Ca}(\text{BH}_4)_2$  produces hydrazinates of composition  $\text{Ca}(\text{BH}_4)_2 \cdot n\text{N}_2\text{H}_4$  ( $n = 1, 4/3, 2, 3$ ) that store 8.8 wt.%  $\text{H}_2$  ( $n = 2$ ), 9.2 wt.%  $\text{H}_2$  ( $n = 1$ ) and 10.8 wt.%  $\text{H}_2$  ( $n = 4/3$ ) (Figure 10).

Z. Li et al. propose a dehydrogenation pathway involving H( $\delta^+$ )...H( $\delta^-$ ) interaction [249] and NH<sub>3</sub>-mediated mechanisms [252]. The dehydrogenation temperature was reduced from 240 °C to 140 °C by utilizing an Fe-based catalyst (2–5 mol% FeCl<sub>3</sub>); however, the Fe<sup>3+</sup> seemed to partially catalyze decomposition of hydrazine as well, as NH<sub>3</sub> was found among the gaseous products (Equation (49)).

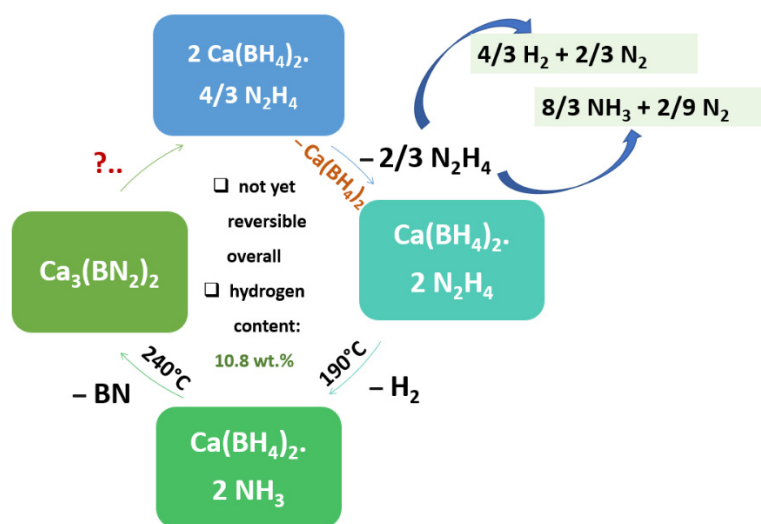
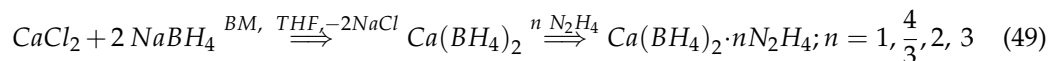
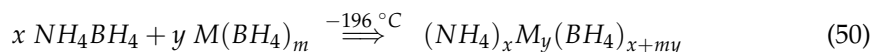


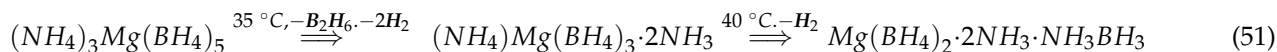
**Figure 10.** Overview of dehydrogenation pathways in Ca(BH<sub>4</sub>)<sub>2</sub>·4/3N<sub>2</sub>H<sub>4</sub> (10.8 wt.% H<sub>2</sub>); the system is not yet reversible [252].

Hydrazine itself (H<sub>2</sub>N-NH<sub>2</sub>) has two competitive decomposition pathways, leading to either (2 H<sub>2</sub> + N<sub>2</sub>), or (4/3 NH<sub>3</sub> + 1/3 N<sub>2</sub>); at least one side-reaction thus leads to enhanced hydrogen storage capacity (Figure 10). However, this system has not achieved reversibility yet and research is due to regenerate Ca(BH<sub>4</sub>)<sub>2</sub> from spent Ca<sub>3</sub>(BN<sub>2</sub>)<sub>2</sub>.

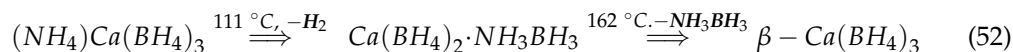
Ammonium-substituted MBH were also produced via the cryo-mechanochemical route for a series of alkali metal (Li<sup>+</sup>, Na<sup>+</sup>), alkali-earth metals (Mg<sup>2+</sup>, Ca<sup>2+</sup>, Sr<sup>2+</sup>), and TM- and RE-borohydrides (Mn<sup>2+</sup>, Y<sup>3+</sup>, La<sup>3+</sup>, Gd<sup>3+</sup>) (Equation (50)) [222].



These ammonium borohydrides show decomposition in the temperature range 30–60 °C and usually release toxic diborane B<sub>2</sub>H<sub>6</sub>, along with dihydrogen H<sub>2</sub> (Equation (51)).



However, not all ammino-stabilized ammonium borohydrides release diborane upon heating; (NH<sub>4</sub>)Ca(BH<sub>4</sub>)<sub>3</sub> decomposes to release an ammonia–borane adduct Ca(BH<sub>4</sub>)<sub>2</sub>·NH<sub>3</sub>BH<sub>3</sub> and hydrogen in the first step, producing β-Ca(BH<sub>4</sub>)<sub>2</sub> upon further heating and loss of a molecule of ammonia borane NH<sub>3</sub>BH<sub>3</sub>. Interestingly, H<sub>2</sub> is only released during the first, lower-temperature decomposition step; (NH<sub>4</sub>)Li(BH<sub>4</sub>)<sub>2</sub> follows a similar decomposition pathway to release hydrogen (Equation (52)) [222].



## 5. Physical and Chemical Properties of M(BH<sub>4</sub>)<sub>x</sub>

Ionic and covalent borohydrides will intrinsically have different properties. For a rough estimation, Pauling's empirical rule and Hannay–Smith formulae have been

employed to estimate the ionicity percentage in known and reported borohydrides. As the electropositivity of the metal increases, the bonding character is more ionic, such that the most ionic borohydrides are those of alkali metal [253]. While the main properties of metal borohydrides have been polarized by their high and potentially reversible hydrogen content, other studies have expanded their field of interest, including optical, magnetic, and semiconductor materials.

### 5.1. Electrochemistry of Metal Hydrides and $M(\text{BH}_4)_x$ : Electrodes, Electrolytes ( $\text{Li}^+$ , $\text{Mg}^{2+}$ , $\text{Ca}^{2+}$ ), Complex Metal Hydrides

Due to their strong reducing character, metal borohydrides have recently been investigated as electrolytes in liquid and solid form, showing conductivities  $\sigma$  higher than  $10^{-4}$  S/cm [21–27,254,255]. Solid-state electrolyte research reached new heights after the discovery that *o*-LiBH<sub>4</sub> (*Prma*, orthorhombic, ionic conductivity  $\sigma_{\text{Li}^+} = 10^{-8}$  S/cm) transforms at 108–110 °C into another high temperature polymorph *h*-LiBH<sub>4</sub> (*P6<sub>3</sub>mc*, hexagonal,  $\sigma_{\text{Li}^+} = 10^{-3}$  at 120 °C, five orders of magnitude higher than that of *o*-LiBH<sub>4</sub>) (Table 2) [256–261]. As shown previously, several strategies have been employed to obtain RT-stable borohydrides with comparable ion conductivity: halide or halide-alike substitution in the complex anion ( $\text{Li}_4(\text{BH}_4)_3\text{I}$ ,  $\text{Li}_2(\text{BH}_4)(\text{NH}_2)$ ), nanoconfinement in mesoporous silica of LiBH<sub>4</sub> or  $\text{Li}_4(\text{BH}_4)_3\text{I}$ , or formation of rare-earth (RE)-containing bimetallic borohydrides  $\text{Li}(\text{RE})(\text{BH}_4)_3\text{Cl}$  (RE = La, Ce, etc.) [262,263]. Ionic conductivity has been expanded by utilizing neutral ligands or larger closo-borate salts which prove to ease the cation migration and represent the state-of-the-art in research on borohydride materials as electrolytes.

**Table 2.** Ion conductivity  $\sigma_{M^{n+}}$  ( $\frac{\text{S}}{\text{cm}}$ ) of representative alkali and alkali-earth metal borohydrides.

Compound	Ion Conductivity $\sigma_{M^{n+}}$ ( $\frac{\text{S}}{\text{cm}}$ )	Experimental Conditions/Observations	Reference
LiBH <sub>4</sub>	$2 \cdot 10^{-3}$	107 °C	[261]
LiBH <sub>4</sub> ·H <sub>2</sub> O	$4.89 \cdot 10^{-4}$	t = 45 °C	[264]
LiBH <sub>4</sub> ·x NH <sub>3</sub>	$2.21 \cdot 10^{-3}$	$0 < x < 2$ ; $\sigma = \sigma(x)$ ; $\sigma_{\text{max}}$ @40 °C	[265,266]
LiBH <sub>4</sub> ·x NH <sub>3</sub> @Li <sub>2</sub> O	$5.4 \cdot 10^{-4}$	$0.67 < x < 0.8$ ; 20 °C; max for 78 wt.% Li <sub>2</sub> O	[267]
LiBH <sub>4</sub> ·x NH <sub>3</sub> BH <sub>3</sub>	$1.47 \cdot 10^{-5}$ – $4.04 \cdot 10^{-4}$	$\frac{1}{2} < x < 1$ ; highest for x = 1	[268]
LiBH <sub>4</sub> ·NH <sub>3</sub> BH <sub>3</sub>	$10^{-1}$	t = 55 °C; record value for Li <sup>+</sup>	[263]
Li <sub>2</sub> B <sub>12</sub> H <sub>12</sub>	$10^{-1}$	110 °C	[257]
Li <sub>2</sub> B <sub>10</sub> H <sub>10</sub>	$3 \cdot 10^{-2}$	81 °C	[258]
Na <sub>2</sub> B <sub>10</sub> H <sub>10</sub>	$3 \cdot 10^{-2}$	RT	[258]
Na <sub>2</sub> B <sub>12</sub> H <sub>12</sub>	$10^{-1}$	256 °C	[259]
LiBH <sub>4</sub> -nano	$10^{-3}$	RT; nanoconfined electrolyte	[260]
Mg(BH <sub>4</sub> ) <sub>2</sub>	$<10^{-12}$	t = 30 °C	[269]
Mg(BH <sub>4</sub> )(NH <sub>2</sub> )	$10^{-6}$	t = 150 °C	[270]
Mg <sub>3</sub> (BH <sub>4</sub> ) <sub>4</sub> (NH <sub>2</sub> ) <sub>2</sub>	$4.1 \cdot 10^{-5}$	100 °C	[271]
Mg(BH <sub>4</sub> ) <sub>2</sub> ·en en = NH <sub>2</sub> CH <sub>2</sub> CH <sub>2</sub> NH <sub>2</sub>	$6 \cdot 10^{-5}$	70 °C, crucial role of [BH <sub>4</sub> <sup>−</sup> ], Mg(en) <sub>2</sub> X <sub>2</sub> showed $\sigma$ very low	[268,272]
Mg(BH <sub>4</sub> ) <sub>2</sub> ·1/2dy dy = diglyme	$2 \cdot 10^{-5}$	80 °C; chelating of flexible dy ligand	[273]
Mg(BH <sub>4</sub> ) <sub>2</sub> ·x NH <sub>3</sub>	$3.3 \cdot 10^{-4}$	x = 1,2,3 6; t = 80 °C; pas-de-deux mechanism proposed	[274]
Mg(BH <sub>4</sub> ) <sub>2</sub> ·1.6NH <sub>3</sub>	$2.2 \cdot 10^{-3}$	t = 55 °C	[275]

Most conductivity studies have been carried out regarding  $\text{LiBH}_4$  and  $\text{Mg}(\text{BH}_4)_2$  complexes, especially on neutral ligand-stabilized solvates of these borohydrides. It becomes apparent that ionic radii increase must be an obstacle in front of ion migration, as  $\text{Ca}^{2+}$  in  $\text{Ca}(\text{BH}_4)_2$  shows slow conductivity ( $r_{\text{Li}^+} = 0.9 \text{ \AA}$ ;  $r_{\text{Mg}^{2+}} = 0.86 \text{ \AA}$ ;  $r_{\text{Ca}^{2+}} = 1.14 \text{ \AA}$ ). It seems that  $\sim 26\%$  increase in ionic radii from  $\text{Li}^+$  to  $\text{Ca}^{2+}$  would inhibit ion migration in the framework. The interaction charge framework is important and increases with the charge of the cation, but it is not essential for conductivity. Although they have the same charge (+2) of  $\text{Mg}^{2+}$  and  $\text{Ca}^{2+}$ , respective borohydrides are different in terms of conductivity, with solvated  $\text{Mg}(\text{BH}_4)_2$  showing real promise as an electrolyte candidate with an oxidation stability of 1.2 V (by CV, cyclic voltammetry) (Table 2) [272,275,276]. Recent trends in improving ionic conductivity have explored complexes with weaker coordinating ligands/counteranions, as is the case for  $\text{CaB}_{12}\text{H}_{12}$  [277]. Despite their low electrochemical stability, borohydrides give rise to rich speciation: nido- (typical tetrahydroborate  $\text{BH}_4^-$ ), planar- ( $\text{B}_6\text{H}_6^{6-}$ ), and closo- ( $\text{B}_{10}\text{H}_{10}^{2-}$ ;  $\text{B}_{12}\text{H}_{12}^{2-}$ ), making their alkali ( $\text{Li}^+$ ,  $\text{Na}^+$ ,  $\text{K}^+$ ) and alkali-earth ( $\text{Mg}^{2+}$ ,  $\text{Ca}^{2+}$ ) salts particularly appealing in ion conduction applications [278–281]. The ionic conductivity trend correlates well with the size of the hydroborate species (Figure 11).

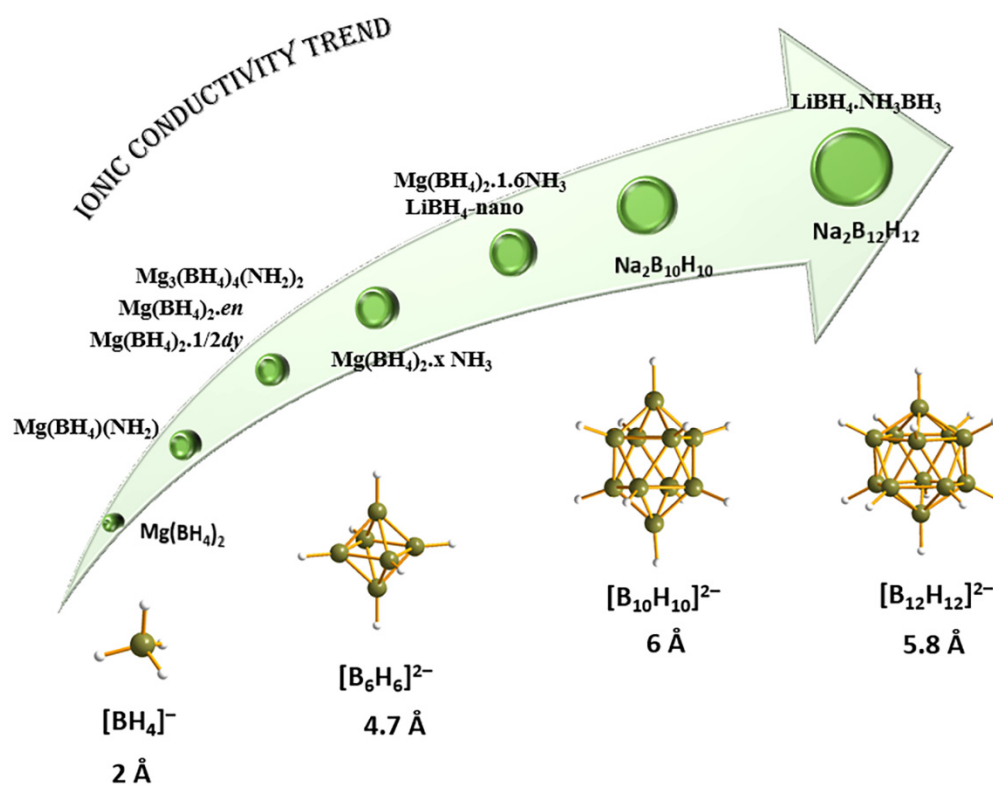


**Figure 11.** Boron–hydrogen speciation and influence on ionic conductivity of corresponding alkali and alkali-earth salts.

The closo-borates are currently under active research due to their rapid ion conduction, due in part to the open structure with channels for ionic conduction [281]. Both  $\text{Li}_2\text{B}_{12}\text{H}_{12}$  and  $\text{Na}_2\text{B}_{12}\text{H}_{12}$  exhibit high ionic conductivities of the order of magnitude of  $10^{-1} \text{ S cm}^{-1}$  which are beneficial for Na-battery electrolytes [257–259]. The superionicity found in these closo-salts could also originate from the high rotational mobility of the large  $\text{B}_{12}\text{H}_{12}^{2-}$  anion [259].

## 5.2. Optical and Magnetic Properties

As expected for RE (RE = rare earth) complexes,  $\text{Eu}(\text{BH}_4)_2 \cdot 2\text{THF}$  has blue luminescence and an impressive quantum yield of  $\sim 75\%$ , due to charge separation of  $\text{Eu}^{2+}$  centers by borohydride  $\text{BH}_4^-$  anions, which avoid quenching. Similar favorable lumines-

cent properties were found in  $Y(BH_4)_2 \cdot 2THF$  [282]. The ionic bond  $Eu^{2+}-BH_4^-$  allows  $d \rightarrow f$  emission in the blue region of the spectrum. A series of mixed metal borohydrides of perovskite-type structure, such as  $KYb(BH_4)_3$  and  $CsEu(BH_4)_3$ , have also been investigated, with a red shift in the latter compared to parent  $Eu(BH_4)_2 \cdot 2THF$  [225,226]. Avoidance of quenching has been proven by addition of a 5%  $Eu^{2+}$  in  $CsEu(BH_4)_3$ , which showed similar luminescence properties regardless of  $[Eu^{2+}]$  doping concentration [225,226].

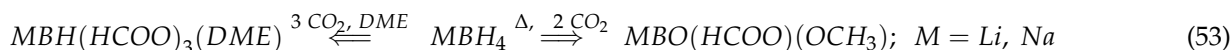
### 5.3. $M(BH_4)_x$ as Semi- and Superconductors

Borohydrides of perovskite structure could be fine-tuned for photovoltaics, as their typical band-gap ( $>5$  eV) could be lowered to  $\sim 1.5$  eV at RT in the particular case of  $CsPb(BH_4)_3$ , which has semiconductor behavior. The reasoning for this seems to lie in the partial covalent bonding in the  $Pb(BH_4)_3$  framework, supported by the p(Pb) states present in the conduction band edge [225].

Superconductivity has been achieved for metal hydrides at very high pressures, exceeding 100 GPa, but providing a solid proof-of-concept. While the lanthanum-based borohydride  $LaBH_8$  is not yet confirmed experimentally, computations predict it to be a superconductor and stable at a considerably lower pressure of about 40 GPa [283–285]. However, recent reports (2021) suggest that under pressure (12 GPa) a ternary alkali borohydride  $KB_2H_8$  shows phonon-mediated high-temperature superconductivity [226].

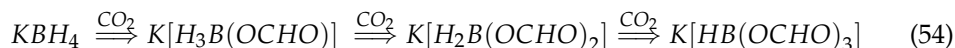
### 5.4. $CO_2$ Capture

Reaction of MBH with  $CO_2(g)$  can be used for carbon dioxide sequestration/removal, or to produce derivatives like formates (Equation (53)) [286,287].

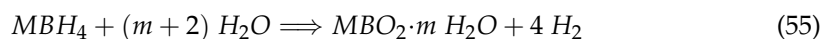


The reaction with  $CO_2$  can follow different pathways, depending on temperature and solvent used (DME, dimethoxyethane), which adds to the growing interest in  $CO_2$  capture globally [288,289].  $LiBH_4$  and  $NaBH_4$  reaction with  $CO_2$  was also monitored in non-catalytic, solvent-free conditions, when IRGA (infrared gas analysis), FTIR,  $^{11}B$  NMR, and  $^{13}C$  NMR confirmed the presence, respectively, of borate, formate, and methoxy species [290].

Reaction of  $KBH_4$  under solvent-free ball-milling with solid  $CO_2$  leads to a formyl-hydroborate species  $K[H_xB(OCHO)_{4-x}]$  ( $x = 1-3$ ) [291]. The synthesis of this interesting substituted borate species follows a three-step, consecutive nucleophilic attachment of the borohydride  $H^-$  on the electron-deficient carbon of  $CO_2$  molecules (Equation (54)).



While reaction of MBH with  $H_2O$  usually follows the pattern seen in Equations (42) and (55), variations including running the reactions under small  $CO_2$  amounts have proven fruitful in synthesizing novel substituted metal borohydrides [292].



Contrary to the  $Li^+$  and  $Na^+$  counterparts,  $KBH_4$  borohydride produces under  $CO_2$ -promoted hydrolysis a metal complex still retaining the  $[BH_4^-]$  moiety:  $K_9[B_4O_5(OH)_4]_3(CO_3)(BH_4) \cdot 7H_2O$ . This complex was investigated by XRD, DSC, TGA, Raman, and IR spectroscopies and fully characterized by solving its single crystal structure, showing a hexagonal crystal structure belonging to the P-62c space group, and high hydrogen gravimetric content. The reaction proposed by Filinchuk et al. is complex and leads to potassium carbonate as by-product (Equation (56)), along with a large amount of hydrogen, so that it can be regarded as having a double utility: removal of  $CO_2$  from car exhaust gases, and efficient conversion of  $CO_2$  to a clean fuel,  $H_2$  [286]:



The porous polymorph of  $\gamma$ -Mg(BH<sub>4</sub>)<sub>2</sub> adsorbs CO<sub>2</sub> under very mild, near-RT conditions and also yields formate and methoxy products, proving suitable for CO<sub>2</sub> sequestration. The highest CO<sub>2</sub> uptake of 12 mol/kg was recorded after 7 days of exposure at 1-bar CO<sub>2</sub> and 30 °C, and was attributed to the very porous nature of magnesium borohydride polymorph, which features a very large specific surface area [293].

## 6. M(BH<sub>4</sub>)<sub>x</sub> as Hydrogen Storage Materials

### 6.1. Thermodynamic Properties of MBH

Thermal decomposition of metal borohydrides is directly related to the electronegativity of the M metal, which roughly displays a clear decrease in decomposition temperature with the increase in M electronegativity [294].

Pauling hypothesized that the energy E(A-B) of a heteroatomic bond (A ≠ B) relates to the difference in electron affinities of A and B by Equation (57), where the second term can be approximated in the case of compounds MR<sub>n</sub> (R-anion) by  $-\Delta H_f/n$ .

$$\chi_A - \chi_B \propto \sqrt{E_{A-B} - \frac{E_{A-A} + E_{B-B}}{2}} \propto \sqrt{\frac{-\Delta H_f}{n}} \quad (57)$$

The decomposition temperature ( $T_d$ , K, and  $t_d$ , °C;  $T_d[\text{K}] = t_d(^\circ\text{C}) + 273.15$ ) can be correlated to the Pauling electronegativity of the cation [295–299]. The empirical formula (Equation (58)) used to determine  $T_d$  was found to be [300]:

$$T_d[\text{K}] = 175.914(\chi_P - 3.11)^2 \text{ or } t_d(^\circ\text{C}) = 175.914 \chi_P^2 - 1094.2 \chi_P + 1428.3 \quad (58)$$

The van't Hoff equation adapted for decomposition of metal borohydrides (Equation (58)) contains the factor 3.11, which can be regarded as the electron attractive coefficient of borohydride anion [BH<sub>4</sub>]<sup>−</sup>, while 175.914 is a coefficient containing entropy values of decomposition (oversimplified as being constant for all compounds, in a first approximation) (Figure 12).

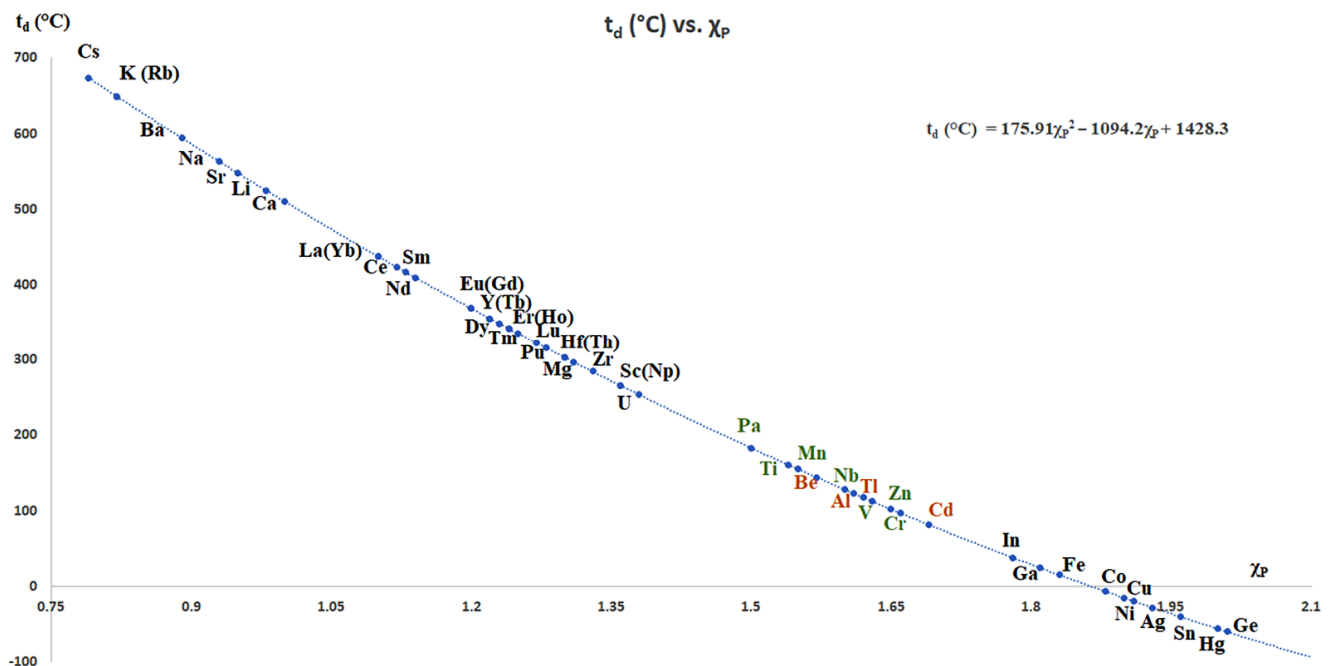


**Figure 12.** Decomposition temperature of M(BH<sub>4</sub>)<sub>x</sub> dependent on cation (\*Pauling) electronegativity following a van't Hoff equation plot. In green are highlighted elements forming borohydrides with predicted decomposition temperature 50–150 °C, suitable for mobile application. Very toxic elements are in red [295–299].

First-principles calculations led to the estimation of formation enthalpies for metal borohydrides, with an absolute error of only 10.4 kJ/mol (Equation (33)) [295–299].

$$\Delta H_{\text{boro}} = 248.7 \chi_P - 390.8 \quad ; \quad T_d = 175.914(\chi_P - 3.11)^2 \quad (59)$$

A representative plot for metal borohydrides presented in Figure 2 is given in Figure 13, where a linear correlation between enthalpy and electronegativity  $\chi_P$  is confirmed.

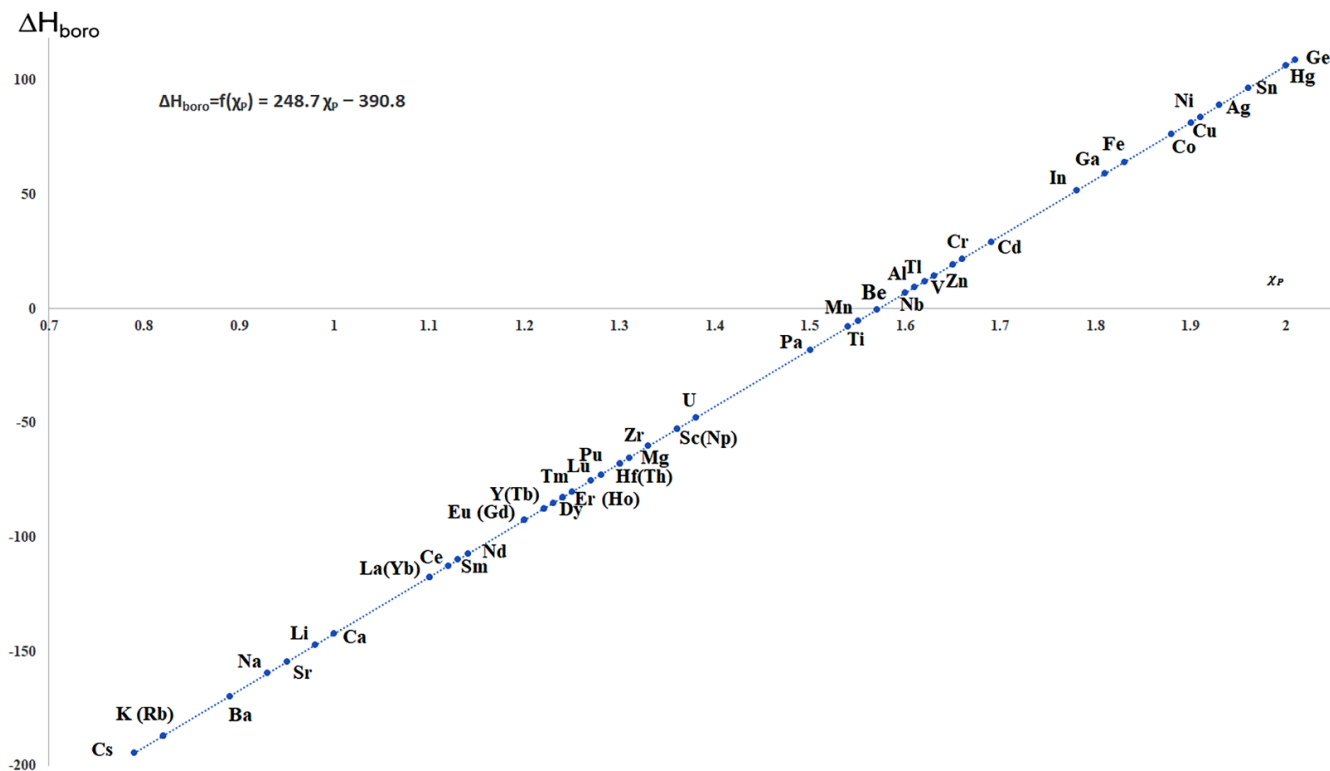


**Figure 13.** Formation enthalpies  $\Delta H_f^0$  ( $\Delta H_{\text{boro}}$ , kJ/mol  $\text{BH}_4$ ) for metal borohydrides that are either reported or believed to exist (Figure 2).

Pauling electronegativities are preferred because when inferring Mulliken scaling ( $\chi_M$ ), the values are fitted for  $\Delta H_{\text{boro}}$  with a higher error (13.1 kJ/mol) and moreover the enthalpies for  $\text{Cu}^+$  and  $\text{Zn}^{2+}$  borohydrides are almost the same (Mulliken electronegativities: 4.48 eV and 4.45 eV, respectively), which cannot explain the differences observed experimentally between the two [294,301,302]. Based on Equation (59), it can be inferred that for metal borohydrides having  $\Delta H_f^0 \geq 0$ , that is for  $\chi_P \geq 1.57$ , the borohydride would have an endothermic formation enthalpy and could be considered unstable (Table 3). For selected  $\text{M}(\text{BH}_4)_x$  the free Gibbs energy  $\Delta G$  has also been computed. Group I and II metal borohydrides have been the most investigated regarding thermodynamic data, and the following suggestive formulae were found (in kJ/mol formula unit);  $\Delta G_{\text{LiBH}_4} = -222466.273 + 751.660356 T - 124.7 T \ln T$  [296],  $\Delta G_{\text{NaBH}_4} = -217735 + 693 T - 119.233 T \ln T$  [296],  $\Delta G_{\text{KfBH}_4} = 16926 - 21.756 T$  [297],  $\Delta G_{\text{KBH}_4} = 19176 - 21.841 T$  [296],  $\Delta G_{\alpha\text{-Mg}(\text{BH}_4)_2} = -222624.9 + 158.46145 T - 35.22138 T \ln T - 0.035975 T^2$  [298],  $\Delta G_{\beta\text{-Mg}(\text{BH}_4)_2} = 12954.437 - 26.4266 T$  [298].

**Table 3.** Thermodynamic parameters characteristic to metal borohydrides:  $\Delta H_{boro}$ ,  $T_d$ , and  $t_d$ . In brown are shown elements with  $\chi_P \geq 1.57$  ( $\Delta H > 0$ , unstable); decomposition temperature is given both as  $T_d$  (K) and  $t_d$  ( $^{\circ}\text{C}$ ), for easier evaluation.

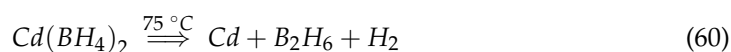
Metal (M)	$\text{M}(\text{BH}_4)_x$	$\chi_P$	$T_d = 175.914(\chi_P - 3.11)^2$ [K] $t_d$ [ $^{\circ}\text{C}$ ]		$\Delta H_{boro} = 248.7 \chi_P - 390.8$ [ $\frac{\text{kJ}}{\text{mol BH}_4}$ ]	Reference
Li	LiBH <sub>4</sub>	0.98	798.1	524.95	−147.074	[30–38,196,199]
Na	NaBH <sub>4</sub>	0.93	836.01	562.86	−159.509	[165,168,169]
K	KBH <sub>4</sub>	0.82	922.51	649.36	−186.866	[165,166,168]
Cu	CuBH <sub>4</sub>	1.9	257.56	−15.59	81.73	[113] forms at 253 K, dec. at 261–273 K
Rb	RbBH <sub>4</sub>	0.82	922.51	649.36	−186.866	[167]
Ag	AgBH <sub>4</sub>	1.93	244.94	−28.21	89.191	[114]; forms at 193 K, dec. at 243 K
Cs	CsBH <sub>4</sub>	0.79	946.84	673.69	−194.327	[165]
Au <sup>I</sup>	AuBH <sub>4</sub>	2.54	57.15	−216	240.898	[115] * unstable
Au <sup>III</sup>	Au(BH <sub>4</sub> ) <sub>3</sub>	2.54	57.15	−216	240.898	[116]
Be	Be(BH <sub>4</sub> ) <sub>2</sub>	1.57	417.2	144.05	−0.341	[170]
Mg	Mg(BH <sub>4</sub> ) <sub>2</sub>	1.31	569.96	296.81	−65.003	[106,158,171–173,189–195]
Ca	Ca(BH <sub>4</sub> ) <sub>2</sub>	1	783.19	510.04	−142.1	[146–151,157]
Cr	Cr(BH <sub>4</sub> ) <sub>2</sub>	1.66	369.86	96.71	22.042	[28,29]
Mn	Mn(BH <sub>4</sub> ) <sub>2</sub>	1.55	428.1	154.95	−5.315	[175,189–191,224]
Fe	Fe(BH <sub>4</sub> ) <sub>2</sub>	1.83	288.22	15.07	64.321	[192,193]
Ni	Ni(BH <sub>4</sub> ) <sub>2</sub>	1.91	253.32	−19.83	84.217	[195] * as heteroleptic complex
Co	Co(BH <sub>4</sub> ) <sub>2</sub>	1.88	266.14	−7.01	76.756	[194] * presumed, but unstable
Zn	Zn(BH <sub>4</sub> ) <sub>2</sub>	1.65	374.98	101.83	19.555	[119–122]
Sr	Sr(BH <sub>4</sub> ) <sub>2</sub>	0.95	820.74	547.59	−154.535	[147,148]
Ba	Ba(BH <sub>4</sub> ) <sub>2</sub>	0.89	866.97	593.82	−169.457	[148]
Cd	Cd(BH <sub>4</sub> ) <sub>2</sub>	1.69	354.71	81.56	29.503	[149]
Hg	Hg(BH <sub>4</sub> ) <sub>2</sub>	2	216.74	−56.41	106.6	[151] * failed attempts
Al	Al(BH <sub>4</sub> ) <sub>3</sub>	1.61	395.81	122.66	9.607	[83–88]
Sc	Sc(BH <sub>4</sub> ) <sub>3</sub>	1.36	538.74	265.59	−52.568	[182,183,295–299]
Ti <sup>III</sup>	Ti(BH <sub>4</sub> ) <sub>3</sub>	1.54	433.61	160.46	−7.802	[176–179,206] * Ti(IV) is reduced in situ to Ti(III)
V	V(BH <sub>4</sub> ) <sub>3</sub>	1.63	385.32	112.17	14.581	[66]
Ga	Ga(BH <sub>4</sub> ) <sub>3</sub>	1.81	297.29	24.14	59.347	[84,85] * as GdH(BH <sub>4</sub> ) <sub>2</sub> (volatile, 203K) and GdH <sub>2</sub> (BH <sub>4</sub> ) (unstable)
Y	Y(BH <sub>4</sub> ) <sub>3</sub>	1.22	628.38	355.23	−87.386	[65,66,68–73]
Nb	Nb(BH <sub>4</sub> ) <sub>3</sub>	1.6	401.1	127.95	7.12	[180] * no homoleptic form; as complex
In	In(BH <sub>4</sub> ) <sub>3</sub>	1.78	311.17	38.02	51.886	[86]
La	La(BH <sub>4</sub> ) <sub>3</sub>	1.1	710.71	437.56	−117.23	[212]
Ce	Ce(BH <sub>4</sub> ) <sub>3</sub>	1.12	696.64	423.49	−112.256	[212]

Table 3. Cont.

Metal (M)	M(BH <sub>4</sub> ) <sub>x</sub>	χ <sub>P</sub>	T <sub>d</sub> = 175.914(χ <sub>P</sub> −3.11) <sup>2</sup> [K]	t <sub>d</sub> [°C]	ΔH <sub>boro</sub> = 248.7 χ <sub>P</sub> −390.8 [ $\frac{\text{kJ}}{\text{mol BH}_4}$ ]	Reference
Nd	Nd(BH <sub>4</sub> ) <sub>3</sub>	1.14	682.7	409.55	−107.282	[69]
Sm <sup>II</sup>	Sm(BH <sub>4</sub> ) <sub>2</sub>	1.13	689.65	416.5	−109.769	[213,214]
Sm <sup>III</sup>	Sm(BH <sub>4</sub> ) <sub>3</sub>	1.13	689.65	416.5	−109.769	[214]
Pr	Pr(BH <sub>4</sub> ) <sub>3</sub>	1.13	689.65	416.5	−109.769	[64]
Eu <sup>II</sup>	Eu(BH <sub>4</sub> ) <sub>2</sub>	1.2	641.75	368.6	−92.36	[213]
Eu <sup>III</sup>	Eu(BH <sub>4</sub> ) <sub>3</sub>	1.2	641.75	368.6	−92.36	[70,148]
Gd	Gd(BH <sub>4</sub> ) <sub>3</sub>	1.2	641.75	368.6	−92.36	[68,71,72,214]
Tb	Tb(BH <sub>4</sub> ) <sub>3</sub>	1.22	628.38	355.23	−87.386	[73,214]
Dy	Dy(BH <sub>4</sub> ) <sub>3</sub>	1.23	621.75	348.6	−84.899	[68]
Ho	Ho(BH <sub>4</sub> ) <sub>4</sub>	1.24	615.15	342	−82.412	[69]
Er	Er(BH <sub>4</sub> ) <sub>3</sub>	1.24	615.15	342	−82.412	[214]
Tm	Tm(BH <sub>4</sub> ) <sub>3</sub>	1.25	608.59	335.44	−79.925	[73]
Yb <sup>II</sup>	Yb(BH <sub>4</sub> ) <sub>2</sub>	1.1	710.71	437.56	−117.23	[215]
Yb <sup>III</sup>	Yb(BH <sub>4</sub> ) <sub>3</sub>	1.1	710.71	437.56	−117.23	[215]
Lu	Lu(BH <sub>4</sub> ) <sub>3</sub>	1.27	595.57	322.42	−74.951	[73]
Th	Th(BH <sub>4</sub> ) <sub>4</sub>	1.3	576.31	303.16	−67.49	[78,206,207]
Pa	Pa(BH <sub>4</sub> ) <sub>3</sub>	1.5	455.99	182.84	−17.75	[78]
U	U(BH <sub>4</sub> ) <sub>4</sub>	1.38	526.49	253.34	−47.594	[78,80,208,209]
Np	Np(BH <sub>4</sub> ) <sub>4</sub>	1.36	538.74	265.59	−52.568	[79,80,210]
Pu <sup>III</sup>	Pu(BH <sub>4</sub> ) <sub>3</sub>	1.28	589.12	315.97	−72.464	[78,80]
Pu <sup>IV</sup>	Pu(BH <sub>4</sub> ) <sub>4</sub>					[79]
Tl <sup>I</sup>	TlBH <sub>4</sub>	1.62	390.55	117.4	12.094	[87]
Tl <sup>III</sup>	Tl(BH <sub>4</sub> ) <sub>3</sub>	1.62	390.55	117.4	12.094	[88] * failed attempts; as TlCl(BH <sub>4</sub> ) <sub>2</sub> (dec. at 178 K)
Ge	Ge(BH <sub>4</sub> ) <sub>4</sub>	2.01	212.86	−60.29	109.087	no conclusive reports
Zr	Zr(BH <sub>4</sub> ) <sub>4</sub>	1.33	557.37	284.22	−60.029	[203,204]
Sn	Sn(BH <sub>4</sub> ) <sub>4</sub>	1.96	232.65	−40.5	96.652	no conclusive reports
Hf	Hf(BH <sub>4</sub> ) <sub>4</sub>	1.3	576.31	303.16	−67.49	[205]

Screening the known borohydrides, one might expect the following elements to form unstable borohydrides: Cu, Ag, (Be), Cr, Fe, Ni, Co, Zn, Cd, Hg, Al, V, Ga, Nb, In, Ge, and Sn. Many of these are known, but either they are stable at very low temperatures or they need other techniques for stabilizations, i.e., formation of adducts with neutral molecules (Table 2).

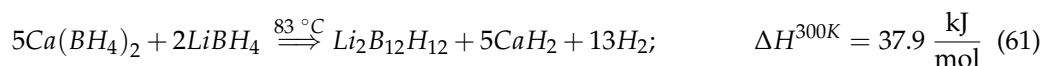
Many borohydrides follow a decomposition scheme leading to production of B<sub>2</sub>H<sub>6</sub> and H<sub>2</sub> in a 1:1 molar ratio (Equation (60)). These pathways that lead to production of diborane (toxic gas) will be, unfortunately, not useful for expanding the class of hydrogen storage material because they lead to a loss of the boron source [300].



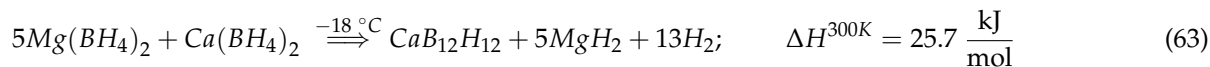
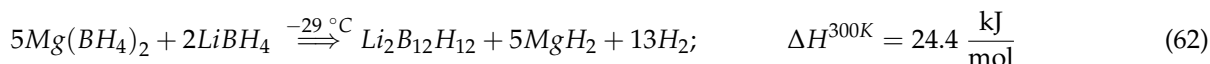
## 6.2. Destabilizing Methods for Complex Metal Borohydrides

*Nanoconfinement* is a valuable method for the synthesis of nano-sized MBH. This route can be utilized to lower energy barriers and speed up kinetics. Nanoscaffolds can be engineered to have highly advantageous textural properties: tunable pore size ( $D_p$ ), as well as high pore volume ( $V_p$ ) and specific surface area (SSA), which in turn will greatly enhance the kinetics of hydrogen release/uptake. These *recyclability enhancements* will be described for representative metal borohydride systems and their composites. Anion substitution in complex metal hydrides can lead to system destabilization:  $\text{TiF}_3$  and  $\text{TiCl}_3$  were investigated in  $\text{NaBH}_4$  and showed a 6.6 kJ/mol decrease in decomposition enthalpy, by altering hydrogen release and uptake [303]. The replacement of  $\text{H}^-$  by  $\text{F}^-$  was investigated in  $\text{LiBH}_4$  as well, showing significant theoretical thermodynamic improvements [304]. Nanoconfinement improvements brought about by size-restriction are discussed in relation to their bulk state in the following chapter (Section 7). Some volatile borohydrides such as  $\text{Zr}(\text{BH}_4)_4$  could be embedded into mesoporous silica (MCM-48 type) to show enhanced stability towards air and moisture, and more importantly, to retain  $\text{Zr}(\text{BH}_4)_4$  inside siloxanic pores, thus mitigating the high volatility issue of neat  $\text{Zr}(\text{IV})$  borohydride.

*Thermal destabilization* by utilizing mixtures of metal borohydrides has proven to be an effective technique [305]. Coupled dehydrogenation of a physical mixture  $(1-x)\text{LiBH}_4 + x\text{Ca}(\text{BH}_4)_2$  comprised of *o*- $\text{LiBH}_4$  and  $\alpha$ -/ $\gamma$ - $\text{Ca}(\text{BH}_4)_2$  (synchrotron XRD patterns) also led to enhanced ionic conductivity of the resulting *cubic*- $\text{CaH}_2$ . Moreover, it seems that the ionic conductivity may be solely due to  $\text{Li}^+$  and irrespective of  $\text{Ca}^{2+}$  content, as shown by samples  $(1-x)\text{LiBH}_4 + x\text{Ca}(\text{BH}_4)_2$  with similar ionic conductivity to that of pure ball-milled  $\text{LiBH}_4$  [305]. Further investigations by first-principles computations of a similarly coupled system by Ozolins et al. have shown that the decomposition reaction yields the complex intermediate  $\text{Li}_2\text{B}_{12}\text{H}_{12}$  alongside the anticipated  $\text{CaH}_2$  and hydrogen  $\text{H}_2$ , with an endothermic enthalpy of 37.9 kJ/mol and 6.7 wt.%  $\text{H}_2$  (Equation (61)) [306].



Using  $\text{Mg}(\text{BH}_4)_2$  with either  $\text{LiBH}_4$  (Equation (62); 8.4 wt.%  $\text{H}_2$ ) or  $\text{Ca}(\text{BH}_4)_2$  (Equation (63); 7.7 wt.%  $\text{H}_2$ ) produces similar chemical reactions, but at negative temperatures which therefore would hinder their usage under ambient conditions.

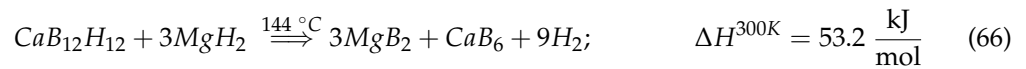


Decomposition of group II metal dodecaborohydrides  $\text{MB}_{12}\text{H}_{12}$  seems to occur around 300 °C (309 °C for  $\text{MgB}_{12}\text{H}_{12}$  and 306 °C for  $\text{CaB}_{12}\text{H}_{12}$ ), but the group I counterpart shows unfavorable thermodynamics ( $\text{LiB}_{12}\text{H}_{12}$ ,  $\Delta H = 116.7$  kJ/mol,  $t_d = 696$  °C) (Equations (64) and (65)).



Further hydrogen release by reaction of  $[\text{B}_{12}\text{H}_{12}]^{2-}$  complex anion with the metal hydrides  $\text{MH}_2$  should lead to additional hydrogen release (Equations (66) and (67)). It is thermodynamically more favored the addition of  $\text{CaH}_2$  rather than  $\text{MgH}_2$  to  $\text{CaB}_{12}\text{H}_{12}$ ,

as the switch from  $\text{MgH}_2$  to  $\text{CaH}_2$  used for destabilization could lower the operating temperature of the system even more, from 144 °C to 86 °C [306].



$\text{Ca}(\text{BH}_4)_2\text{-M}(\text{NH}_2)_2$  destabilized system ( $M = \text{Mg}, \text{Ca}$ ) is a typical and representative system producing significant thermodynamic alteration for decomposition of  $\text{Ca}(\text{BH}_4)_2$ . Destabilization of  $\text{Ca}(\text{BH}_4)_2$  was attempted with various group II amides ( $\text{Mg}(\text{NH}_2)_2$ ,  $\text{Ca}(\text{NH}_2)_2$ ) leading to mixed-metal-/metal nitridoborates [ $\text{Ca}_3\text{Mg}_6(\text{BN}_2)_6$ ] and  $\text{Ca}_9(\text{BN}_2)_6$ , respectively. The reasoning for such an outcome lies in the interaction of  $[\text{BH}_4]^-$  and  $[\text{NH}_2]^-$  anions, and more precisely in the B-H...H-N interaction of dihydrogen bonding type (Figure 14) [307,308].

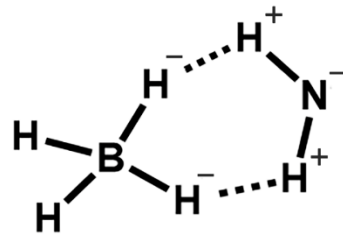
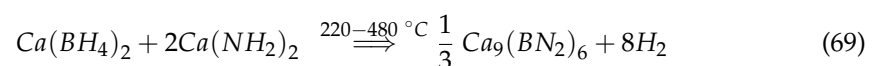
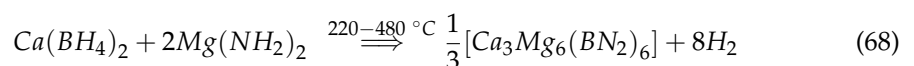


Figure 14. Dihydrogen bonding represented between borohydride  $[\text{BH}_4]^-$  and amidic  $[\text{NH}_2]^-$  moieties.

While the dehydrogenation onset of bulk  $\text{Ca}(\text{BH}_4)_2$  is roughly 320° ( $290_{\text{onset}}\text{-}361_{\text{peak}}$ ), the binary system  $\text{Ca}(\text{BH}_4)_2\text{-}2\text{Mg}(\text{NH}_2)_2$  (8.3 wt.%  $\text{H}_2$ ) and  $\text{Ca}(\text{BH}_4)_2\text{-}2\text{Ca}(\text{NH}_2)_2$  (6.8 wt.%  $\text{H}_2$ ) starts to release hydrogen at 220 °C, so that a significant  $\Delta T$  of 100 degrees is produced. Although some  $\text{NH}_3$  release was recorded, XRD study of the final dehydrogenated binary systems indicates Equations (68) and (69) as taking place when heating the samples below 480 °C [309].



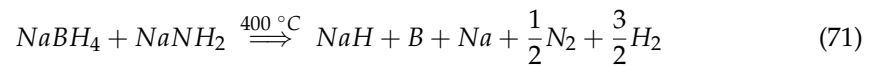
The binary systems were prepared by BM (ball-milling technique, 200 rpm, 5 h, Ar) while the nature of the evolved gases was assessed by MS-coupled TPD (temperature-programmed desorption) [309]. This pattern of destabilization has been reported as well for  $\text{LiBH}_4\text{-LiNH}_2$  [310],  $\text{NaBH}_4\text{-NaNH}_2$  [311],  $\text{Ca}(\text{BH}_4)_2\text{-LiNH}_2$  [312,313], and  $\text{Ca}(\text{BH}_4)_2\text{-NaNH}_2$  [313] systems, and they all led to new complex hydrides.

Table 4 summarizes the main destabilization systems known for metal borohydrides; these include destabilization by metal, metal oxide, metal chloride, amides, and even metal borohydrides. The decomposition pathway is often altered by the molar ratio  $M(\text{BH}_4)_x$ : destabilizing agent. For instance, a clear dehydrogenation proposal (Equation (70)) was advanced by Aoki et al. for  $\text{LiBH}_4\text{-}2\text{LiNH}_2$  [314], while others reported the dehydrogenation for  $\text{LiBH}_4\text{-LiNH}_2$  without an explicit mechanism.



Somer et al. propose two possible reactions in the  $\text{NaBH}_4\text{:NaNH}_2$  1:1 and 1:2 systems (Equations (71) and (72)), with very different outcomes. The 1:1 system leads to the

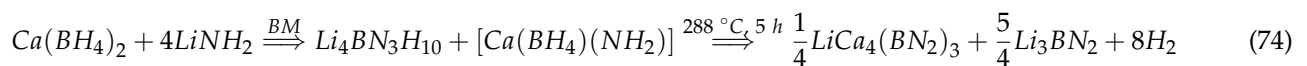
production of amorphous boron B and Na metal, whereas the 1:2 mixture leads to hydrogen evolution and a unique solid product, trisodium dinitridoborate  $\text{Na}_2\text{BN}_2$  [311].



When LiH was mixed with  $\gamma\text{-Mg}(\text{BH}_4)_2$  in various molar ratios (1:0.5, 1:0.97, and 1:1.89), it was found that the decomposition follows the one of pure products resulting from a meta-theoretical reaction (Equation (73)). The sample 1  $\gamma\text{-Mg}(\text{BH}_4)_2$ : 0.5 LiH showed the highest hydrogen storage capacity, essentially equal to the theoretical value [315].



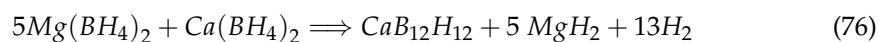
Destabilization of  $\text{Ca}(\text{BH}_4)_2$  with  $\text{LiNH}_2$  in a 1:4 molar ratio yields a cubic phase of an anion-substituted borohydride [ $\text{Ca}(\text{BH}_4)(\text{NH}_2)$ ], alongside a hydro-nitridoborate phase of  $\text{Li}_4\text{BN}_3\text{H}_{10}$ . Upon heating to either 288 °C (5 h, undoped sample) or 178 °C (5 h, 5 wt.%  $\text{CoCl}_2$ ), the system 1  $\text{Ca}(\text{BH}_4)_2$ : 4  $\text{LiNH}_2$  releases 8 wt.% and 7 wt.% hydrogen, respectively (Equation (74)).



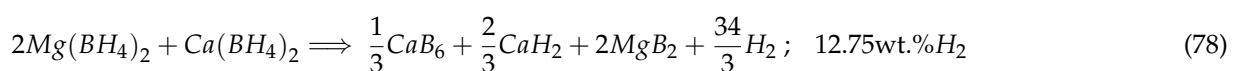
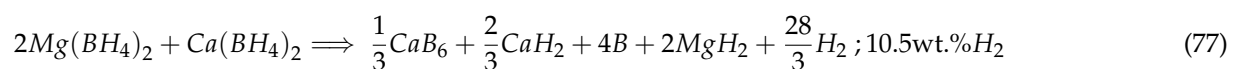
DFT computation by Ozolins et al. showed various dehydrogenation pathways for binary borohydride–borohydride, borohydride–amide and borohydride–metal systems (Equation (75)) [306]. The system  $5\text{Mg}(\text{BH}_4)_2 + 2\text{LiBH}_4$  (8 wt.%  $\text{H}_2$ ) has a decomposition temperature of  $-29^\circ\text{C}$  and is therefore ruled out from usage in mobility applications; however, the  $\text{Ca}^{2+}$ -counterpart  $5\text{Ca}(\text{BH}_4)_2 + 2\text{LiBH}_4$  (6.7 wt.%  $\text{H}_2$ ) has a reasonably low hydrogen release temperature of  $83^\circ\text{C}$  [306].



Similarly, the system  $5\text{Mg}(\text{BH}_4)_2 + \text{Ca}(\text{BH}_4)_2$  with 7.7 wt.%  $\text{H}_2$  (theoretical) was predicted by first-principles computations to release  $\text{H}_2$  at  $-18^\circ\text{C}$  [306], but was actually found experimentally to only dehydrogenate around  $150^\circ\text{C}$ , and the reaction was not reversible (Equation (76)) [316,317].



Assuming that in composites of type  $2\text{Mg}(\text{BH}_4)_2 + \text{Ca}(\text{BH}_4)_2$  a temperature high enough is reached (above  $306\text{--}309^\circ\text{C}$ , the decomposition temperature for plausible intermediates  $\text{CaB}_{12}\text{H}_{12}$  and  $\text{MgB}_{12}\text{H}_{12}$ ), one may consider that final decomposition products are those expected from individual borohydrides, so that the overall decomposition can be formulated as in Equations (77) and (78), with a theoretical hydrogen storage capacity of 10.5–12.75 wt.% [316–318].



Combined Kissinger plot and Arrhenius equation allowed establishing the first-order kinetic parameters for dehydrogenation reaction of binary borohydride–amine systems (Table 5).

**Table 4.** Representative examples of destabilized borohydride systems: binary *borohydride–amide* systems  $M(\text{BH}_4)_x\text{-RNH}_2$ , *borohydride–borohydride* systems  $M(\text{BH}_4)_x\text{-R}(\text{BH}_4)_y$ , *borohydride–chloride*  $M^I\text{BH}_4\text{-MgCl}_2$ , *borohydride–TM oxide*, *borohydride–metal*. ( $t_d$ : decomposition temperature).

System	Catalyst	$t_d$ (°C)	Obs.	Reference
$\text{LiBH}_4\text{-LiNH}_2$	- via metastable $\text{Li}_2[\text{BH}_4][\text{NH}_2]$ and $\text{Li}_4[\text{BH}_4][\text{NH}_2]_3$	$95_{\text{melt}}\text{-}160_{\text{onset}}\text{-}315_{\text{peak}}, 230_{\text{mean}}$	5.8 wt.% $\text{H}_2$ ; $\text{H}_2$ major; small traces of $\text{NH}_3$ (TPD-MS data)	[310]
$\text{LiBH}_4\text{-}2\text{LiNH}_2$	- (LiH possible intermediate)	249	7.8 wt.% $\text{H}_2$ $\text{LiBH}_4$ : 75 kJ/mol $\text{H}_2$ ; $\text{LiBH}_4\text{-}2\text{LiNH}_2$ : 23 kJ/mol $\text{H}_2$	[314]
$x \text{NaBH}_4\text{-NaNH}_2$ ( $x = 1,2,3,4$ )	- via $\alpha\text{-}/\beta\text{-Na}_2[\text{BH}_4][\text{NH}_2]$	$265_{\text{onset}}\text{-}350_{\text{peak}}, 297$ (2:1); 400 (1:1)	8 wt.%	[311]
$\gamma\text{-Mg}(\text{BH}_4)_2\text{-}0.5\text{LiH}$	-	380–420	15.5 wt.%exp., 14.78 wt.% (theoretical)* * higher wt.% exp. due to usage of solvated $\gamma\text{-Mg}(\text{BH}_4)_2$	[315]
$\text{Ca}(\text{BH}_4)_2\text{-}4 \text{LiNH}_2$	-	$250_{\text{onset}}\text{-}320_{\text{peak}}$ (288 <sub>mean</sub> )	8 wt.%	[312,313]
$\text{Ca}(\text{BH}_4)_2\text{-}4\text{LiNH}_2\text{-}5 \text{wt.}\% \text{CoCl}_2$	$\text{Co}^{2+}$ ( $\text{CoCl}_2$ )	$150_{\text{onset}}\text{-}207_{\text{peak}}$ (178 <sub>mean</sub> )	>7 wt.%	[312]
$\text{Ca}(\text{BH}_4)_2\text{-}2\text{Mg}(\text{NH}_2)_2$	-	220–480 (270, 290 and 310–multistep)	8.3 (8.8 wt.% theoretical) not reversible (50-bar $\text{H}_2$ , 20–300 °C)	[309]
$\text{Ca}(\text{BH}_4)_2\text{-}2\text{Ca}(\text{NH}_2)_2$	-	220–480 (270, 290 and 310–multistep)	6.8 (7.5 wt.% theoretical) not reversible (50-bar $\text{H}_2$ , 20–300 °C)	[309]
$5\text{Ca}(\text{BH}_4)_2\text{-}2\text{LiBH}_4$	-	83	6.7 wt.%* * theoretical	[306]
$5\text{Mg}(\text{BH}_4)_2\text{-}2\text{LiBH}_4$	-	–29	8.4 wt.%* * theoretical	[306]
$2\text{Mg}(\text{BH}_4)_2\text{-Ca}(\text{BH}_4)_2$	-	272, 326, 346, 398 (rehydrogenation at $288_{\text{onset}}, 273_{\text{peak}}$ )	10.5 wt.%* * theoretical	[316–318]
$5\text{Mg}(\text{BH}_4)_2\text{-Ca}(\text{BH}_4)_2$	-	–18 °C ( $p = 1\text{atm}$ )* * predicted based on DFT calculations; 150 °C	7.73 wt.% $\text{H}_2$ * * predicted based on DFT calculations	[306]* [316,317]
$\text{LiBH}_4 + 0.2 \text{MgCl}_2 + 0.1 \text{TiCl}_3$ ; $\text{LiBH}_4 + 0.076 \text{MgCl}_2 + 0.047 \text{TiCl}_3$	$\text{MgCl}_2, \text{TiCl}_3$	$60_{\text{onset}}\text{-}400_{\text{peak}}$	5 wt.% $\text{H}_2$	[319,320]
$\text{LiBH}_4 + 0.09 \text{TM oxides}$ ( $\text{TiO}_2, \text{V}_2\text{O}_3$ )	$\text{TiB}_2$ -possible active intermediate	200	7–9 wt.% $\text{H}_2$ ; reversible	[319]
$\text{LiBH}_4 + 0.2 \text{M}$ ( $\text{M} = \text{Mg}, \text{Al}$ )	$\text{Mg}/\text{Al}$	$60\text{-}300_{\text{fast}}\text{-}600$	9 wt.% $\text{H}_2$ ; $\text{Al}$ -based yields material probably volatile, only recharges to 3.5 wt.% capacity	[320]
$\text{LiBH}_4 + 0.0897 \text{Al}$	$\text{Al}$	450	12.4 wt.%, partially reversible	[321]

**Table 5.** Kinetic parameters for dehydrogenation of binary destabilized systems  $\text{Ca}(\text{BH}_4)_2\text{-M}^{\text{II}}(\text{NH}_2)_2$  ( $\text{M} = \text{Mg}, \text{Ca}$ ).

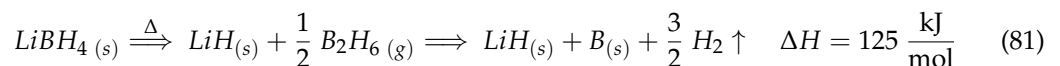
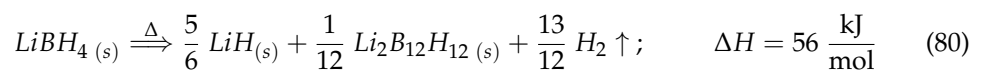
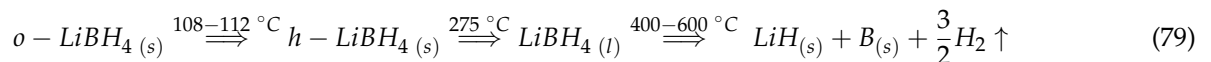
Binary System	$E_a$ (kJ/mol)	$A \times 10^{-9}$ ( $\text{min}^{-1}$ )	$k \times 10^2$ ( $\text{min}^{-1}$ )	Reference
$\text{Ca}(\text{BH}_4)_2\text{-}2\text{Mg}(\text{NH}_2)_2$	132.7	15	1.2	[309]
$\text{Ca}(\text{BH}_4)_2\text{-}2\text{Ca}(\text{NH}_2)_2$	119.3	3.2	4.3	[309]

The specific rate for  $\text{Ca}(\text{BH}_4)_2\text{-}2\text{Ca}(\text{NH}_2)_2$  shows a 3.5-fold increase in reaction rate, when compared to  $\text{Ca}(\text{BH}_4)_2\text{-}2\text{Mg}(\text{NH}_2)_2$  system. For comparison, pristine  $\text{Ca}(\text{BH}_4)_2$  has slow desorption kinetics that onsets at  $290^\circ$  and peaks at  $361^\circ\text{C}$  [309].

## 7. Model Systems for Hydrogen Storage of MBH and Other RMH (Reactive Metal Hydrides): Nanoconfinement vs. Bulk Behavior for Improved Thermodynamics and Kinetics

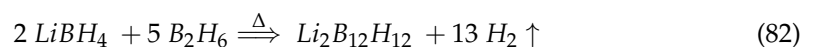
### 7.1. $\text{LiBH}_4$

Being the lightest metal borohydride and potentially having some of the highest hydrogen storage capacity (18.4 wt.%),  $\text{LiBH}_4$  was first prepared in 1940 by Schlesinger and Brown by an organolithium compound and diborane  $\text{B}_2\text{H}_6$  (Equation (18)) [102], and afterwards investigated in detail by many researchers [125,322–325]. Transition to a  $h\text{-LiBH}_4$  phase at  $108\text{--}112^\circ\text{C}$  exhibiting unexpectedly fast  $\text{Li}^+$  ion conductivity drove even further the pace of MBH research. Following melting ( $275^\circ\text{C}$ ), decomposition occurs above  $400^\circ\text{C}$  with an endothermic reaction enthalpy of  $\Delta H_d = 74\text{ kJ/mol}$  [326], and leads to formation of  $\text{LiH}$ ,  $\text{B}$ , and  $\text{H}_2$ , which account for a real practical hydrogen storage of 13.8 wt.%  $\text{H}_2$  (Equations (79)–(81)) [327].



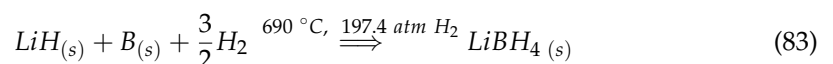
Synchrotron radiation XRD (SR-PXD) showed the presence of many intermediate phases during decomposition of  $\text{LiBH}_4$  [322]. These intermediates (Equations (80) and (81)) are supported by Raman spectroscopy and  $^{11}\text{B}$ -NMR experiments [328,329]. The data provided by Zuttel et al. show that the two-step dehydrogenation of  $\text{LiBH}_4$  proceeds via  $\text{Li}_2\text{B}_{12}\text{H}_{12}$  formation (10 wt.%  $\text{H}_2$  release,  $\Delta H = 56\text{ kJ/mol}$ , Equation (80)), and a highly endothermic second step leading to  $\text{LiH}$  and  $\text{B}$ , releasing 4 wt.%  $\text{H}_2$  ( $\Delta H = 125\text{ kJ/mol}$ ) [200]. A thermodynamic data scheme is pictured by Y. Yan et al., who assigned enthalpy effects to the intermediate species formation during  $o\text{-LiBH}_4$  decomposition [164].

The  $^{11}\text{B}$  NMR data showed  $\text{B}_2\text{H}_6$  to be an impurity during dehydrogenation processes. Therefore, running the reaction of  $\text{LiBH}_4$  with  $\text{B}_2\text{H}_6$  confirmed the formation of the hypothesized  $\text{Li}_2\text{B}_{12}\text{H}_{12}$  during the dehydrogenation pathway (Equation (82)) [330].



Attempts to lower the hydrogen desorption to temperatures below  $400^\circ\text{C}$  have been successful when using  $\text{SiO}_2$  powder addition ( $\text{LiBH}_4\text{:SiO}_2 = 1\text{:}3$ ) [331]. Three important peaks in TPD spectra of  $\text{LiBH}_4$  corroborated the NMR studies, Raman spectroscopy, and XRD data, all of which point to the formation of dodecahydro-closo-dodecaborate species  $[\text{B}_{12}\text{H}_{12}]^{2-}$ , and possibly other boron hydrides as intermediates [328,329].

Rehydrogenation to reform  $\text{LiBH}_4$  is possible, but it requires extreme conditions ( $70\text{--}350\text{-bar H}_2$ ,  $t > 600^\circ\text{C}$ ) and will not proceed to completion, thus leading to continual decrease in hydrogen capacity with the number of hydrogen release–uptake cycles (Equations (10) and Equation (83)) [48,326,332,333].



Nanoconfinement of  $\text{LiBH}_4$  was investigated in a variety of supports (2–25 nm), such as mesoporous silica (MSU-H, SBA-15 etc.) or mesoporous carbon (carbon replica of MSU-H silica: C-MSU-H, or of SBA-15 silica: C-SBA-15 i.e., CMK-3) (Figure 15) [334–336]. A pertinent overview of C-replica synthesis of mesoporous silicas comes from M. Kruk et al. [337]

and R. Ryoo et al. [338]. Mesoporous SiO<sub>2</sub>, however, is to be avoided, since an irreversible reaction with LiBH<sub>4</sub> during dehydrogenation could lead to lithium silicates (Figure 16) [335,339]. Attempts to improve hydrogen uptake by using Mo-decorated mesoporous silica (MSU-H type) increased the reversible hydrogen capacity from 3.2 wt.% (pristine LiBH<sub>4</sub>) to 5.2 wt.% H<sub>2</sub> in the nanocomposite LiBH<sub>4</sub>-Mo:MSU-H [335].

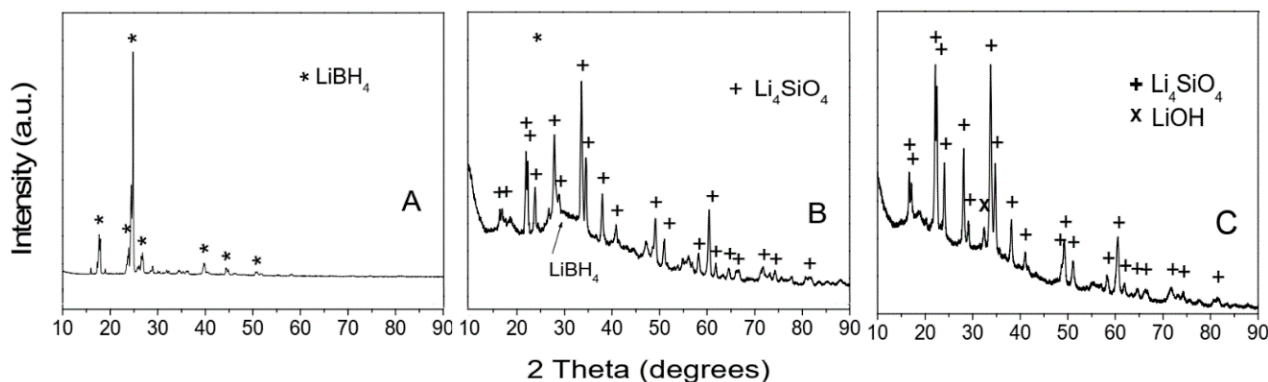


**Figure 15.** XRD data showing the evolution of phases in a Mo-catalyzed LiBH<sub>4</sub>-Mo:MSU-H mesoporous silica nanocomposite: commercial LiBH<sub>4</sub> (A), rehydrogenated LiBH<sub>4</sub> - Mo:MSU-H (B) and dehydrogenated LiBH<sub>4</sub> Mo:MSU-H (C). Reprinted with permission from [335].

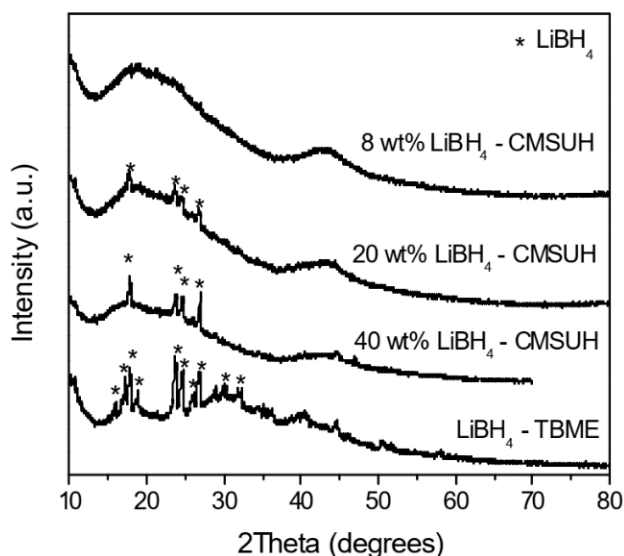
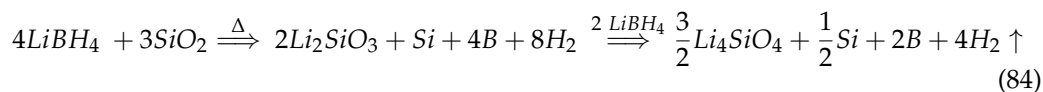


**Figure 16.** XRD diffraction spectra of MTBE-recrystallized LiBH<sub>4</sub> and of three nanocomposites LiBH<sub>4</sub>-C-MSU-H (8 wt.%, 20 wt.%, and 40 wt.% LiBH<sub>4</sub>). Reprinted with permission from [334].

Formation of lithium silicates (Li<sub>2</sub>SiO<sub>3</sub>, Li<sub>4</sub>SiO<sub>4</sub>) was confirmed by XRD and synchrotron powder XRD, but only after LiBH<sub>4</sub> decomposed in the as-synthesized composite LiBH<sub>4</sub>@meso-SiO<sub>2</sub>; the nanocomposite seems otherwise stable at temperatures  $t < 275$  °C (Equation (84)) [89,335,340].



Nanoconfinement can be performed by melt infiltration or solvent infiltration, both of which lead to a decrease in the crystallite size of the LiBH<sub>4</sub> [341,342]. Incipient wetness technique has been used to infiltrate MTBE (methyl *tert*-butyl ether) solution of LiBH<sub>4</sub> in mesoporous carbon (C-MSU-H). The maximum loading attempted was about 40 wt.% LiBH<sub>4</sub>, but the XRD data confirms that even for a 20 wt.% loading some diffraction peaks

of  $\text{LiBH}_4$  appear. This is indicative of the borohydride species crystallizing outside of the mesopores [334].

Interestingly, the lowest onset for the as-prepared nanocomposites  $\text{LiBH}_4@\text{C-MSU-H}$  was recorded at 150 °C for the lowest investigated borohydride loading (8 wt.%), while the others showed decomposition starting at 170 °C (20 wt.%  $\text{LiBH}_4$ ) and 200 °C (40 wt.%  $\text{LiBH}_4$ ), with effect ascribed to the better dispersion of the borohydride inside the mesoporous support at lower loadings (Figure 17) [334,335].

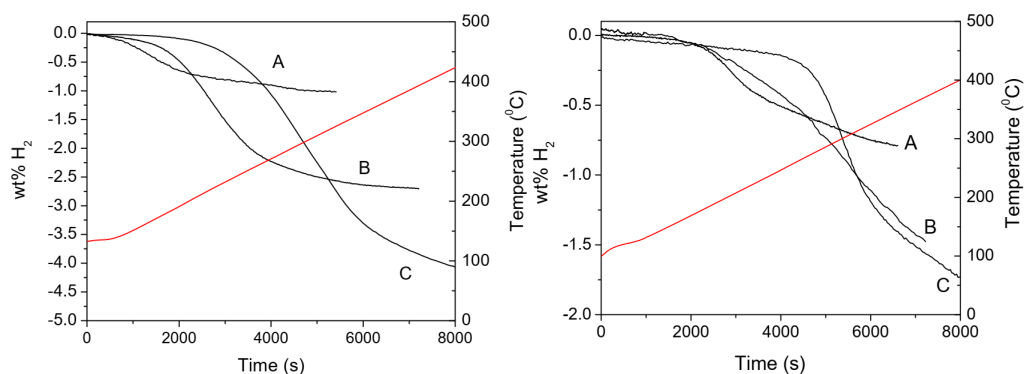


**Figure 17.** Hydrogen desorption kinetics of nanoconfined  $\text{LiBH}_4@\text{C-MSU-H}$  with a heating ramp of 2 °C/min (initial nanocomposites, left; rehydrogenated samples, right). A: 8 wt.%, B: 20 wt.%, and C: 40 wt.% loading of  $\text{LiBH}_4$ . Reprinted with permission from [334].

The influence of carbon porosity was investigated showing that a proper impregnation of  $\text{LiBH}_4$  inside 1.8–3.2 nm activated carbon ( $S_{\text{BET}} = 1341 \text{ m}^2/\text{g}$ ;  $V_p = 0.87 \text{ cm}^3/\text{g}$ ) is accompanied by reduction of both surface area (to  $245 \text{ m}^2/\text{g}$ ) and pore volume (to  $0.2 \text{ cm}^3/\text{g}$ ) [336,343]. The size of the scaffold alters the activation energy  $E_a$  of dehydrogenation: non-porous graphite (146 kJ/mol  $\text{LiBH}_4$ ), 24 nm RF-CA (111 kJ/mol  $\text{LiBH}_4$ ), and 13 nm RF-CA (103 kJ/mol  $\text{LiBH}_4$ ), consistent with inverse proportionality between nanoscaffold size and activation energy  $E_a$  [344,345]. The Arrhenius Equation (85) shows that, taking solely into account the  $E_a$  of these three supports, one might expect the dehydrogenation rates to follow this order:  $k_{\text{graphite}}:k_{24\text{nm}}:k_{13\text{nm}} = 1:e^{14.03}:e^{17.20}$  (at 298.15 K), and  $k_{\text{graphite}}:k_{24\text{nm}}:k_{13\text{nm}} = 1:e^{11.28}:e^{13.86}$  (at 373.15 K).

$$k = A e^{-\frac{E_a}{RT}} \quad (85)$$

This approximation was performed assuming the same pre-exponential Arrhenius factor  $A$  (an oversimplification), but this shows that nonporous carbon barely has any benefit from confinement, whereas the rate in nanoconfined composites is  $\sim 10^6$  times faster. Moreover, reducing the nanoscaffold from 24 nm to 13 nm affords a rate that is 23.8 times higher (at 25 °C) or 13.2 times higher (at 100 °C, a temperature considered optimal for operation of fuel cell operation). Nanoconfined  $\text{LiBH}_4$  shows a decrease in melting temperature of 30 °C (in 13 nm RF-CA) or 23 °C (in 24 nm RF-CA), but only when melt infiltration was employed; a modest 1 °C decrease was recorded for the solvent infiltration technique [341,346].

When a 33.67 wt.% loading of  $\text{LiBH}_4$  was achieved in C-SBA-15 (CMK-3 carbon, average diameter 4 nm) prepared by the concentrated solution infiltration technique, a clear reduction in temperature onset of dehydrogenation was recorded, and the composite  $\text{LiBH}_4@\text{CMK-3}$  exhibited complete dehydrogenation up to 400 °C [336]. The solvent infiltration approach can alter the dehydrogenation pathway, as well as the reaction kinetics; for comparison, a ball-milled sample containing  $\text{LiBH}_4$  affords full dehydrogenation above 450 °C [347].

While bulk dehydrogenated  $\text{LiBH}_4$  ( $\text{LiH}$  and  $\text{B}$ ) can be rehydrogenated under harsh conditions ( $p$ ,  $t$ , Equation (83)), the nanoconfined borohydride can be regenerated using

100-bar H<sub>2</sub> at below 400 °C within 2 h when microporous carbon was used as scaffold. The improved recyclability of such a composite points to better reversibility when pore size decreases to a microporous range ( $D_{\text{pore}} < 2 \text{ nm}$ ) [341]. A comparison between nanoconfinement of LiBH<sub>4</sub> in carbon and silica supports of pore radii 8–20 Å showed improvement in desorption kinetics, reversibility, and Li<sup>+</sup> ionic conductivity with decreasing pore size. It was shown that similarly sized silica and carbon scaffolds produce different effects upon the melt infiltration of LiBH<sub>4</sub>, with silica-based support showing obvious improvements compared to carbon scaffolds, an aspect attributed to increased LiBH<sub>4</sub> interfacial layer thickness “*t*” for SiO<sub>2</sub> ( $1.94 \pm 0.13 \text{ nm}$ ) compared to C-based support ( $1.41 \pm 0.16 \text{ nm}$ ). In this regard, the Gibbs–Thomson equation correlates with the shift (depression) in melting temperature ( $\Delta T$ ) to interfacial effects, namely, it increases with the interface energy ( $\Delta\gamma$ : 0.053 J/m<sup>2</sup> for LiBH<sub>4</sub>/SiO<sub>2</sub> and 0.033 J/m<sup>2</sup> for LiBH<sub>4</sub>/C system) and decreases with pore radius ( $r_p$ ) (Equation (86)) [348,349].

$$\frac{\Delta T}{T_0} = \frac{2\Delta\gamma V_m}{\Delta H(r_p - 1)} \quad (86)$$

The phase transition shift for LiBH<sub>4</sub> (~114 °C for bulk) was observed at 65 °C for LiBH<sub>4</sub>/SiO<sub>2</sub> (3.3 nm) and at 19 °C for LiBH<sub>4</sub>/C<sub>m-4.9</sub> (of high microporosity). P. Ngene et al. assumed a core-shell model and found a direct relation for computing the enthalpy for the confined material, which could allow fine-tuning of thermodynamic parameter by adjusting pore size and interfacial thickness (Equation (87)) [350].

$$\frac{\Delta H_{\text{confined}}}{\Delta H_{\text{bulk}}} = \left(1 - \frac{t}{r}\right)^2 \quad (87)$$

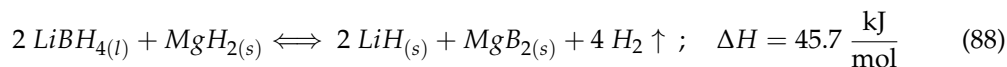
Pore size distribution (PSD) and pore geometry should always play a decisive role in nanoconfinement results, especially for C-nanoscaffolds where microporosity percentage could be dominant [351]. The nano-synergy effect has recently made possible a reversible hydrogen capacity of 9.2 wt.% [352]. Investigation of possible side-pathways in a dehydrogenation reaction and particularly establishing the nature of intermediate species (such as Li<sub>2</sub>B<sub>12</sub>H<sub>12</sub>) could trigger new directions in nanoconfined borohydride materials [41,323–325].

## 7.2. LiBH<sub>4</sub> + MgH<sub>2</sub>

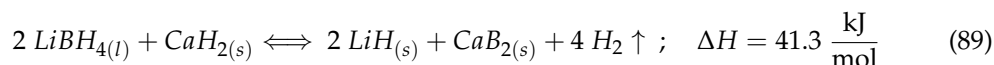
Magnesium-based materials (alloys, hydrides, alanates, borohydrides, etc.) have sparked interest as promising hydrogen storage materials due to their low cost, high wt.% hydrogen storage, and interesting properties, including the much sought-after recyclability/reversibility condition for any future energy storage material [353]. Among all hydrides, MgH<sub>2</sub> is very promising due to high abundance of magnesium, low cost, and reversibility behavior in hydrogenation studies, along with high hydrogen uptake capacity (7.7 wt.%) and very high energy density (9 kJ/g Mg) [354–359]. However, the desorption kinetics are slow at 300 °C and 1-bar H<sub>2</sub>, while the reactivity towards air (oxygen in particular) and the hydrogen desorption has a high enthalpy—thus requiring operation at high temperature [355,360]. Lowering desorption enthalpy can be achieved by introducing high-reactivity defects in the structure (high-energy ball-milling) reaction with a destabilizing element or with a catalyst [361].

Given the advantages of using the Mg-based hydrides mentioned above, inclusion of MgH<sub>2</sub> in various reactive hydride composites (RHCs) has been attempted. The most studied such reactive composite is 2LiBH<sub>4</sub> + MgH<sub>2</sub> (11.6 wt.% hydrogen storage capacity, according to the decomposition pathway in Equation (88)). While taken individually, both LiBH<sub>4</sub> and MgH<sub>2</sub> have unfavorably high thermal stability and slow kinetics, and their

2:1 mixture is found to produce  $MgB_2$  instead of the rock-stable boron B, which brought new hopes in pursuit of a viable energy-storage material (Equation (88)) [92,306,362].



This RHC has favorable thermodynamics and the formation of  $MgB_2$  reduces the dehydrogenation enthalpy to  $\Delta H_{(88)} = -46 \text{ kJ/mol } H_2$ , which makes the reaction reversible under mild conditions (3–20-bar  $H_2$ , 315–450 °C) [92,362–369]. Similar destabilization has been observed for the ( $LiBH_4 + 2CaH_2$ ) system, with an endothermic enthalpy slightly less than 41.3 kJ/mol and 11.7 wt.%  $H_2$  storage (Equation (89)) [306].



Nanoconfinement of the ( $2LiBH_4 + MgH_2$ ) system was attempted in 21 nm RF-CA porous scaffolds showing 4 wt.% reversible hydrogen storage capacity (92% of theoretical storage of the composite RHC@RF-CA, after three cycles), and it was found that decomposition in the nanoconfined state mirrors that from the bulk (Equation (88)) [346]. The hydrogen capacity is higher than that of nanoconfined  $MgH_2@RF-CA_{22nm}$  (1.4 wt.%) [133].

DSC analysis of the composite  $2LiBH_4-MgH_2$  shows four endothermic peaks: 113, 267, 332, and 351 °C for the nanoconfined state in 21 nm RF-CA vs. 117, 290, 364, and 462 °C in bulk (Table 6) [346]. The hydrogen desorption kinetics are clearly improved by nanoconfinement, with  $MgH_2$  registering a 32 °C lowering of dehydrogenation temperature, while dehydrogenation of  $LiBH_4$  is lowered by a significant 111 °C.

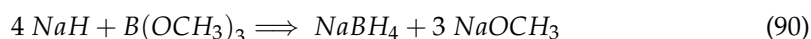
**Table 6.** DSC analysis data for RF-CA-nanoconfined  $2LiBH_4-MgH_2$  vs.  $2LiBH_4-MgH_2$ -bulk [346].

Compound	DSC Peak 1; Polymorphic Transformation $o-LiBH_4 \Rightarrow h-LiBH_4$	DSC Peak 2; Melting Point	DSC Peak 3; Dehydrogenation ( $MgH_2$ )	DSC Peak 4; Dehydrogenation ( $LiBH_4$ )
$2LiBH_4-MgH_2@RF-CA_{21nm}$	113 °C	267 °C	332 °C	351 °C
$2LiBH_4-MgH_2$ -bulk	117 °C	290 °C	364 °C	462 °C

Regardless of the kinetic improvements during recyclability studies, the high thermal stability of bulk metal borohydrides remains an obstacle in their use as hydrogen storage materials.

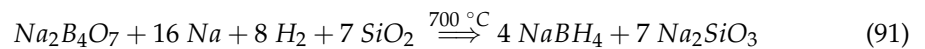
### 7.3. $NaBH_4$

With a hydrogen storage capacity of 10.6 wt.%,  $NaBH_4$  is a valuable reducing reagent used in organic synthesis and decomposes at a high temperature typical of ionic compounds like metal salts (534 °C) [370–374]. The synthesis was reported first by Schlesinger, who reacted trimethyl borate with sodium hydride in hydrocarbon oil, at boiling point (250 °C) (Equation (90)) [375]. The sodium methoxide is hydrolyzed ( $NaOCH_3 + H_2O \Rightarrow NaOH + CH_3OH$ ) to form  $CH_3OH$ , which allows separation of the reactive mixture, and a sodium hydroxide solution of  $NaBH_4$  that allows borohydride extraction using isopropylamine.

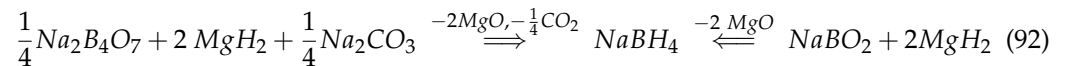


An alternative method (Bayer process) utilizes  $Na_2B_4O_7 \cdot 7SiO_2$  with Na and 3 atm  $H_2$  at 400–500 °C in a one-pot synthesis [376,377]. This process allows for obtaining large quantities of  $NaBH_4$ , but it does present the risk of explosion (the working temperature

is above decomposition of  $\text{NaBH}_4$ ) and it produces large quantities of  $\text{Na}_2\text{SiO}_3$  of lower market demand or value (Equation (91)).



Given the lower cost of Mg as compared to Na, a modified Bayer process uses  $\text{MgH}_2$  as reducing reagent (Equation (92)) [378–380].

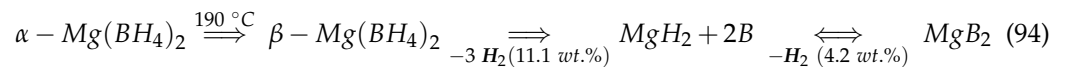


The decomposition is different to that of  $\text{LiBH}_4$  analogue, due to the lower stability of  $\text{NaH}$  compared to  $\text{LiH}$ , and it leads to the formation of the parent elements (Equation (93)). The decomposition process of  $\text{NaBH}_4$  starts at  $\sim 240^\circ\text{C}$  and releases the greatest amount of hydrogen above  $450^\circ\text{C}$ .



#### 7.4. $\text{Mg}(\text{BH}_4)_2$

With a high theoretical gravimetric energy storage capacity (14.8 wt.%), and reasonably low dehydrogenation enthalpy ( $\Delta H = -39.3 \text{ kJ/mol H}_2$ ),  $\text{Mg}(\text{BH}_4)_2$  remains an attractive candidate for hydrogen storage. First-principles calculations on the ground-state crystal structure of  $\text{Mg}(\text{BH}_4)_2$  confirm these energetic characteristics [381]. Decomposition shows several steps in order to finally produce  $\text{MgB}_2$  and  $\text{H}_2$  (Equation (94)). Formation of intermediate species such as  $\text{MgB}_{12}\text{H}_{12}$  is also implied [382–386].



In fact, an alternative reaction mechanism has been proposed concerning formation of the  $\text{MgB}_{12}\text{H}_{12}$  species in a first step ( $-15 \text{ ppm}$ , singlet, in  $^{11}\text{B}$ -MAS NMR spectrum), dehydrogenation of  $\text{MgH}_2$  in a second step, and a final reaction of Mg and  $\text{MgB}_{12}\text{H}_{12}$  forming  $\text{MgB}_2$ —which we know is the final dehydrogenation “resting-state” of magnesium (Figure 18).

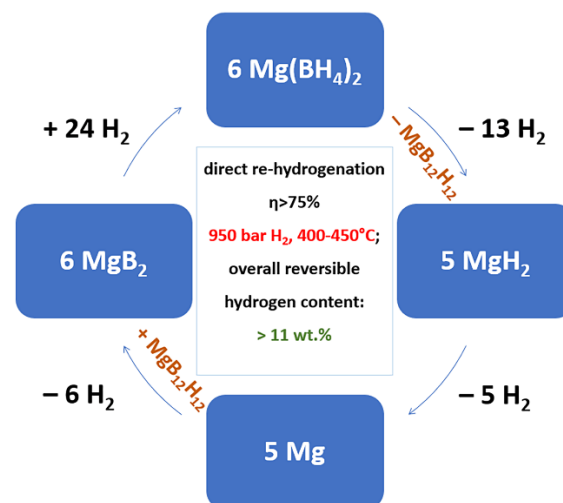


**Figure 18.** Direct re-hydrogenation of  $\text{MgB}_2$  under extreme conditions (950-bar  $\text{H}_2$ ,  $450^\circ\text{C}$ ) to regenerate  $\text{Mg}(\text{BH}_4)_2$  material with  $\sim 11 \text{ wt.}\%$  reversible hydrogen capacity. Figure compiled from reaction data presented in [386].

The decomposition temperature could be lowered to  $100^\circ\text{C}$  by the addition of  $\text{TiCl}_3$  catalyst [109]. Rehydrogenation of  $\text{MgB}_2$  under 100-bar  $\text{H}_2$  at  $350^\circ\text{C}$  showed  $\sim 3 \text{ wt.}\%$

hydrogen capacity, confirming the reversibility of this dehydrogenation step [156,385]. The intermediacy of  $\text{MgB}_{12}\text{H}_{12}$  was investigated, as in the case of other metal borohydrides, and is considered plausible [387].

The first decomposition step (277 °C) has an enthalpy of  $-40 \dots 57$  kJ/mol, depending on experimental data [385,387], and a computed value of 38 kJ/mol (DFT computations) [388]. In situ synchrotron radiation SR-PXD data show as final dehydrogenation products a mixture of Mg, MgO, and  $\text{MgH}_2$ , but these results should be considered with care given the high affinity of Mg for oxygen and proneness to subsequent oxidation [118].

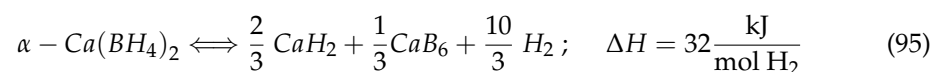
Regeneration of  $\text{Mg}(\text{BH}_4)_2$  by hydrogenation of  $\text{MgB}_2$  requires high  $\text{H}_2$  pressure and temperature (950-bar  $\text{H}_2$ , 400 °C), but also prolonged time (108 h), which makes the bulk material impractical for use in a tank for mobile applications [386]. When starting from nano-sized  $\text{MgB}_2$  synthesized at RT, a partial rehydrogenation to  $\text{Mg}(\text{BH}_4)_2$  occurred at 300 °C and 30-bar  $\text{H}_2$ , leading to a material with 2.9 wt.% hydrogen storage, but quite far off the theoretical value for magnesium borohydride (14.8 wt.%) [389,390].

Another polymorph of magnesium borohydride,  $\gamma\text{-Mg}(\text{BH}_4)_2$ , has recently shown promising results when Co-based additives were used (2 mol%  $\text{CoX}_2$ , X = F, Cl), desorbing 4 wt.%  $\text{H}_2$  at 285 °C and 2.5-bar  $\text{H}_2$  backpressure. The reverse reaction took place at 285 °C, reforming the more stable  $\beta\text{-Mg}(\text{BH}_4)_2$ , but using 120-bar  $\text{H}_2$  was needed to yield a material with 2 wt.% hydrogen storage capacity. In addition, the  $\gamma \implies \epsilon$  phase transition temperature of  $\text{Mg}(\text{BH}_4)_2$  was reduced using  $\text{CoX}_2$  by  $\sim 50$  °C [391,392].

Mg-based materials greatly benefit from nanoconfinement in carbon nanotubes, which reduces the enthalpy of dehydrogenation even by 50% (for  $\text{MgH}_2$ , a reduction from 36 kJ/mol<sub>H</sub> in bulk, to 17 kJ/mol<sub>H</sub> in 9-unit cell thick  $\text{MgH}_2$  thin film slab) [393]. Nanoconfinement of  $\text{Mg}(\text{BH}_4)_2$  in microporous carbon AC resulted in nanocomposites with loadings as high as 44 wt.%, albeit at the cost of partially crystallizing on the outer surface of AC (as seen by powder-XRD and EDS data analysis) [382,383]. The total weight loss of 6 wt.% corresponds to 44% borohydride loading in the nanocomposite [382]. Small angle neutron scattering (SANS) is a technique allowing for the study of particle size and distribution. Using isotopically labeled magnesium borohydride,  $\text{Mg}^{(11}\text{BD}_4)_2@AC$ , Sartori et al. observed nanoconfined borohydride particles of less than 4 nm [383]. Improved hydrogen release is obvious from the shifting of the endothermic peak events from 269 °C to 257 °C ( $-12$  °C decrease) and from 376 °C to 317 °C ( $-50$  °C decrease), and it can be ascribed to the nanoconfinement effect.

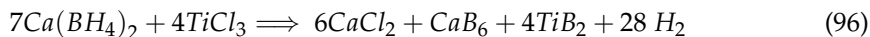
### 7.5. $\text{Ca}(\text{BH}_4)_2$

$\text{Ca}(\text{BH}_4)_2$  has a hydrogen storage capacity of 11.5 wt.% (maximum theoretical capacity), but the real capacity is only 9.6 wt.% considering the actual dehydrogenation reaction (Equations (12) and (95)). Equation (95) is essentially the same as Equation (12), but written for one mol  $\text{Ca}(\text{BH}_4)_2$ , as the reaction is reversible and decomposition and rehydrogenation processes follow the same reaction, having a  $\Delta H = 32$  kJ/mol [188].

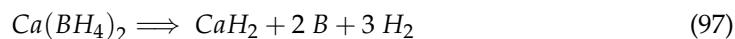


The orthorhombic ( $\alpha$ -phase) can be obtained free of THF solvent by evacuation under vacuum of the commercially available THF adduct. There is another low-temperature orthorhombic phase proposed for  $\text{Ca}(\text{BH}_4)_2$  ( $\gamma$ -phase polymorph) [118]. The decomposition temperatures are higher than those anticipated based on thermodynamic data, partly due to sluggish kinetics [394]. Heating  $\alpha\text{-Ca}(\text{BH}_4)_2$  to 170 °C leads to a phase transition to  $\beta\text{-Ca}(\text{BH}_4)_2$  and upon further heating the DSC scan data shows two endothermic peaks at 360 °C and 500 °C [395,396]. The rehydrogenation of this reversible system can proceed at 400 °C and 690 atm  $\text{H}_2$ , but these conditions are too harsh to warrant the use of bulk  $\text{Ca}(\text{BH}_4)_2$  in vehicular applications [95]. The influence of using catalysts (Nb, Ti) showed beneficial reduction in hydrogen desorption temperature, but the rehydrogenation conditions are far from ideal (350 °C, 150-bar  $\text{H}_2$ , 12–24 h) and the re-hydrogenated material

exhibits 4.5 wt.% H<sub>2</sub> capacity [397]. Using additives like TiCl<sub>3</sub> could lower even further re-hydrogenation kinetics, making it possible when dehydrogenated material was subjected at 350 °C for 24 h at a lower pressure of 90-bar H<sub>2</sub> [394]. Ball-milling Ca(BH<sub>4</sub>)<sub>2</sub> with 5 mol%TiCl<sub>3</sub> (Ca(BH<sub>4</sub>)<sub>2</sub>:TiCl<sub>3</sub> = 1:0.05) leads to hydrogen evolution and formation of CaCl<sub>2</sub>, according to Equation (96) [394].



This is also an example where the additive (TiCl<sub>3</sub>) alters the dehydrogenation pathway (commonly accepted as described by Equation (95)), as the proposed weight-loss based on DSC and TGA curves conform to about 7.1 to 8.7% reduction. This is consistent with the following decomposition pathway, producing CaH<sub>2</sub>, B, and H<sub>2</sub> (7.2 wt.% hydrogen storage capacity based on Equation (97)) [394]. The hydrogen storage capacity after rehydrogenation is only 3.8 wt.%; complete rehydrogenation was thus not achieved. It is, however, apparent that TiCl<sub>3</sub> additive plays an important role in lowering activation energy for the hydrogenation reaction.



A proof-of-concept process for complete hydrogen release/uptake was shown for a ball-milled mixture CaB<sub>6</sub> + 2 CaH<sub>2</sub> + 8 wt.% TiCl<sub>3</sub>/Pd, but the reaction conditions were harsh (700-bar H<sub>2</sub>, 400–440 °C); however, almost complete recyclability with 9.6 wt.% hydrogen storage has been demonstrated [95]. A key role in this achievement is thought to be played by the deposition of TiCl<sub>3</sub> on porous Pd, which is itself known for absorbing record amounts of hydrogen and giving interstitial hydrides, while other TM halides (RuCl<sub>3</sub>) led to polymorphs of Ca(BH<sub>4</sub>)<sub>2</sub> and other unknown phases, confirming the alteration in the rehydrogenation pathway [95,398].

Nanoconfined Ca(BH<sub>4</sub>)<sub>2</sub> in microporous carbon showed tangible improvements in the recyclability behavior of as-prepared nanocomposites [143]. Using carefully engineered chemically activated micro-mesoporous carbon as scaffolds (specific surface area SSA = 1780 m<sup>2</sup>/g, V<sub>pore</sub>~1 cm<sup>3</sup>/g and 60% microporosity), Comanescu et al. obtained by the incipient wetness method Ca(BH<sub>4</sub>)<sub>2</sub>@MC-a nanocomposites with 36 wt.% borohydride loading (Figure 19).

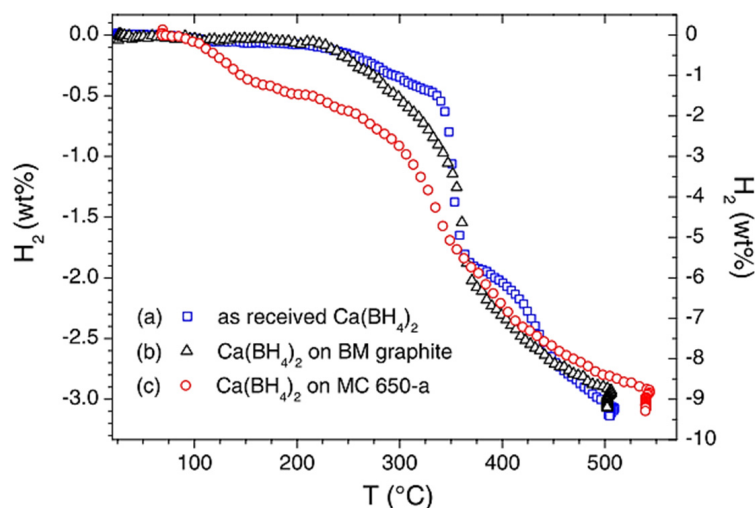


**Figure 19.** TPD curves of Ca(BH<sub>4</sub>)<sub>2</sub>@MC-a nanocomposites with a heating rate of 2.5 °C/min. Reprinted with permission from [143].

These Ca(BH<sub>4</sub>)<sub>2</sub>@MC-a composites started the hydrogen release step at about 100 °C and managed to retain 2.4 wt.% hydrogen capacity even after 18 cycles of hydrogen release/uptake. The rehydrogenation of the desorbed composites needed rather mild

conditions (25–40 atm H<sub>2</sub>, 6.5 h), confirming the important role of the nanoporous scaffold of choice (Figure 20) [143].

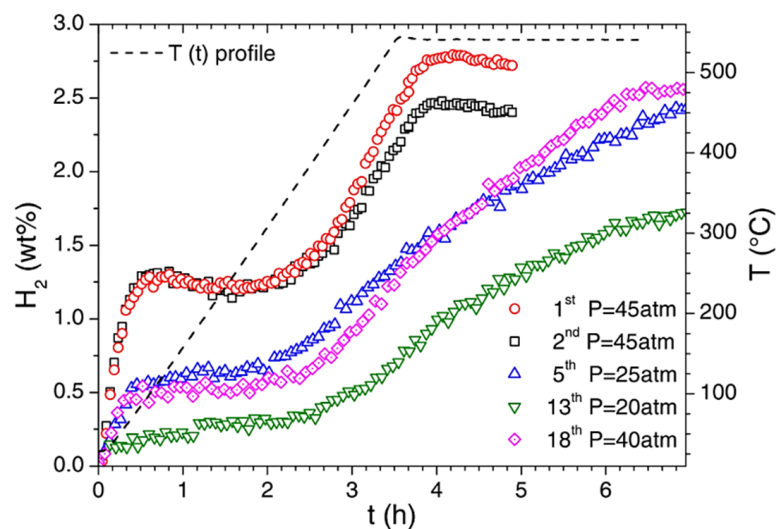
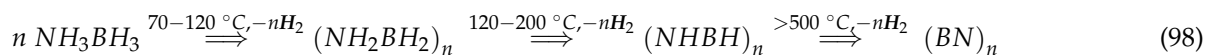


**Figure 20.** TPA curves of nanocomposite Ca.(BH<sub>4</sub>)<sub>2</sub> = MC 650-a for successive hydrogenation cycles at pressures in the range 20–45 atm. Reprinted with permission from [143].

The result obtained for the composite Ca.(BH<sub>4</sub>)<sub>2</sub> = MC 650-a (containing 36 wt.% Ca(BH<sub>4</sub>)<sub>2</sub>) is an improvement over previously reported data on reversibility studies on Ca(BH<sub>4</sub>)<sub>2</sub>, confirming that about 68% of Ca(BH<sub>4</sub>)<sub>2</sub> behaves reversibly [143].

### 7.6. Ammonia Borane NH<sub>3</sub>BH<sub>3</sub>

A special place is reserved to ammonia–borane, an interesting adduct with 19.6 wt.% hydrogen. NH<sub>3</sub>BH<sub>3</sub> (ammonia–borane, AB) and ammonium borohydride (NH<sub>4</sub>BH<sub>4</sub>) have been reported from 1958, but NH<sub>4</sub>BH<sub>4</sub> is far too unstable releasing H<sub>2</sub> at even −40 °C to form AB [399]. NH<sub>3</sub>BH<sub>3</sub> is a stable solid, water-sensitive, and susceptible to oxidation or attack by acidic reagents, having a high solubility in water (33.6 g/100 g H<sub>2</sub>O). The AB molecules present dipole–dipole interactions due to the dihydrogen bonding, i.e., interaction between a hydridic hydrogen (−NH<sub>3</sub>) and an acidic one (BH<sub>3</sub>) [400], and organizes in an orthorhombic phase at low temperature (<225 K) due to these interactions. While it is not a proper metal borohydride, NH<sub>3</sub>BH<sub>3</sub> has the advantageous property of being RT-stable, exhibiting a two-step dehydrogenation at very reasonable temperatures: 114 °C (melting point, 6.5 wt.% H<sub>2</sub> release, forming polyaminoboranes (NH<sub>2</sub>BH<sub>2</sub>)<sub>n</sub>), and 150 °C (remaining H<sub>2</sub> release, formation of polyiminoborane (NHBH)<sub>n</sub>), with the downsides of irreversibility, slow kinetics, and formation of “inorganic benzene” as by-product during dehydrogenation (borazine, *c*-(NHBH)<sub>3</sub>) (Equation (98)). The N-B (nitrogen–boron) units are isoelectronic to C-C (carbon–carbon) moieties, and they can therefore be regarded as hydrocarbon analogues [145,401,402].



Mesoporous silica or carbon have served as scaffolds for NH<sub>3</sub>BH<sub>3</sub> impregnation, and this nano-reduction strategy bypassed borazine formation [145,402,403]. Even NH<sub>3</sub> release is suppressed when Li<sup>+</sup>-based dopants are used [402]. Some key thermodynamic aspects connected to NH<sub>3</sub>BH<sub>3</sub> confinement in nanoporous substrates are summarized in Table 7. A common denominator is that using lower-size pores, the decomposition temperature is decreased due to the lowered activation energy *E*<sub>a</sub> caused by nanoconfinement [404,405].

**Table 7.** Nanoconfinement of ammonia borane in nanoporous silica (MCM-41, SBA-15) or carbon (CMK-3 OMC, RF-CC).

Substance	Scaffold	Scaffold Pore	Loading (wt.%)	$t_d$ (°C)	$E_a$ (kJ/mol)	$\Delta H$ (kJ/mol)	Ref.
NH <sub>3</sub> BH <sub>3</sub>	-	-	100	114 (110), 155	184	−19.6 to −21	[145,406]
NH <sub>3</sub> BH <sub>3</sub>	MCM-41	4 nm	33, 50, 75 (outside pores)	100, 182	N/A	34.09 (2 steps: 30.33 and 3.76)	[404,407]
NH <sub>3</sub> BH <sub>3</sub>	SBA-15	7.5 nm	50	50–100, 130	67	−1	[145]
NH <sub>3</sub> BH <sub>3</sub>	OMC	4.5 nm		(50–)95		−2.1	[402]
NH <sub>3</sub> BH <sub>3</sub>	RF-CC (carbon cryogel)	2–20 (mean 5) nm	24	85–150; 80–90 for CC(exo- peak)	N/A	−120 (CC)	[403,408]
NH <sub>3</sub> BH <sub>3</sub>	AC (activated carbon)	3 nm	17.6 wt.% (computed from pore volume decrease from 0.36 cm <sup>3</sup> /g to 0.14 cm <sup>3</sup> /g for AC@AB <sub>THF</sub> )	3–4; RT(25)	N/A	−1.6 (AC@AB <sub>THF</sub> ), −3.0 (AC@AB <sub>MET</sub> ) and −5.9 (AC@AB <sub>milled</sub> )	[409]
NH <sub>3</sub> BH <sub>3</sub>	MOF (Fe–MIL-53)	11–13 nm	AB:Fe = 6.5% (0.5:1 molar); 13% (1:1 molar)	80–110	130 +/− 7; 135 +/− 3	N/A	[410]

The porosity of the MOF scaffolds (IRMOF-1, IRMOF-10, UiO-66, UiO-67, MIL-52(Al)) for AB nanoconfinement (8.38 wt.%, 3.51 wt.%, 12.95 wt.%, 14.70 wt.%, and 11.26 wt.%, respectively, computed from SI data) has been investigated, showing that AB impregnation does not change MOF crystallinity. A low desorption temperature of 64°C was recorded for AB@UiO-66 (12.95 wt.% loading), which also featured the smallest pore size among investigated MOFs, of only 1.17 nm [411].

The reduction in decomposition temperature of AB@MOF was found to be linearly proportional to the reciprocal of AB size; in other words, the expectations are that a lower pore size nano-restriction would yield the best destabilization in ammonia borane nanocomposites [411].

Another advantage of utilizing SiO<sub>2</sub>-based scaffolds in AB nanoconfinement is that this does not lead to a reaction with the framework, as was the case for typical M(BH<sub>4</sub>)<sub>x</sub>. It is also apparent from Table 7 that 1D-structured mesosilica (MCM-41) are less attractive as scaffolds than 2D-mesostructured silica (SBA-15) of hexagonal pore arrangement, although the pore size might suggest otherwise (4 nm for MCM-41 vs. 7.5 nm for SBA-15). These conclusions could be extended to other borohydride@silica nanosystems as well, and could provide a starting point for further nanoscaffold engineering research. Nanoconfinement alters the dehydrogenation pathway in AB, as utilizing mesoporous carbons like CMK-3 manages to avoid toxic gas evolution; borazine or ammonia are not detected in that case. It can be hypothesized that nanoconfinement might help rehydrogenation by ammonia borane restructuring inside scaffold nanopores, and by lowering activation energies to improve the thermodynamics of hydrogen release/uptake. Some advances have been made by suggesting a methanolysis cycle, where [NH<sub>4</sub>][B(OCH<sub>3</sub>)<sub>4</sub>] and B(OCH<sub>3</sub>)<sub>3</sub> are key intermediates [412]. Complete elucidation of a yet-unclear dehydrogenation mechanism, combined with collaborative theoretical/experimental research efforts, could pave the way to the ultimate hydrogen-storage material.

## 8. Conclusions and Outlook

It has been almost half a century since hydrogen was first considered a renewable energy carrier, aiming at replacing fossil fuel and building up towards a “hydrogen economy” goal. While not without its pitfalls, solid-state hydrogen storage exhibits obvious

advantages compared to the physical storage of H<sub>2</sub> gas: it is safer, requires less extreme conditions for storage and regeneration, and occupies less space.

Among various metal hydrides, metal borohydrides have inherited structural flexibility, accommodating both mixed cations and anion substitutions, and can be tailored towards multi-functional materials. Borohydrides can be engineered to form novel composites that reversibly store hydrogen chemically, reaching very good hydrogen storage capacities, in line with the DOE's expectations for the near future. Recent studies conducted under high temperature and pressure (hydrogen, diborane) have shed new light on mechanistic aspects regarding formation and decomposition pathways of complex metal borohydrides.

Very recent progress on alkali metal borohydrides is directed towards controlling the kinetics of hydrogen production by utilizing nanoporous silica and carbon, Co-based catalysts, bimetallic catalysts (NiPt, NiCo<sub>9</sub>, RuPd, Co-Ru) and nano-catalyst composites, or harnessing the latent potential in alcoholysis (methanolysis, in particular) of said metal borohydrides. Kinetic studies on metal borohydrides currently target PEM fuel cell applications, and have shown that the hydrolysis mechanism has as a rate-limiting step the splitting of the H-OH bond. Transition metal nanoparticles (Ni, Pt, Zr, Co, Mn, Cu), mixed-valence oxides (Co<sub>3</sub>O<sub>4</sub>), transition metal complexes (of Ru<sup>3+</sup>, for instance), and MOFs have shown controlled hydrolysis of alkali metal borohydrides. Engineered catalysts (Mg<sub>95</sub>Ni<sub>5</sub>) have managed to suppress ammonia release from borohydride ammoniates by improving hydrogen release at very reasonable temperatures (70–80 °C). Exploring new decomposition pathways of such ligand-stabilized borohydrides has also gained new momentum. Divalent metal borohydrides stabilized by neutral molecules show high ionic conductivity and a real promise for use in solid-state batteries. The rich boron–hydrogen chemistry, together with the open channels of closo-structured borohydrides (B<sub>10</sub>H<sub>10</sub><sup>2-</sup>, B<sub>12</sub>H<sub>12</sub><sup>2-</sup>), currently make research on closo-borate salts of alkali and alkali-earth metals a hot topic in ionic conductivity for solid-state electrolytes. Direct borohydride fuel cell (DBFC) and direct borohydride–hydrogen peroxide fuel cell (DBHPFC) systems research has expanded recently towards high-performance applications aimed at space exploration, by harnessing the power of nanoparticle catalysis (Ni, Cu, or bimetallic PdFe, PdAg, PdAu) to control the resultant power density. Various destabilization strategies of borohydride compounds have now included novel catalyst systems and complementary in-depth mechanistic insights. Nanostructuring of employed catalysts for hydrolysis reactions or de-/redhydrogenation studies has confirmed a positive effect by lowering activation energies associated with individual mechanistic steps. The porous polymorph of Mg(BH<sub>4</sub>)<sub>2</sub> has gained attention recently by involvement in a core-shell, oxidation-resistant nanostructure (γ-Mg(BH<sub>4</sub>)<sub>2</sub>@MgCl<sub>2</sub>) to afford dehydrogenation onset as low as 100 °C. Theoretical computations on ternary borohydride materials (K<sub>2</sub>B<sub>2</sub>H<sub>8</sub>) predict superconducting properties at high pressures and around 140 K. Fundamental research is constantly expanding the class of structurally characterized metal borohydrides with new members (Th(BH<sub>4</sub>)<sub>4</sub> is a new addition from 2021), while more cost-effective and high-yielding synthesis routes emerge—the synthesis of NaBH<sub>4</sub> was reported by milling sodium tetraborate with Al and NaH as additive.

Meeting targets related to performance range, refueling time, car performance, and passenger space and safety are at the forefront of development of novel hydrogen storage materials and material-based storage system technologies. Mobile applications and vehicular applications in particular could receive a new breath of life when a proper hydride-based material is engineered by scientists, in line with safety, performance, and cost estimation goals.

**Funding:** This work was supported by the Romanian Ministry of Research and Innovation through the Core Program PN19-03 (contract no. PN21N/2019), PN-III-P2-2.1-PED-2019-4816 within PNCD III, and Project No. PN-III-P1-1.1-TE-2021-1657.

**Institutional Review Board Statement:** Not applicable.

**Informed Consent Statement:** Not applicable.

**Data Availability Statement:** Not applicable.

**Conflicts of Interest:** The author declares that there are no commercial or financial relationships that could be considered as a potential conflict of interest.

## References

1. Yue, M.; Lambert, H.; Pahon, E.; Roche, R.; Jemei, S.; Hissel, D. Hydrogen energy systems: A critical review of technologies, applications, trends and challenges. *Renew. Sustain. Energ. Rev.* **2021**, *146*, 111180. [CrossRef]
2. Abe, J.O.; Popoola, A.P.I.; Ajenifuja, E.; Popoola, O.M. Hydrogen energy, economy and storage: Review and recommendation. *Int. J. Hydrogen Energy* **2019**, *44*, 15072–15086. [CrossRef]
3. Lai, Q.W.; Sun, Y.H.; Wang, T.; Modi, P.; Cazorla, C.; Demirci, U.B.; Ares Fernandez, J.R.; Leardini, F.; Aguey-Zinsou, K.F. How to design hydrogen storage materials? Fundamentals, synthesis, and storage tanks. *Adv. Sustain. Syst.* **2019**, *3*, 1900043. [CrossRef]
4. Ong, B.C.; Kamarudin, S.K.; Basri, S. Direct liquid fuel cells: A review. *Int. J. Hydrogen Energy* **2017**, *42*, 10142–10157. [CrossRef]
5. Mohtadi, R.; Orimo, S.I. The renaissance of hydrides as energy materials. *Nat. Rev. Mater.* **2017**, *2*, 16091. [CrossRef]
6. Veras, T.D.; Mozer, T.S.; dos Santos, D.D.R.M.; Cesar, A.D. Hydrogen: Trends, production and characterization of the main process worldwide. *Int. J. Hydrogen Energy* **2017**, *42*, 2018–2033. [CrossRef]
7. He, T.; Pachfule, P.; Wu, H.; Xu, Q.; Chen, P. Hydrogen carriers. *Nat. Rev. Mater.* **2016**, *1*, 16067. [CrossRef]
8. Lai, Q.W.; Paskevicius, M.; Sheppard, D.A.; Buckley, C.E.; Thornton, A.W.; Hill, M.R.; Gu, Q.F.; Mao, J.F.; Huang, Z.G.; Liu, H.K.; et al. Hydrogen storage materials for mobile and stationary applications: Current state of the art. *ChemSusChem* **2015**, *8*, 2789–2825. [CrossRef] [PubMed]
9. Huang, Y.J.; Cheng, Y.H.; Zhang, J.Y. A review of high density solid hydrogen storage materials by pyrolysis for promising mobile applications. *Ind. Eng. Chem. Res.* **2021**, *60*, 2737–2771. [CrossRef]
10. Schüth, F.; Bogdanović, B.; Felderhoff, M. Light metal hydrides and complex hydrides for hydrogen storage. *Chem. Commun.* **2004**, *20*, 2249–2258. [CrossRef]
11. Schneemann, A.; White, J.L.; Kang, S.Y.; Jeong, S.; Wan, L.F.; Cho, E.S.; Heo, T.W.; Prendergast, D.; Urban, J.J.; Wood, B.C.; et al. Nanostructured metal hydrides for hydrogen storage. *Chem. Rev.* **2018**, *118*, 10775–10839. [CrossRef]
12. Grahame, A.; Aguey-Zinsou, K.F. properties and applications of metal (M) dodecahydro-closo-dodecaborates ( $M_{n=1,2}B_{12}H_{12}$ ) and their implications for reversible hydrogen storage in the borohydrides. *Inorganics* **2018**, *6*, 106. [CrossRef]
13. Wang, K.; Pan, Z.X.; Yu, X.B. Metal B-N-H hydrogen-storage compound: Development and perspectives. *J. Alloys Compd.* **2019**, *794*, 303–324. [CrossRef]
14. Kumar, R.; Karkamkar, A.; Bowden, M.; Autrey, T. Solid-state hydrogen rich boron-nitrogen compounds for energy storage. *Chem. Soc. Rev.* **2019**, *48*, 5350–5380. [CrossRef]
15. Ley, M.B.; Jepsen, L.H.; Lee, Y.S.; Cho, Y.W.; von Colbe, J.M.B.; Dornheim, M.; Rokni, M.; Jensen, J.O.; Sloth, M.; Filinchuk, Y.; et al. Complex hydrides for hydrogen storage—New perspectives. *Mater. Today* **2014**, *17*, 122–128. [CrossRef]
16. Ouyang, L.Z.; Chen, K.; Jiang, J.; Yang, X.S.; Zhu, M. Hydrogen storage in light-metal based systems: A review. *J. Alloys Compd.* **2020**, *829*, 154597. [CrossRef]
17. Singh, R.; Altaee, A.; Gautam, S. Nanomaterials in the advancement of hydrogen energy storage. *Heliyon* **2020**, *6*, e04487. [CrossRef]
18. Santos, D.M.F.; Sequeira, C.A.C. Sodium borohydride as a fuel for the future. *Renew. Sustain. Energ. Rev.* **2011**, *15*, 3980–4001. [CrossRef]
19. Available online: <https://www.energy.gov/eere/fuelcells/doe-technical-targets-onboard-hydrogen-storage-light-duty-vehicles> (accessed on 31 January 2022).
20. Available online: [https://www.energy.gov/sites/default/files/2017/05/f34/fcto\\_targets\\_onboard\\_hydro\\_storage\\_explanation.pdf](https://www.energy.gov/sites/default/files/2017/05/f34/fcto_targets_onboard_hydro_storage_explanation.pdf) (accessed on 31 January 2022).
21. Paskevicius, M.; Jepsen, L.H.; Schouwink, P.; Cerny, R.; Ravnsbæk, D.B.; Filinchuk, Y.; Dornheim, M.; Besenbacher, F.; Jensen, T.R. Metal borohydrides and derivatives—Synthesis, structure and properties. *Chem. Soc. Rev.* **2017**, *46*, 1565–1634. [CrossRef] [PubMed]
22. Abdelhamid, H.N. A review on hydrogen generation from the hydrolysis of sodium borohydride. *Int. J. Hydrogen Energy* **2021**, *46*, 726–765. [CrossRef]
23. Liu, X.; Zhang, X.Y.; Li, D.S.; Zhang, S.Q.; Zhang, Q.C. Recent advances in the “on-off” approaches for on-demand liquid-phase hydrogen evolution. *J. Mater. Chem. A* **2021**, *9*, 18164–18174. [CrossRef]
24. Nunes, H.X.; Silva, D.L.; Rangel, C.M.; Pinto, A.M.F.R. Rehydrogenation of sodium borates to close the  $NaBH_4-H_2$  cycle: A review. *Energies* **2021**, *14*, 3567. [CrossRef]
25. Gras, M.; Lota, G. Control of hydrogen release during borohydride electrooxidation with porous carbon materials. *RSC Adv.* **2021**, *11*, 15639–15655. [CrossRef]
26. Yao, Q.L.; Ding, Y.Y.; Lu, Z.H. Noble-metal-free nanocatalysts for hydrogen generation from boron- and nitrogen-based hydrides. *Inorg. Chem. Front.* **2020**, *7*, 3837–3874. [CrossRef]
27. Deng, J.F.; Chen, S.P.; Wu, X.J.; Zheng, J.; Li, X.G. Recent progress on materials for hydrogen generation via hydrolysis. *J. Inorg. Mater.* **2021**, *36*, 1–8. [CrossRef]
28. Dionne, M.; Hao, S.; Gambarotta, S. Preparation and characterization of a new series of Cr(II) hydroborates. *Can. J. Chem.* **1995**, *73*, 1126–1134. [CrossRef]

29. Nöth, H.; Seitz, M. Preparation and characterization of chromium(ii) tetrahydroborate-tetrahydrofuran (1/2). *J. Chem. Soc. Chem. Commun.* **1976**, *24*, 1004a. [CrossRef]
30. Soulie, J.P.; Renaudin, G.; Cerny, R.; Yvon, K. Lithium borohydride LiBH<sub>4</sub> I. Crystal structure. *J. Alloys Compd.* **2002**, *346*, 200–205. [CrossRef]
31. Puzskiel, J.; Gasnier, A.; Amica, G.; Gennari, F. Tuning LiBH<sub>4</sub> for hydrogen storage: Destabilization, additive, and nanoconfinement approaches. *Molecules* **2020**, *25*, 163. [CrossRef]
32. Skripov, A.V.; Soloninin, A.V.; Babanova, O.A.; Skoryunov, R.V. Anion and cation dynamics in polyhydroborate salts: NMR studies. *Molecules* **2020**, *25*, 2940. [CrossRef] [PubMed]
33. Le, T.T.; Pistidda, C.; Nguyen, V.H.; Singh, P.; Raizada, P.; Klassen, T.; Dornheim, M. Nanoconfinement effects on hydrogen storage properties of MgH<sub>2</sub> and LiBH<sub>4</sub>. *Int. J. Hydrogen Energy* **2021**, *46*, 23723–23736. [CrossRef]
34. Skoryunov, R.V.; Babanova, O.A.; Soloninin, A.V.; Grinderslev, J.B.; Skripov, A.V.; Jensen, T.R. Dynamical properties of lithium borohydride-ammine composite LiBH<sub>4</sub>.NH<sub>3</sub>: A nuclear magnetic resonance study. *J. Alloys Compd.* **2022**, *894*, 162446. [CrossRef]
35. Ye, J.K.; Xia, G.L.; Yu, X.B. In-situ constructed destabilization reaction of LiBH<sub>4</sub> wrapped with graphene toward stable hydrogen storage reversibility. *Mater. Today Energy* **2021**, *22*, 100885. [CrossRef]
36. Yang, G.Y.; Xie, C.; Li, Y.T.; Li, H.W.; Liu, D.M.; Chen, J.G.; Zhang, Q.G. Enhancement of the ionic conductivity of lithium borohydride by silica supports. *Dalton Trans.* **2021**, *50*, 15352–15358. [CrossRef] [PubMed]
37. De Kort, L.M.; Gulino, V.; de Jongh, P.E.; Ngene, P. Ionic conductivity in complex metal hydride-based nanocomposite materials: The impact of nanostructuring and nanocomposite formation. *J. Alloys Compd.* **2022**, *901*, 163474. [CrossRef]
38. Zhang, Q.; Gao, Z.Q.; Shi, X.M.; Zhang, C.; Liu, K.; Zhang, J.; Zhou, L.; Ma, C.J.; Du, Y.P. Recent advances on rare earths in solid lithium ion conductors. *J. Rare Earths* **2021**, *39*, 1–10. [CrossRef]
39. Bogdanovic, B.; Schwickardi, M. Ti-doped alkali metal aluminium hydrides as potential novel reversible hydrogen storage materials. *J. Alloys Compd.* **1997**, *253*, 1–9. [CrossRef]
40. Schlesinger, H.I.; Sanderson, R.T.; Burg, A.B. A volatile compound of aluminum, boron and hydrogen. *J. Am. Chem. Soc.* **1939**, *61*, 536. [CrossRef]
41. Ravnsbæk, D.B.; Filinchuk, Y.; Cerenius, Y.; Jakobsen, H.J.; Besenbacher, F.; Skibsted, J.; Jensen, T.R. A series of mixed-metal borohydrides. *Angew. Chem. Int. Ed.* **2009**, *48*, 6659–6663. [CrossRef] [PubMed]
42. Hagemann, H.; Cerny, R. Synthetic approaches to inorganic borohydrides. *Dalton Trans.* **2010**, *39*, 6006–6012. [CrossRef]
43. Wang, T.; Aguey-Zinsou, K.F. Synthesis of borohydride nanoparticles at room temperature by precipitation. *Int. J. Hydrogen Energy* **2021**, *46*, 24286–24292. [CrossRef]
44. Suarez-Alcantara, K.; Garcia, J.R.T. Metal borohydrides beyond groups I and II: A review. *Materials* **2021**, *14*, 2561. [CrossRef] [PubMed]
45. Cerny, R.; Brighi, M.; Murgia, F. The crystal chemistry of inorganic hydroborates. *Chemistry* **2020**, *2*, 53. [CrossRef]
46. Gu, T.T.; Gu, J.; Zhang, Y.; Ren, H. Metal borohydride-based system for solid-state hydrogen storage. *Prog. Chem.* **2020**, *32*, 665–686. [CrossRef]
47. Suryanarayana, C. Mechanical alloying and milling. *Prog. Mater. Sci.* **2001**, *46*, 1–184. [CrossRef]
48. Dornheim, M.; Eigen, N.; Barkhordarian, G.; Klassen, T.; Bormann, R. Tailoring hydrogen storage materials towards application. *Adv. Eng. Mater* **2006**, *8*, 377–385. [CrossRef]
49. Eigen, N.; Keller, C.; Dornheim, M.; Klassen, T.; Bormann, R. Industrial production of light metal hydrides for hydrogen storage. *Scr. Mater.* **2007**, *56*, 847–851. [CrossRef]
50. Hassan, I.A.; Ramadan, H.S.; Saleh, M.A.; Hissel, D. Hydrogen storage technologies for stationary and mobile applications: Review, analysis and perspectives. *Renew. Sustain. Energ. Rev.* **2021**, *149*, 111311. [CrossRef]
51. Takacs, L. Self-sustaining reactions induced by ball milling. *Prog. Mater. Sci.* **2002**, *47*, 355–414. [CrossRef]
52. Balema, V.P.; Wiench, J.W.; Pruski, M.; Pecharsky, V.K. Solvent-free mechanochemical synthesis of phosphonium salts. *Chem. Commun.* **2002**, *7*, 724–725. [CrossRef]
53. Pistidda, C.; Santhosh, A.; Jerabek, P.; Shang, Y.Y.; Girella, A.; Milanese, C.; Dore, M.; Garroni, S.; Bordignon, S.; Chierotti, M.R.; et al. Hydrogenation via a low energy mechanochemical approach: The MgB<sub>2</sub> case. *J. Phys. Energy* **2021**, *3*, 044001. [CrossRef]
54. Balema, V.P. Mechanical processing in hydrogen storage research and development. *Mater. Matter.* **2007**, *2*, 16–18. Available online: <https://www.sigmaaldrich.com/deepweb/assets/sigmaaldrich/marketing/global/documents/190/337/material-matters-v2n2.pdf> (accessed on 31 January 2022). [CrossRef]
55. Bateni, A.; Scherpe, S.; Acar, S.; Somer, M. Novel approach for synthesis of Magnesium Borohydride, Mg(BH<sub>4</sub>)<sub>2</sub>. *Energy Procedia* **2012**, *29*, 26–33. [CrossRef]
56. Xu, D.Y.; Zhang, Y.; Guo, Q.J. Research progress on catalysts for hydrogen generation through sodium borohydride alcoholysis. *Int. J. Hydrogen Energy* **2022**, *47*, 5929–5946. [CrossRef]
57. Ouyang, L.Z.; Jiang, J.; Chen, K.; Zhu, M.; Liu, Z.W. Hydrogen production via hydrolysis and alcoholysis of light metal-based materials: A review. *Nano-Micro Lett.* **2021**, *13*, 134. [CrossRef] [PubMed]
58. Al-Msrhad, T.M.H.; Devrim, Y.; Uzundurukan, A.; Budak, Y. Investigation of hydrogen production from sodium borohydride by carbon nano tube-graphene supported PdRu bimetallic catalyst for PEM fuel cell application. *Int. J. Energy Res.* **2021**. [CrossRef]
59. Faghihi, M.; Akbarbandari, F.; Zabihi, M.; Pazouki, M. Synthesis and characterization of the magnetic supported metal-organic framework catalysts (CuCoBTC@MAC and CuBTC@MAC) for the hydrogen production from sodium borohydride. *Mater. Chem. Phys.* **2021**, *267*, 124599. [CrossRef]

60. Schlesinger, H.I.; Brown, H.C.; Hyde, E.K. The preparation of other borohydrides by metathetical reactions utilizing the alkali metal borohydrides. *J. Am. Chem. Soc.* **1953**, *75*, 209–213. [[CrossRef](#)]
61. Schlesinger, H.I.; Brown, H.C.; Hoekstra, H.R.; Rapp, L.R. Reactions of diborane with alkali metal hydrides and their addition compounds. New syntheses of borohydrides. Sodium and potassium borohydrides. *J. Am. Chem. Soc.* **1953**, *75*, 199–204. [[CrossRef](#)]
62. Schlesinger, H.I.; Brown, H.C.; Finholt, A.E. The preparation of sodium borohydride by the high temperature reaction of sodium hydride with borate esters. *J. Am. Chem. Soc.* **1953**, *75*, 205–209. [[CrossRef](#)]
63. Schlesinger, H.I.; Brown, H.C. Uranium(IV) Borohydride. *J. Am. Chem. Soc.* **1953**, *75*, 219–221. [[CrossRef](#)]
64. Payandeh Gharibdoust, S.; Heere, M.; Nervi, C.; Sørby, M.H.; Hauback, B.C.; Jensen, T.R. Synthesis, structure, and polymorphic transitions of praseodymium(III) and neodymium(III) borohydride, Pr(BH<sub>4</sub>)<sub>3</sub> and Nd(BH<sub>4</sub>)<sub>3</sub>. *Dalt. Trans.* **2018**, *47*, 8307–8319. [[CrossRef](#)] [[PubMed](#)]
65. Frommen, C.; Aliouane, N.; Deledda, S.; Fonneløp, J.E.; Grove, H.; Lieutenant, K.; Llamas-Jansa, I.; Sartori, S.; Sørby, M.H.; Hauback, B.C. Crystal structure, polymorphism, and thermal properties of yttrium borohydride Y(BH<sub>4</sub>)<sub>3</sub>. *J. Alloys Compd.* **2010**, *496*, 710–716. [[CrossRef](#)]
66. Yang, C.H.; Tsai, W.T.; Chang, J.K. Hydrogen desorption behavior of vanadium borohydride synthesized by modified mechanochemical process. *Int. J. Hydrogen Energy* **2011**, *36*, 4993–4999. [[CrossRef](#)]
67. Ravnsbæk, D.B.; Filinchuk, Y.; Cerny, R.; Ley, M.B.; Haase, D.; Jakobsen, H.J.; Skibsted, J.; Jensen, T.R. Thermal polymorphism and decomposition of Y(BH<sub>4</sub>)<sub>3</sub>. *Inorg. Chem.* **2010**, *49*, 3801–3809. [[CrossRef](#)]
68. Sato, T.; Miwa, K.; Nakamori, Y.; Ohoyama, K.; Li, H.; Noritake, T.; Aoki, M.; Towata, S.I.; Orimo, S.I. Experimental and computational studies on solvent-free rare-earth metal borohydrides R(BH<sub>4</sub>)<sub>3</sub> (R=Y, Dy, and Gd). *Phys. Rev. B* **2008**, *77*, 104114. [[CrossRef](#)]
69. Wegner, W.; Jaron, T.; Grochala, W. Polymorphism and hydrogen discharge from holmium borohydride, Ho(BH<sub>4</sub>)<sub>3</sub>, and KHo(BH<sub>4</sub>)<sub>4</sub>. *Int. J. Hydrogen Energy* **2014**, *39*, 20024–20030. [[CrossRef](#)]
70. Wegner, W.; Jaron, T.; Grochala, W. Preparation of a series of lanthanide borohydrides and their thermal decomposition to refractory lanthanide borides. *J. Alloys Compd.* **2018**, *744*, 57–63. [[CrossRef](#)]
71. Andrade-Gamboa, J.; Puzkiel, J.A.; Fernández-Albanesi, L.; Gennari, F.C. A novel polymorph of gadolinium tetrahydroborate produced by mechanical milling. *Int. J. Hydrogen Energy* **2010**, *35*, 10324–10328. [[CrossRef](#)]
72. Ley, M.B.; Paskevicius, M.; Schouwink, P.; Richter, B.; Sheppard, D.A.; Buckley, C.E.; Jensen, T.R. Novel solvates M(BH<sub>4</sub>)<sub>3</sub>S(CH<sub>3</sub>)<sub>2</sub> and properties of halide-free M(BH<sub>4</sub>)<sub>3</sub> (M = Y or Gd). *Dalton Trans.* **2014**, *43*, 13333–13342. [[CrossRef](#)]
73. Grinderslev, J.B.; Møller, K.T.; Bremholm, M.; Jensen, T.R. Trends in synthesis, crystal structure, and thermal and magnetic properties of rare-earth metal borohydrides. *Inorg. Chem.* **2019**, *58*, 5503–5517. [[CrossRef](#)] [[PubMed](#)]
74. Jaron, T.; Grochala, W. Y(BH<sub>4</sub>)<sub>3</sub>—An old–new ternary hydrogen store *akalearning* from a multitude of failures. *Dalton Trans.* **2010**, *39*, 160–166. [[CrossRef](#)] [[PubMed](#)]
75. Lee, Y.-S.; Shim, J.-H.; Cho, Y.W. Polymorphism and thermodynamics of Y(BH<sub>4</sub>)<sub>3</sub> from first principles. *J. Phys. Chem. C* **2010**, *114*, 12833–12837. [[CrossRef](#)]
76. Yan, Y.; Li, H.W.; Sato, T.; Umeda, N.; Miwa, K.; Towata, S.; Orimo, S. Dehydrogenating and rehydrogenating properties of yttrium borohydride Y(BH<sub>4</sub>)<sub>3</sub> prepared by liquid-phase synthesis. *Int. J. Hydrogen Energy* **2009**, *34*, 5732–5736. [[CrossRef](#)]
77. Haaland, A.; Shorokhov, D.J.; Tutukin, A.V.; Volden, H.V.; Swang, O.; McGrady, G.S.; Kaltsoyannis, N.; Downs, A.J.; Tang, C.Y.; Turner, J.F.C. Molecular structures of two metal tetrakis(tetrahydroborates), Zr(BH<sub>4</sub>)<sub>4</sub> and U(BH<sub>4</sub>)<sub>4</sub>: Equilibrium conformations and barriers to internal rotation of the triply bridging BH<sub>4</sub> groups. *Inorg. Chem.* **2002**, *41*, 6646–6655. [[CrossRef](#)] [[PubMed](#)]
78. Banks, R.H.; Edelstein, N.M. Synthesis and Characterization of Protactinium(IV), Neptunium(IV), and Plutonium (IV) Borohydrides. In *Lanthanide and Actinide Chemistry and Spectroscopy*; American Chemical Society Publications: Washington, DC, USA, 1980; pp. 331–348. [[CrossRef](#)]
79. Rajnak, K.; Gamp, E.; Shinomoto, R.; Edelstein, N. Optical and magnetic properties of uranium borohydride and tetrakis(methyl)borohydride. *J. Chem. Phys.* **1984**, *80*, 5942–5950. [[CrossRef](#)]
80. Banks, R.H.; Edelstein, N.M.; Rietz, R.R.; Templeton, D.H.; Zalkin, A. Preparation and properties of the actinide borohydrides: Protactinium(IV), neptunium(IV), and plutonium(IV) borohydrides. *J. Am. Chem. Soc.* **1978**, *100*, 1957–1958. [[CrossRef](#)]
81. Desch, C.H. *Henry Louis Le Chatelier, 1850–1936*; Royal Society: London, UK, 1938; Volume 2, pp. 250–259. [[CrossRef](#)]
82. Atkins, P.; de Paula, J. *Physical Chemistry*, 8th ed.; Chemical Equilibrium; Oxford University Press: Oxford, UK, 2006; ISBN 0716787598.
83. Aldridge, S.; Blake, A.J.; Downs, A.J.; Gould, R.O.; Parsons, S.; Pulham, C.R. Some tetrahydroborate derivatives of aluminium: Crystal structures of dimethylaluminium tetrahydroborate and the  $\alpha$  and  $\beta$  phases of aluminium tris(tetrahydroborate) at low temperature. *J. Chem. Soc. Dalton Trans.* **1997**, *6*, 1007–1012. [[CrossRef](#)]
84. Downs, A.J.; Thomas, P.D.P. Gallium borohydrides: The synthesis and properties of HGa(BH<sub>4</sub>)<sub>2</sub>. *J. Chem. Soc. Chem. Commun.* **1976**, *20*, 825–827. [[CrossRef](#)]
85. Pulham, C.R.; Brain, P.T.; Downs, A.J.; Rankin, D.W.H.; Robertson, H.E. Gallaborane, H<sub>2</sub>Ga( $\mu$ -H)<sub>2</sub>BH<sub>2</sub>: Synthesis, properties, and structure of the gaseous molecule as determined by electron diffraction. *J. Chem. Soc. Chem. Commun.* **1990**, *2*, 177–178. [[CrossRef](#)]
86. Wiberg, E.; Nöth, H. Notizen: Über Wasserstoff-Verbindungen des Indiums. *Z. Naturforsch. B* **1957**, *12*, 59–60. [[CrossRef](#)]
87. Wiberg, E.; Dittmann, O.; Nöth, H.; Schmidt, M. Notizen: Über Wasserstoff-Verbindungen des Thalliums. V. Zur Kenntnis eines Thallium(I)-boranats TlBH<sub>4</sub> und Thallium(I)-alanats TlAlH<sub>4</sub>. *Z. Naturforsch. B* **1957**, *12*, 62–63. [[CrossRef](#)]

88. Wiberg, E.; Nöth, H. Notizen: Über Wasserstoff-Verbindungen des Thalliums. VI. Zur Kenntnis eines Thallium(III)-boranats  $\text{TlCl}(\text{BH}_4)_2$ . *Z. Naturforsch. B* **1957**, *12*, 63–65.
89. Mosegaard, L.; Møller, B.; Jørgensen, J.; Filinchuk, Y.; Cerenius, Y.; Hanson, J.C.; Dimasi, E.; Besenbacher, F.; Jensen, T.R. Reactivity of  $\text{LiBH}_4$ : In Situ Synchrotron Radiation Powder X-ray Diffraction Study. *J. Phys. Chem. C* **2008**, *112*, 1299–1303. [[CrossRef](#)]
90. Goerrig, D. Verfahren zur Herstellung von Boranaten. German Patent No. DE 000001077644 A, 17 March 1960.
91. Friedrichs, O.; Buchter, F.; Zwicky, C.N.; Borgschulte, A.; Remhof, A.; Mauron, P.; Biemann, M.; Züttel, A. Direct synthesis of  $\text{Li}[\text{BH}_4]$  and  $\text{Li}[\text{BD}_4]$  from the elements. *Acta Mater.* **2008**, *56*, 949–954. [[CrossRef](#)]
92. Barkhodarian, G.; Klassen, T.; Dornheim, M.; Bormann, R. Unexpected kinetic effect of  $\text{MgB}_2$  in reactive hydride composites containing complex borohydrides. *J. Alloys Compd.* **2007**, *440*, L18–L21. [[CrossRef](#)]
93. Friedrichs, O.; Remhof, A.; Borgschulte, A.; Buchter, F.; Orimo, S.I.; Züttel, A. Breaking the passivation—the road to a solvent free borohydride synthesis. *Phys. Chem. Chem. Phys.* **2010**, *12*, 10919–10922. [[CrossRef](#)] [[PubMed](#)]
94. Barkhodarian, G.; Jensen, T.R.; Doppiu, S.; Bosenberg, U.; Borgschulte, A.; Gremaud, R.; Cerenius, Y.; Dornheim, M.; Klassen, T.; Bormann, R. Formation of  $\text{Ca}(\text{BH}_4)_2$  from Hydrogenation of  $\text{CaH}_2+\text{MgB}_2$  Composite. *J. Phys. Chem. C* **2008**, *112*, 2743–2749. [[CrossRef](#)]
95. Ronnebro, E.; Majzoub, E.H. Calcium borohydride for hydrogen storage: Catalysis and reversibility. *J. Phys. Chem. B* **2007**, *111*, 12045–12047. [[CrossRef](#)]
96. Yan, Y.; Rentsch, D.; Remhof, A. Controllable decomposition of  $\text{Ca}(\text{BH}_4)_2$  for reversible hydrogen storage. *Phys. Chem. Chem. Phys.* **2017**, *19*, 7788–7792. [[CrossRef](#)]
97. Pinkerton, F.E.; Meyer, M.S. Reversible hydrogen storage in the lithium borohydride—Calcium hydride coupled system. *J. Alloys Compd.* **2008**, *464*, L1–L4. [[CrossRef](#)]
98. Sahle, C.J.; Sternemann, C.; Giacobbe, C.; Yan, Y.; Weis, C.; Harder, M.; Forov, Y.; Spiekermann, G.; Tolan, M.; Krisch, M.; et al. Formation of  $\text{CaB}_6$  in the thermal decomposition of the hydrogen storage material  $\text{Ca}(\text{BH}_4)_2$ . *Phys. Chem. Chem. Phys.* **2016**, *18*, 19866–19872. [[CrossRef](#)] [[PubMed](#)]
99. Castilla-Martinez, C.A.; Moury, R.; Ould-Amara, S.; Demirci, U.B. Destabilization of boron-based compounds for hydrogen storage in the solid-state: Recent advances. *Energies* **2021**, *14*, 7003. [[CrossRef](#)]
100. Rongeat, C.; D’Anna, V.; Hagemann, H.; Borgschulte, A.; Züttel, A.; Schultz, L.; Gutfleisch, O. Effect of additives on the synthesis and reversibility of  $\text{Ca}(\text{BH}_4)_2$ . *J. Alloys Compd.* **2010**, *493*, 281–287. [[CrossRef](#)]
101. Nakamori, Y.; Li, H.W.; Kikuchi, K.; Aoki, M.; Miwa, K.; Towata, S.; Orimo, S. Thermodynamical stabilities of metal-borohydrides. *J. Alloys Compd.* **2007**, *446–447*, 296–300. [[CrossRef](#)]
102. Schlesinger, H.I.; Brown, H.C. Metallo Borohydrides. III. Lithium borohydride. *J. Am. Chem. Soc.* **1940**, *62*, 3429–3435. [[CrossRef](#)]
103. Kollonitsch, J.; Fuchs, O. Preparation of aluminium borohydride and its applications in organic reductions. *Nature* **1955**, *176*, 1081. [[CrossRef](#)]
104. Brown, H.C.; Choi, Y.M.; Narasimhan, S. Addition compounds of alkali metal hydrides. 22. Convenient procedures for the preparation of lithium borohydride from sodium borohydride and borane-dimethyl sulfide in simple ether solvents. *Inorg. Chem.* **1982**, *21*, 3657–3661. [[CrossRef](#)]
105. Rittmeyer, P.; Wietelmann, U. *Ullmann’s Encyclopaedia of Industrial Chemistry*; Wiley-VCH: Weinheim, Germany, 2000.
106. Cerny, R.; Filinchuk, Y.; Hagemann, H.; Yvon, K. Magnesium borohydride: Synthesis and crystal structure. *Angew. Chem. Int. Ed.* **2007**, *46*, 5765–5767. [[CrossRef](#)]
107. Soloveichik, G.L.; Andrus, M.; Gao, Y.; Zhao, J.-C.; Kniajanski, S. Magnesium borohydride as a hydrogen storage material: Synthesis of unsolvated  $\text{Mg}(\text{BH}_4)_2$ . *Int. J. Hydrogen Energy* **2009**, *34*, 2144–2152. [[CrossRef](#)]
108. Huang, H.X.; Liu, B.G.; Lv, Y.J.; Lv, W.; Yuan, J.G.; Wu, Y. Double regulation of  $\text{Mg}_{95}\text{Ni}_5$  hydride in suppressing ammonia and promoting hydrogen evolution for  $\text{Mg}(\text{BH}_4)_2\cdot 2\text{NH}_3$ . *J. Alloys Compd.* **2022**, *901*, 163468. [[CrossRef](#)]
109. Li, H.W.; Kikuchi, K.; Nakamori, Y.; Miwa, K.; Towata, S.; Orimo, S. Effects of ball milling and additives on dehydrogenating behaviors of well-crystallized  $\text{Mg}(\text{BH}_4)_2$ . *Scr. Mater.* **2007**, *57*, 679–682. [[CrossRef](#)]
110. Zanella, P.; Crociani, L.; Masciocchi, N.; Giunchi, G. Facile high-yield synthesis of pure, crystalline  $\text{Mg}(\text{BH}_4)_2$ . *Inorg. Chem.* **2007**, *46*, 9039–9041. [[CrossRef](#)] [[PubMed](#)]
111. Wiberg, E.; Hartwimmer, R.Z. Zur Kenntnis von Erdalkaliboranaten  $\text{Me}[\text{BH}_4)_2$  III. Synthese aus Erdalkalihydriden und Diboran. *Z. Naturforsch. B Chem. Sci.* **1955**, *10*, 295–296. [[CrossRef](#)]
112. Wiberg, E.; Noth, H.; Hartwimmer, R.Z. Zur Kenntnis von Erdalkaliboranaten  $\text{Me}[\text{BH}_4)_2$  I. Darstellung aus Erdalkali-tetramethoxoboranen und Diboran. *Z. Naturforsch. B Chem. Sci.* **1955**, *10*, 292–294. [[CrossRef](#)]
113. Wiberg, E. Zur Kenntnis eines kupfer-bor-wasserstoffs  $\text{CuBH}_4$ . *Z. Naturforsch. B* **1952**, *7b*, 582.
114. Wiberg, E.; Henle, W. Notizen: Zur Kenntnis eines Silber-bor-wasserstoffs  $\text{AgBH}_4$ . *Z. Naturforsch. B* **1952**, *7*, 575–576. [[CrossRef](#)]
115. Wiberg, E. Neuere Ergebnisse der präparativen Hydrid-Forschung. *Angew. Chem.* **1953**, *65*, 16–33. [[CrossRef](#)]
116. Musaev, D.G.; Morokuma, K. Does the Tetrahydroborate Species  $\text{AuBH}_4$  Exist? Ab Initio MO Study of the Structure and Stability of  $\text{CuBH}_4$ ,  $\text{AgBH}_4$ , and  $\text{AuBH}_4$ . *Organometallics* **1995**, *14*, 3327–3334. [[CrossRef](#)]
117. Jain, I.P.; Jain, P.; Jain, A. Novel hydrogen storage materials: A review of lightweight complex hydrides. *J. Alloys Compd.* **2010**, *503*, 303–339. [[CrossRef](#)]
118. Riktor, M.D.; Sørby, M.H.; Chlopek, K.; Fichtner, M.; Buchter, F.; Züttel, A.; Hauback, B.C. In situ synchrotron diffraction studies of phase transitions and thermal decomposition of  $\text{Mg}(\text{BH}_4)_2$  and  $\text{Ca}(\text{BH}_4)_2$ . *J. Mater. Chem.* **2007**, *17*, 4939–4942. [[CrossRef](#)]

119. Jeon, E.; Cho, Y.W. Mechanochemical synthesis and thermal decomposition of zinc borohydride. *J. Alloys Compd.* **2006**, *422*, 273–275. [CrossRef]
120. Srinivasan, S.; Escobar, D.; Jurczyk, M.; Goswami, Y.; Stefanakos, E. Nanocatalyst doping of  $Zn(BH_4)_2$  for on-board hydrogen storage. *J. Alloys Compd.* **2008**, *462*, 294–302. [CrossRef]
121. Wiberg, E.; Henle, W. Notizen: Zur Kenntnis eines ätherlöslichen Zink-bor-wasser-stoffs  $Zn(BH_4)_2$ . *Z. Naturforsch. B* **1952**, *7*, 579–580. [CrossRef]
122. Nöth, H.; Wiberg, E.; Winter, L.P. Boranate und Boranato-metallate. I. Zur Kenntnis von Solvaten des Zinkboranats. *Z. Anorg. Allg. Chem.* **1969**, *370*, 209–223. [CrossRef]
123. Banus, M.D.; Bragdon, R.W.; Hinckley, A.A. Potassium, rubidium and cesium borohydrides. *J. Am. Chem. Soc.* **1954**, *76*, 3848–3849. [CrossRef]
124. Hagemann, H.; Gomes, S.; Renaudin, G.; Yvon, K. Raman studies of reorientation motions of  $[BH_4]^-$  anions in alkali borohydrides. *J. Alloys Compd.* **2004**, *363*, 129–132. [CrossRef]
125. Friedrichs, O.; Borgschulte, A.; Kato, S.; Buchter, F.; Gremaud, R.; Remhof, A.; Zuttel, A. Low-temperature synthesis of  $LiBH_4$  by gas-solid reaction. *Chem. Eur. J.* **2009**, *15*, 5531–5534. [CrossRef]
126. James, B.D.; Wallbridge, M.G.H. Metal tetrahydroborates. *Prog. Inorg. Chem.* **1970**, *11*, 99–231.
127. Paskevicius, M.; Sheppard, D.A.; Buckley, C.E. Thermodynamic changes in mechanochemically synthesized magnesium hydride nanoparticles. *J. Am. Chem. Soc.* **2010**, *132*, 5077–5083. [CrossRef]
128. Berube, V.; Radtke, G.; Dresselhaus, M.; Chen, G. Size effects on the hydrogen storage properties of nanostructured metal hydrides: A review. *Int. J. Energy Res* **2007**, *31*, 637–663. [CrossRef]
129. Gertsman, V.; Birringer, R. On the room-temperature grain growth in nanocrystalline copper. *Scr. Metall. Mater.* **1994**, *30*, 577–581. [CrossRef]
130. Vigeholm, B.; Kjoller, J.; Larsen, B.; Schroder Pedersen, A. Hydrogen sorption performance of pure magnesium during continued cycling. *Int. J. Hydrogen Energy* **1983**, *8*, 809–817. [CrossRef]
131. Berlouis, L.; Cabrera, E.; Hall-Barientos, E.; Hall, P.; Dodd, S.; Morris, S.; Imam, M. Thermal analysis investigation of hydriding properties of nanocrystalline Mg–Ni- and Mg–Fe-based alloys prepared by high-energy ball milling. *J. Mater. Res.* **2001**, *16*, 45–57. [CrossRef]
132. Nielsen, T.K.; Besenbacher, F.; Jensen, T.R. Nanoconfined hydrides for energy storage. *Nanoscale* **2011**, *3*, 2086–2098. [CrossRef]
133. Nielsen, T.K.; Manickam, K.; Hirscher, M.; Besenbacher, F.; Jensen, T.R. Confinement of  $MgH_2$  Nanoclusters within Nanoporous Aerogel Scaffold Materials. *ACS Nano* **2009**, *3*, 3521–3528. [CrossRef]
134. Zhang, S.; Gross, A.F.; Atta, S.L.; Lopez, M.; Liu, P.; Ahn, C.C.; Vajo, J.J.; Jensen, C.M. The synthesis and hydrogen storage properties of a  $MgH_2$  incorporated carbon aerogel scaffold. *Nanotechnology* **2009**, *20*, 204027. [CrossRef] [PubMed]
135. de Gennes, P.G. Wetting: Statics and dynamics. *Rev. Mod. Phys.* **1985**, *57*, 827–863. [CrossRef]
136. Dujardin, E.; Ebbesen, T.W.; Hiura, H.; Tanigaki, K. Capillarity and wetting of carbon nanotubes. *Science* **1994**, *265*, 1850–1852. [CrossRef] [PubMed]
137. Gao, J.; Adelhelm, P.; Verkuijlen, M.H.W.; Rongeat, C.; Herrich, M.; van Bentum, P.J.M.; Gutfleisch, O.; Kentgens, A.P.M.; de Jong, K.P.; de Jongh, P.E. Confinement of  $NaAlH_4$  in nanoporous carbon: Impact on  $H_2$  release, reversibility, and thermodynamics. *J. Phys. Chem. C* **2010**, *114*, 4675–4682. [CrossRef]
138. Dilts, J.A.; Ashby, E.C. A study of the thermal decomposition of complex metal hydrides. *Inorg. Chem.* **1972**, *11*, 1230–1236. [CrossRef]
139. Bogdanović, B.; Brand, R.A.; Marjanović, A.; Schwickardi, M.; Tölle, J. Metal-doped sodium aluminium hydrides as potential new hydrogen storage materials. *J. Alloys Compd.* **2000**, *302*, 36–58. [CrossRef]
140. Verkuijlen, M.H.W.; Gao, J.; Adelhelm, P.; van Bentum, P.J.M.; de Jongh, P.E.; Kentgens, A.P.M. Solid-state NMR studies of the local structure of  $NaAlH_4/C$  nanocomposites at different stages of hydrogen desorption and rehydrogenation. *J. Phys. Chem. C* **2010**, *114*, 4683–4692. [CrossRef]
141. Lohstroh, W.; Roth, A.; Hahn, H.; Fichtner, M. Thermodynamic effects in nanoscale  $NaAlH_4$ . *ChemPhysChem* **2010**, *11*, 789–792. [CrossRef] [PubMed]
142. Stephens, R.D.; Gross, A.F.; Atta, S.L.; Vajo, J.J.; Pinkerton, F.E. The kinetic enhancement of hydrogen cycling in  $NaAlH_4$  by melt infusion into nanoporous carbon aerogel. *Nanotechnology* **2009**, *20*, 204018. [CrossRef]
143. Comanescu, C.; Capurso, G.; Maddalena, A. Nanoconfinement in activated mesoporous carbon of calcium borohydride for improved reversible hydrogen storage. *Nanotechnology* **2012**, *23*, 385401. [CrossRef]
144. Gutowski, M.; Autrey, T. Computational studies of boron/nitrogen and aluminum/nitrogen compounds for chemical hydrogen storage. *Prepr. Pap. Am. Chem. Soc. Div. Fuel Chem.* **2004**, *49*, 275–276. Available online: <http://citeseerx.ist.psu.edu/viewdoc/download?doi=10.1.1.459.4955&rep=rep1&type=pdf> (accessed on 31 January 2022).
145. Gutowska, A.; Li, L.; Shin, Y.; Wang, C.M.; Li, X.S.; Linehan, J.C.; Smith, R.S.; Kay, B.D.; Schmid, B.; Shaw, W.; et al. Nanoscaffold mediates hydrogen release and the reactivity of ammonia borane. *Angew. Chem. Int. Ed.* **2005**, *44*, 3578–3582. [CrossRef] [PubMed]
146. Filinchuk, Y.; Ronnebro, E.; Chandra, D. Crystal structures and phase transformations in  $Ca(BH_4)_2$ . *Acta Mater.* **2009**, *57*, 732–738. [CrossRef]
147. Ravnsbæk, D.B.; Nickels, E.A.; Cerny, R.; Olesen, C.H.; David, W.I.F.; Edwards, P.P.; Filinchuk, Y.; Jensen, T.R. Novel Alkali Earth Borohydride  $Sr(BH_4)_2$  and Borohydride-Chloride  $Sr(BH_4)Cl$ . *Inorg. Chem.* **2013**, *52*, 10877–10885. [CrossRef]

148. Sharma, M.; Didelot, E.; Spyratou, A.; Daku, L.M.L.; Cerny, R.; Hagemann, H. Halide Free  $M(\text{BH}_4)_2$  ( $M = \text{Sr}, \text{Ba}, \text{and Eu}$ ) Synthesis, Structure, and Decomposition. *Inorg. Chem.* **2016**, *55*, 7090–7097. [[CrossRef](#)] [[PubMed](#)]
149. Ravnsbæk, D.B.; Sørensen, L.H.; Filinchuk, Y.; Besenbacher, F.; Jensen, T.R. Screening of Metal Borohydrides by Mechanochemistry and Diffraction. *Angew. Chem. Int. Ed.* **2012**, *51*, 3582–3586. [[CrossRef](#)]
150. Wiberg, E.; Henle, W. Zur Kenntnis eines Cadmium-bor-wasserstoffs  $\text{Cd}(\text{BH}_4)_2$ . *Z. Naturforsch. B* **1952**, *7*, 582. [[CrossRef](#)]
151. Nöth, H.; Winter, L.P. Metallboranate und Boranato-metallate. V. Solvate des Cadmiumboranats und Boranatocadmate. *Z. Anorg. Allg. Chem.* **1972**, *389*, 225–234. [[CrossRef](#)]
152. Stockmayer, W.H.; Rice, D.W.; Stephenson, C.C. Thermodynamic properties of sodium borohydride and aqueous borohydride ion. *J. Am. Chem. Soc.* **1955**, *77*, 1980–1983. [[CrossRef](#)]
153. Filinchuk, Y.; Hagemann, H. Structure and properties of  $\text{NaBH}_4 \cdot 2\text{H}_2\text{O}$  and  $\text{NaBH}_4$ . *Eur. J. Inorg. Chem.* **2008**, *20*, 3127–3133. [[CrossRef](#)]
154. Hagemann, H.; D’Anna, V.; Carbonniere, P.; Bardaji, E.G.; Fichtner, M. Synthesis and characterization of  $\text{NaBD}_3\text{H}$ , a potential structural probe for hydrogen storage materials. *J. Phys. Chem. A* **2009**, *113*, 13932–13936. [[CrossRef](#)] [[PubMed](#)]
155. Davis, R.E.; Kenson, R.E. Boron Hydrides. XII. The synthesis and infrared spectra of  $\text{NaBH}_3\text{D}$  and  $\text{NaBD}_3\text{H}$ . *Proc. Indiana Acad. Sci.* **1966**, *76*, 236–240.
156. Chłopek, K.; Frommen, C.; Leon, A.; Zabara, O.; Fichtner, M. Synthesis and properties of magnesium tetrahydroborate,  $\text{Mg}(\text{BH}_4)_2$ . *J. Mater. Chem.* **2007**, *17*, 3496–3503. [[CrossRef](#)]
157. Buchter, F.; Łodziana, Z.; Remhof, A.; Friedrichs, O.; Borgschulte, A.; Mauron, P.; Zuttel, A.; Sheptyakov, D.; Barkhordarian, G.; Bormann, R.; et al. Structure of  $\text{Ca}(\text{BD}_4)_2$   $\beta$ -phase from combined neutron and synchrotron x-ray powder diffraction data and density functional calculations. *J. Phys. Chem. B* **2008**, *112*, 8042–8048. [[CrossRef](#)] [[PubMed](#)]
158. Filinchuk, Y.; Richter, B.; Jensen, T.R.; Dmitriev, V.; Chernyshov, D.; Hagemann, H. Porous and dense magnesium borohydride frameworks: Synthesis, stability, and reversible absorption of guest species. *Angew. Chem. Int. Ed.* **2011**, *50*, 11162–11166. [[CrossRef](#)] [[PubMed](#)]
159. Ehrlich, R.; Rice, G. The chemistry of alane. XII. The lithium tetrahydroalane-triethylamine complex. *Inorg. Chem.* **1966**, *5*, 1284–1286. [[CrossRef](#)]
160. Plešek, J.; Heřmánek, S. Chemistry of boranes. IV. On preparation, properties, and behavior towards Lewis bases of magnesium borohydride. *Collect. Czech. Chem. Commun.* **1966**, *31*, 3845–3858. [[CrossRef](#)]
161. Brown, H.C.; Yoon, N.M. Selective reductions. X. reaction of aluminum hydride with selected organic compounds containing representative functional groups. Comparison of the reducing characteristics of lithium aluminum hydride and its derivatives. *J. Am. Chem. Soc.* **1966**, *88*, 1464–1472. [[CrossRef](#)]
162. Ruff, J.K.; Hawthorne, M.F. The amine complexes of aluminum hydride. II. *J. Am. Chem. Soc.* **1961**, *83*, 535–538. [[CrossRef](#)]
163. Kuzdrowska, M.; Annunziata, L.; Marks, S.; Schmid, M.; Jaffredo, C.G.; Roesky, P.W.; Guillaume, S.M.; Maron, L. Organometallic calcium and strontium borohydrides as initiators for the polymerization of epsilon-caprolactone and L-lactide: Combined experimental and computational investigations. *Dalton Trans.* **2013**, *42*, 9352–9360. [[CrossRef](#)] [[PubMed](#)]
164. Yan, Y.; Remhof, A.; Hwang, S.-J.; Li, H.-W.; Mauron, P.; Orimo, S.-I.; Zuttel, A. Pressure and temperature dependence of the decomposition pathway of  $\text{LiBH}_4$ . *Phys. Chem. Chem. Phys.* **2012**, *14*, 6514–6519. [[CrossRef](#)] [[PubMed](#)]
165. Abrahams, S.C.; Kalnajs, J. The lattice constants of the alkali borohydrides and the low-temperature phase of sodium borohydride. *J. Chem. Phys.* **1954**, *22*, 434–436. [[CrossRef](#)]
166. Kumar, R.S.; Kim, E.; Cornelius, A.L. Structural Phase Transitions in the Potential Hydrogen Storage Compound  $\text{KBH}_4$  under Compression. *J. Phys. Chem. C* **2008**, *112*, 8452–8457. [[CrossRef](#)]
167. Filinchuk, Y.; Talyzin, A.V.; Hagemann, H.; Dmitriev, V.; Chernyshov, D.; Sundqvist, B. Cation Size and Anion Anisotropy in Structural Chemistry of Metal Borohydrides. The Peculiar Pressure Evolution of  $\text{RbBH}_4$ . *Inorg. Chem.* **2010**, *49*, 5285–5292. [[CrossRef](#)]
168. Babanova, O.A.; Soloninin, A.V.; Stepanov, A.P.; Skripov, A.V.; Filinchuk, Y. Structural and Dynamical Properties of  $\text{NaBH}_4$  and  $\text{KBH}_4$ : NMR and Synchrotron X-ray Diffraction Studies. *J. Phys. Chem. C* **2010**, *114*, 3712–3718. [[CrossRef](#)]
169. Filinchuk, Y.; Talyzin, A.V.; Chernyshov, D.; Dmitriev, V. High-pressure phase of  $\text{NaBH}_4$ : Crystal structure from synchrotron powder diffraction data. *Phys. Rev. B Condens. Matter Mater. Phys.* **2007**, *76*, 092104. [[CrossRef](#)]
170. Marynick, D.S.; Lipscomb, W.N. Crystal structure of beryllium borohydride. *Inorg. Chem.* **1972**, *11*, 820–823. [[CrossRef](#)]
171. Filinchuk, Y.; Cerny, R.; Hagemann, H. Insight into  $\text{Mg}(\text{BH}_4)_2$  with Synchrotron X-ray diffraction: Structure revision, crystal chemistry, and anomalous thermal expansion. *Chem. Mater.* **2009**, *21*, 925–933. [[CrossRef](#)]
172. Her, J.H.; Stephens, P.W.; Gao, Y.; Soloveichik, G.L.; Rijssenbeek, J.; Andrus, M.; Zhao, J.C. Structure of unsolvated magnesium borohydride  $\text{Mg}(\text{BH}_4)_2$ . *Acta Crystallogr. Sect. B Struct. Sci.* **2007**, *63*, 561–568. [[CrossRef](#)] [[PubMed](#)]
173. Pitt, M.P.; Webb, C.J.; Paskevicius, M.; Sheptyakov, D.; Buckley, C.E.; Gray, E.M. In situ neutron diffraction study of the deuteration of isotopic  $\text{Mg}^{11}\text{B}_2$ . *J. Phys. Chem. C* **2011**, *115*, 22669–22679. [[CrossRef](#)]
174. Cerny, R.; Penin, N.; Hagemann, H.; Filinchuk, Y. The first crystallographic and spectroscopic characterization of a 3d-metal borohydride:  $\text{Mn}(\text{BH}_4)_2$ . *J. Phys. Chem. C* **2009**, *113*, 9003–9007. [[CrossRef](#)]
175. Tumanov, N.A.; Roedern, E.; Łodziana, Z.; Nielsen, D.B.; Jensen, T.R.; Talyzin, A.V.; Černý, R.; Chernyshov, D.; Dmitriev, V.; Palasyuk, T.; et al. High-Pressure study of  $\text{Mn}(\text{BH}_4)_2$  reveals a stable polymorph with high hydrogen density. *Chem. Mater.* **2016**, *28*, 274–283. [[CrossRef](#)]
176. Łodziana, Z. Multivalent metal tetrahydroborides of Al, Sc, Y, Ti, and Zr. *Phys. Rev. B* **2010**, *81*, 144108. [[CrossRef](#)]

177. Dain, C.J.; Downs, A.J.; Goode, M.J.; Evans, D.G.; Nicholls, K.T.; Rankin, D.W.H.; Robertson, H.E. Molecular structure of gaseous titanium tris(tetrahydroborate),  $Ti(BH_4)_3$ : Experimental determination by electron diffraction and molecular orbital analysis of some  $Ti(BH_4)_3$  derivatives. *J. Chem. Soc. Dalt. Trans.* **1991**, 967–977. [CrossRef]
178. Franz, K.; Fusstetter, H.; Nöth, H. Metallboranate und Boranatometallate. IX [1]; Äther-Addukte von Tris(boranato)-titan(III) und dimere Alkoxy-bis(boranato)-titan(III)-Verbindungen. *Z. Anorg. Allg. Chem.* **1976**, 427, 97–113. [CrossRef]
179. Fang, Z.Z.; Ma, L.P.; Kang, X.D.; Wang, P.J.; Wang, P.; Cheng, H.M. In situ formation and rapid decomposition of  $Ti(BH_4)_3$  by mechanical milling  $LiBH_4$  with  $TiF_3$ . *Appl. Phys. Lett.* **2009**, 94, 1–4. [CrossRef]
180. Nöth, H. Anorganische Reaktionen der Alkaliboranate. *Angew. Chem.* **1961**, 73, 371–383. [CrossRef]
181. Hagemann, H.; Longhini, M.; Kaminski, J.W.; Wesolowski, T.A.; Cerny, R.; Penin, N.; Sørby, M.H.; Hauback, B.C.; Severa, G.; Jensen, C.M.  $LiSc(BH_4)_4$ : A novel salt of  $Li^+$  and discrete  $Sc(BH_4)_4^-$  complex anions. *J. Phys. Chem. A* **2008**, 112, 7551–7555. [CrossRef] [PubMed]
182. Kim, C.; Hwang, S.-J.; Bowman, R.C.J.; Reiter, J.W.; Zan, J.A.; Kulleck, J.G.; Kabbour, H.; Majzoub, E.H.; Ozolins, V.  $LiSc(BH_4)_4$  as a hydrogen storage material: Multinuclear high-resolution solid-state nmr and first-principles density functional theory studies. *J. Phys. Chem. C* **2009**, 113, 9956–9968. [CrossRef]
183. Morris, J.H.; Smith, W.E. Synthesis and characterisation of a tetrahydrofuran derivative of scandium tetrahydroborate. *J. Chem. Soc. D Chem. Commun.* **1970**, 245a. [CrossRef]
184. Cerny, R.; Kim, K.C.; Penin, N.; D’Anna, V.; Hagemann, H.; Sholl, D.S.  $AZn_2(BH_4)_5$  (A = Li, Na) and  $NaZn(BH_4)_3$ : Structural studies. *J. Phys. Chem. C* **2010**, 114, 19127–19133. [CrossRef]
185. Møller, K.T.; Ley, M.B.; Schouwink, P.; Černý, R.; Jensen, T.R. Synthesis and thermal stability of perovskite alkali metal strontium borohydrides. *Dalton Trans.* **2016**, 45, 831–840. [CrossRef] [PubMed]
186. Grinderslev, J.B.; Møller, K.T.; Yan, Y.; Chen, X.M.; Li, Y.; Li, H.W.; Zhou, W.; Skibsted, J.; Chen, X.; Jensen, T.R. Potassium octahydridotriborate: Diverse polymorphism in a potential hydrogen storage material and potassium ion conductor. *Dalton Trans.* **2019**, 48, 8872–8881. [CrossRef]
187. Fischer, P.; Züttel, A. Order-disorder phase transition in  $NaBD_4$ . *Mater. Sci. Forum* **2004**, 443, 287–290. [CrossRef]
188. Miwa, K.; Aoki, M.; Noritake, T.; Ohba, N.; Nakamori, Y.; Towata, S.; Züttel, A.; Orimo, S. Thermodynamical stability of calcium borohydride  $Ca(BH_4)_2$ . *Phys. Rev. B Condens. Matter Mater. Phys.* **2006**, 74, 155122. [CrossRef]
189. Richter, B.; Ravnsbaek, D.B.; Tumanov, N.; Filinchuk, Y.; Jensen, T.R. Manganese borohydride; synthesis and characterization. *Dalton Trans.* **2015**, 44, 3988–3996. [CrossRef]
190. Severa, G.; Hagemann, H.; Longhini, M.; Kaminski, J.W.; Wesolowski, T.A.; Jensen, C.M. Thermal desorption, vibrational spectroscopic, and DFT computational studies of the complex manganese borohydrides  $Mn(BH_4)_2$  and  $[Mn(BH_4)_4]^{2-}$ . *J. Phys. Chem. C* **2010**, 114, 15516–15521. [CrossRef]
191. Makhaev, V.D.; Borisov, A.P.; Gnilomedova, T.P.; Lobkovskii, É.B.; Chekhlov, A.N. Production of manganese borohydride complexes of manganese solvated with THF, and the structure of  $Mn(BH_4)_2$  (THF)<sub>3</sub>. *Bull. Acad. Sci. USSR Div. Chem. Sci.* **1987**, 36, 1582–1586. [CrossRef]
192. Schaeffer, G.W.; Roscoe, J.S.; Stewart, A.C. The Reduction of Iron(III) Chloride with Lithium Aluminohydride and Lithium Borohydride: Iron(II) Borohydride. *J. Am. Chem. Soc.* **1956**, 78, 729–733. [CrossRef]
193. Varin, R.A.; Bidabadi, A.S. Rapid, ambient temperature hydrogen generation from the solid state Li-B-Fe-H system by mechanochemical activation synthesis. *J. Power Sources* **2015**, 284, 554–565. [CrossRef]
194. Stewart, A.C.; Schaeffer, G.W. The reaction of cobalt(II) bromide with lithium borohydride and lithium aluminohydride. *J. Inorg. Nucl. Chem.* **1956**, 3, 194–197. [CrossRef]
195. Raje, S.; Angamuthu, R. Solvent-free synthesis and reactivity of nickel(II) borohydride and nickel(II) hydride. *Green Chem.* **2019**, 21, 2752–2758. [CrossRef]
196. Filinchuk, Y.; Chernyshov, D.; Cerny, R. Lightest borohydride probed by synchrotron x-ray diffraction: Experiment calls for a new theoretical revision. *J. Phys. Chem. C* **2008**, 112, 10579–10584. [CrossRef]
197. Filinchuk, Y.; Chernyshov, D. Looking at hydrogen atoms with X-rays: Comprehensive synchrotron diffraction study of  $LiBH_4$ . *Acta Crystallogr. Sect. A Found. Crystallogr.* **2007**, 63, s240–s241. Available online: <http://scripts.iucr.org/cgi-bin/paper?a38061> (accessed on 31 January 2022). [CrossRef]
198. Soldate, A.M. Crystal structure of sodium borohydride. *J. Am. Chem. Soc.* **1947**, 69, 987–988. [CrossRef]
199. Dmitriev, V.; Filinchuk, Y.; Chernyshov, D.; Talyzin, A.V.; Ilewski, A.; Andersson, O.; Sundqvist, B.; Kurnosov, A. Pressure-temperature phase diagram of  $LiBH_4$ : Synchrotron x-ray diffraction experiments and theoretical analysis. *Phys. Rev. B Condens. Matter Mater. Phys.* **2008**, 77, 174112. [CrossRef]
200. Ohba, N.; Miwa, K.; Aoki, M.; Noritake, T.; Towata, S.-i.; Nakamori, Y.; Orimo, S.-i.; Züttel, A. First-principles study on the stability of intermediate compounds of  $LiBH_4$ . *Phys. Rev. B* **2006**, 74, 075110. [CrossRef]
201. Rude, L.H.; Nielsen, T.K.; Ravnsbæk, D.B.; Bosenberg, U.; Ley, M.B.; Richter, B.; Arnbjerg, L.M.; Dornheim, M.; Filinchuk, Y.; Besenbacher, F.; et al. Tailoring properties of borohydrides for hydrogen storage: A review. *Phys. Status Solidi A* **2011**, 208, 1754–1773. [CrossRef]
202. Roedern, E.; Jensen, T.R. Ammine-stabilized transition-metal borohydrides of iron, cobalt, and chromium: Synthesis and characterization. *Inorg. Chem.* **2015**, 54, 10477–10482. [CrossRef] [PubMed]

203. Rude, L.H.; Corno, M.; Ugliengo, P.; Baricco, M.; Lee, Y.-S.; Cho, Y.W.; Besenbacher, F.; Overgaard, J.; Jensen, T.R. Synthesis and Structural Investigation of  $Zr(BH_4)_4$ . *J. Phys. Chem. C* **2012**, *116*, 20239–20245. [[CrossRef](#)]
204. Bird, P.H.; Churchill, M.R. The crystal structure of zirconium(IV) borohydride (at  $-160^\circ$ ). *Chem. Commun. (London)* **1967**, 403. [[CrossRef](#)]
205. Broach, R.W.; Chuang, I.S.; Marks, T.J.; Williams, J.M. Metrical characterization of tridentate tetrahydroborate ligation to a transition-metal ion. Structure and bonding in  $Hf(BH_4)_4$  by single-crystal neutron diffraction. *Inorg. Chem.* **1983**, *22*, 1081–1084. [[CrossRef](#)]
206. Hoekstra, H.R.; Katz, J.J. The Preparation and Properties of the Group IV-B Metal Borohydrides. *J. Am. Chem. Soc.* **1949**, *71*, 2488–2492. [[CrossRef](#)]
207. Dunbar, A.C.; Wright, J.C.; Grant, D.J.; Girolami, G.S. X-ray Crystal Structure of Thorium Tetrahydroborate,  $Th(BH_4)_4$ , and Computational Studies of  $An(BH_4)_4$  ( $An = Th, U$ ). *Inorg. Chem.* **2021**, *60*, 12489–12497. [[CrossRef](#)]
208. Bernstein, E.R.; Hamilton, W.C.; Keiderling, T.A.; La Placa, S.J.; Lippard, S.J.; Mayerle, J.J. 14-Coordinate uranium(IV). Structure of uranium borohydride by single-crystal neutron diffraction. *Inorg. Chem.* **1972**, *11*, 3009–3016. [[CrossRef](#)]
209. Charpin, P.; Nierlich, M.; Vigner, D.; Lance, M.; Baudry, D. Structure of the second crystalline form of uranium(IV) tetrahydroborate. *Acta Crystallogr. Sect. C Cryst. Struct. Commun.* **1987**, *43*, 1465–1467. [[CrossRef](#)]
210. Banks, R.H.; Edelstein, N.M.; Spencer, B.; Templeton, D.H.; Zalkin, A. Volatility and molecular structure of neptunium(IV) borohydride. *J. Am. Chem. Soc.* **1980**, *102*, 620–623. [[CrossRef](#)]
211. Tumanov, N.A.; Safin, D.A.; Richter, B.; Lodziana, Z.; Jensen, T.R.; Garcia, Y.; Filinchuk, Y. Challenges in the synthetic routes to  $Mn(BH_4)_2$ : Insight into intermediate compounds. *Dalton Trans.* **2015**, *44*, 6571–6580. [[CrossRef](#)] [[PubMed](#)]
212. Ley, M.B.; Jørgensen, M.; Cerny, R.; Filinchuk, Y.; Jensen, T.R. From  $M(BH_4)_3$  ( $M = La, Ce$ ) borohydride frameworks to controllable synthesis of porous hydrides and ion conductors. *Inorg. Chem.* **2016**, *55*, 9748–9756. [[CrossRef](#)] [[PubMed](#)]
213. Humphries, T.D.; Ley, M.B.; Frommen, C.; Munroe, K.T.; Jensen, T.R.; Hauback, B.C. Crystal structure and in situ decomposition of  $Eu(BH_4)_2$  and  $Sm(BH_4)_2$ . *J. Mater. Chem. A* **2015**, *3*, 691–698. [[CrossRef](#)]
214. Olsen, J.E.; Frommen, C.; Jensen, T.R.; Riktor, M.D.; Sorby, M.H.; Hauback, B.C. Structure and thermal properties of composites with RE-borohydrides ( $RE = La, Ce, Pr, Nd, Sm, Eu, Gd, Tb, Er, Yb$  or  $Lu$ ) and  $LiBH_4$ . *RSC Adv.* **2014**, *4*, 1570–1582. [[CrossRef](#)]
215. Olsen, J.E.; Frommen, C.; Sorby, M.H.; Hauback, B.C. Crystal structures and properties of solvent-free  $LiYb(BH_4)_{4-x}Cl_x$ ,  $Yb(BH_4)_3$  and  $Yb(BH_4)_{2-x}Cl_x$ . *RSC Adv.* **2013**, *3*, 10764–10774. [[CrossRef](#)]
216. Jaron, T.; Orłowski, P.A.; Wegner, W.; Fijałkowski, K.J.; Leszczynski, P.J.; Grochala, W. Hydrogen storage materials: Room-temperature wet-chemistry approach toward mixed-metal borohydrides. *Angew. Chem. Int. Ed.* **2015**, *54*, 1236–1239. [[CrossRef](#)]
217. Jaron, T.; Wegner, W.; Fijałkowski, K.J.; Leszczynski, P.J.; Grochala, W. Facile formation of thermodynamically unstable novel borohydride materials by a wet chemistry route. *Chem. Eur. J.* **2015**, *21*, 5689–5692. [[CrossRef](#)]
218. Nickels, E.A.; Jones, M.O.; David, W.I.F.; Johnson, S.R.; Lowton, R.L.; Sommariva, M.; Edwards, P.P. Tuning the decomposition temperature in complex hydrides: Synthesis of a mixed alkali metal borohydride. *Angew. Chem. Int. Ed.* **2008**, *47*, 2817–2819. [[CrossRef](#)] [[PubMed](#)]
219. Seballos, L.; Zhang, J.Z.; Ronnebro, E.; Herberg, J.L.; Majzoub, E.H. Metastability and crystal structure of the bialkali complex metal borohydride  $NaK(BH_4)_2$ . *J. Alloys Compd.* **2009**, *476*, 446–450. [[CrossRef](#)]
220. Semenenko, K.N.; Chavgun, A.P.; Surov, V.N. Interaction of sodium tetrahydroborate with potassium and lithium tetrahydroborates. *Russ. J. Inorg. Chem.* **1971**, *16*, 271–273.
221. Jensen, S.R.H.; Jepsen, L.H.; Skibsted, J.; Jensen, T.R. Phase diagram for the  $NaBH_4$ – $KBH_4$  system and the stability of a  $Na_{1-x}K_xBH_4$  Solid Solution. *J. Phys. Chem. C* **2015**, *119*, 27919–27929. [[CrossRef](#)]
222. Grinderslev, J.B.; Jepsen, L.H.; Lee, Y.-S.; Møller, K.T.; Cho, Y.W.; Černý, R.; Jensen, T.R. Structural diversity and trends in properties of an array of hydrogen-rich ammonium metal borohydrides. *Inorg. Chem.* **2020**, *59*, 12733–12747. [[CrossRef](#)]
223. Černý, R.; Schouwink, P. The crystal chemistry of inorganic metal borohydrides and their relation to metal oxides. *Acta Crystallogr. Sect. B* **2015**, *B71*, 619–640. [[CrossRef](#)]
224. Schouwink, P.; D’Anna, V.; Ley, M.B.; Daku, L.M.L.; Richter, B.; Jensen, T.R.; Hagemann, H.; Černý, R. Bimetallic borohydrides in the system  $M(BH_4)_2$ – $KBH_4$  ( $M = Mg, Mn$ ): On the structural diversity. *J. Phys. Chem. C* **2012**, *116*, 10829–10840. [[CrossRef](#)]
225. Schouwink, P.; Ley, M.B.; Tissot, A.; Hagemann, H.; Jensen, T.R.; Smrčok, L.; Černý, R. Structure and properties of complex hydride perovskite materials. *Nat. Commun.* **2014**, *5*, 5706. [[CrossRef](#)]
226. Gao, M.; Yan, X.W.; Lu, Z.Y.; Xiang, T. Phonon-mediated high-temperature superconductivity in the ternary borohydride  $KB_2H_8$  under pressure near 12 GPa. *Phys. Rev. B* **2021**, *104*, L100504. [[CrossRef](#)]
227. Møller, K.T.; Jørgensen, M.; Fogh, A.S.; Jensen, T.R. Perovskite alkali metal samarium borohydrides: Crystal structures and thermal decomposition. *Dalton Trans.* **2017**, *46*, 11905–11912. [[CrossRef](#)] [[PubMed](#)]
228. Matsuo, M.; Takamura, H.; Maekawa, H.; Li, H.-W.; Orimo, S.-I. Stabilization of lithium superionic conduction phase and enhancement of conductivity of  $LiBH_4$  by  $LiCl$  addition. *Appl. Phys. Lett.* **2009**, *94*, 084103. [[CrossRef](#)]
229. D’Anna, V.; Daku, L.M.L.; Hagemann, H.; Kubel, F. Ionic layered  $BaFCl$  and  $Ba_{1-x}Sr_xFCl$  compounds: Physical- and chemical-pressure effects. *Phys. Rev. B* **2010**, *82*, 024108. [[CrossRef](#)]
230. Shannon, R.D. Revised effective ionic radii and systematic studies of interatomic distances in halides and chalcogenides. *Acta Cryst.* **1976**, *A32*, 751–767. [[CrossRef](#)]
231. Arnbjerg, L.M.; Ravnsbæk, D.B.; Filinchuk, Y.; Vang, R.T.; Cerenius, Y.; Besenbacher, F.; Jørgensen, J.-E.; Jakobsen, H.J.; Jensen, T.R. Structure and dynamics for  $LiBH_4$ – $LiCl$  solid solutions. *Chem. Mater.* **2009**, *21*, 5772–5782. [[CrossRef](#)]

232. Blanchard, D.; Maronsson, J.B.; Riktor, M.D.; Kheres, J.; Sveinbjörnsson, D.; Bardají, E.G.; Léon, A.; Juranyi, F.; Wuttke, J.; Lefmann, K.; et al. Hindered rotational energy barriers of  $\text{BH}_4^-$  tetrahedra in  $\beta\text{-Mg}(\text{BH}_4)_2$  from quasielastic neutron scattering and DFT calculations. *J. Phys. Chem. C* **2012**, *116*, 2013–2023. [[CrossRef](#)]
233. Rude, L.H.; Zavorotynska, O.; Arnbjerg, L.M.; Ravnsbæk, D.B.; Malmkjær, R.A.; Grove, H.; Hauback, B.C.; Baricco, M.; Filinchuk, Y.; Besenbacher, F.; et al. Bromide substitution in lithium borohydride,  $\text{LiBH}_4\text{-LiBr}$ . *Int. J. Hydrogen Energy* **2011**, *36*, 15664–15672. [[CrossRef](#)]
234. Ravnsbæk, D.B.; Rude, L.H.; Jensen, T.R. Chloride substitution in sodium borohydride. *J. Solid State Chem.* **2011**, *184*, 1858–1866. [[CrossRef](#)]
235. Llamas-Jansa, I.; Aliouane, N.; Deledda, S.; Fonnelløp, J.E.; Frommen, C.; Humphries, T.; Lieutenant, K.; Sartori, S.; Sørby, M.H.; Hauback, B.C. Chloride substitution induced by mechano-chemical reactions between  $\text{NaBH}_4$  and transition metal chlorides. *J. Alloys Compd.* **2012**, *530*, 186–192. [[CrossRef](#)]
236. Olsen, J.E.; Sørby, M.H.; Hauback, B.C. Chloride-substitution in sodium borohydride. *J. Alloys Compd.* **2011**, *509*, L228–L231. [[CrossRef](#)]
237. Rude, L.H.; Groppo, E.; Arnbjerg, L.M.; Ravnsbæk, D.B.; Malmkjær, R.A.; Filinchuk, Y.; Baricco, M.; Besenbacher, F.; Jensen, T.R. Iodide substitution in lithium borohydride,  $\text{LiBH}_4\text{-LiI}$ . *J. Alloys Compd.* **2011**, *509*, 8299–8305. [[CrossRef](#)]
238. Borgschulte, A.; Gremaud, R.; Kato, S.; Stadie, N.P.; Remhof, A.; Züttel, A.; Matsuo, M.; Orimo, S.-I. Anharmonicity in  $\text{LiBH}_4\text{-LiI}$  induced by anion exchange and temperature. *Appl. Phys. Lett.* **2010**, *97*, 031916. [[CrossRef](#)]
239. Custelcean, R.; Jackson, J.E. Dihydrogen bonding: Structures, energetics, and dynamics. *Chem. Rev.* **2001**, *101*, 1963–1980. [[CrossRef](#)]
240. Noritake, T.; Aoki, M.; Matsumoto, M.; Miwa, K.; Towata, S.; Li, H.W.; Orimo, S. Crystal structure and charge density analysis of  $\text{Ca}(\text{BH}_4)_2$ . *J. Alloys Compd.* **2010**, *491*, 57–62. [[CrossRef](#)]
241. Grinderslev, J.B.; Ley, M.B.; Lee, Y.-S.; Jepsen, L.H.; Jørgensen, M.; Cho, Y.W.; Skibsted, J.; Jensen, T.R. Ammine lanthanum and cerium borohydrides,  $\text{M}(\text{BH}_4)_3\cdot\text{NH}_3$ ; trends in synthesis, structures, and thermal properties. *Inorg. Chem.* **2020**, *59*, 7768–7778. [[CrossRef](#)]
242. Grinderslev, J.B.; Jensen, T.R. Trends in the series of ammine rare-earth-metal borohydrides: Relating structural and thermal properties. *Inorg. Chem.* **2021**, *60*, 2573–2589. [[CrossRef](#)]
243. Johnson, S.R.; David, W.I.F.; Royse, D.M.; Sommariva, M.; Tang, C.Y.; Fabbiani, F.P.A.; Jones, M.O.; Edwards, P.P. The monoammoniate of lithium borohydride,  $\text{Li}(\text{NH}_3)\text{BH}_4$ : An effective ammonia storage compound. *Chem. Asian J.* **2009**, *4*, 849–854. [[CrossRef](#)] [[PubMed](#)]
244. Jepsen, L.H.; Ley, M.B.; Filinchuk, Y.; Besenbacher, F.; Jensen, T.R. Tailoring the properties of ammine metal borohydrides for solid-state hydrogen storage. *ChemSusChem* **2015**, *8*, 1452–1463. [[CrossRef](#)] [[PubMed](#)]
245. Soloveichik, G.; Her, J.-H.; Stephens, P.W.; Gao, Y.; Rijssenbeek, J.; Andrus, M.; Zhao, J.C. Ammine magnesium borohydride complex as a new material for hydrogen storage: Structure and properties of  $\text{Mg}(\text{BH}_4)_2\cdot 2\text{NH}_3$ . *Inorg. Chem.* **2008**, *47*, 4290–4298. [[CrossRef](#)]
246. Yang, Y.; Liu, Y.; Li, Y.; Gao, M.; Pan, H. Synthesis and thermal decomposition behaviors of magnesium borohydride ammoniates with controllable composition as hydrogen storage materials. *Chem. Asian J.* **2013**, *8*, 476–481. [[CrossRef](#)]
247. Huang, J.; Tan, Y.; Su, J.; Gu, Q.; Cerny, R.; Ouyang, L.; Sun, D.; Yu, X.; Zhu, M. Synthesis, structure and dehydrogenation of zirconium borohydride octaammoniate. *Chem. Commun.* **2015**, *51*, 2794–2797. [[CrossRef](#)]
248. Konoplev, V.N.; Silina, T.A. Ammonia derivatives of magnesium borohydride. *Zh. Neorg. Khim.* **1985**, *30*, 1125–1128.
249. Chu, H.; Wu, G.; Xiong, Z.; Guo, J.; He, T.; Chen, P. Structure and hydrogen storage properties of calcium borohydride diammoniate. *Chem. Mater.* **2010**, *22*, 6021–6028. [[CrossRef](#)]
250. He, T.; Wu, H.; Wu, G.; Wang, J.; Zhou, W.; Xiong, Z.; Chen, J.; Zhang, T.; Chen, P. Borohydride hydrazinates: High hydrogen content materials for hydrogen storage. *Energy Environ. Sci.* **2012**, *5*, 5686–5689. [[CrossRef](#)]
251. He, T.; Wu, H.; Chen, J.; Zhou, W.; Wu, G.; Xiong, Z.; Zhang, T.; Chen, P. Alkali and alkaline-earth metal borohydride hydrazinates: Synthesis, structures and dehydrogenation. *Phys. Chem. Chem. Phys.* **2013**, *15*, 10487–10493. [[CrossRef](#)] [[PubMed](#)]
252. Li, Z.; He, T.; Wu, G.; Ju, X.; Chen, P. The synthesis, structure and dehydrogenation of calcium borohydride hydrazinates. *Int. J. Hydrogen Energy* **2015**, *40*, 5333–5339. [[CrossRef](#)]
253. Shriver, D.; Weller, M.; Overton, T.; Rourke, J.; Armstrong, F. *Inorganic Chemistry*, 6th ed.; Oxford University Press: Oxford, UK, 2014; ISBN-10: 1-4292-9906-1.
254. Unemoto, A.; Matsuo, M.; Orimo, S. Complex hydrides for electrochemical energy storage. *Adv. Funct. Mater.* **2014**, *24*, 2267–2279. [[CrossRef](#)]
255. Møller, K.T.; Sheppard, D.; Ravnsbæk, D.B.; Buckley, C.E.; Akiba, E.; Li, H.-W.; Jensen, T.R. Complex metal hydrides for hydrogen, thermal and electrochemical energy storage. *Energies* **2017**, *10*, 1645. [[CrossRef](#)]
256. Matsuo, M.; Nakamori, Y.; Orimo, S.; Maekawa, H.; Takamura, H. Lithium superionic conduction in lithium borohydride accompanied by structural transition. *Appl. Phys. Lett.* **2007**, *91*, 224103. [[CrossRef](#)]
257. Tang, W.S.; Unemoto, A.; Zhou, W.; Stavila, V.; Matsuo, M.; Wu, H.; Orimo, S.-I.; Udovic, T.J. Unparalleled lithium and sodium superionic conduction in solid electrolytes with large monovalent cage-like anions. *Energy Environ. Sci.* **2015**, *8*, 3637–3645. [[CrossRef](#)] [[PubMed](#)]
258. Lu, Z.; Ciucci, F. Metal Borohydrides as Electrolytes for Solid-State Li, Na, Mg, and Ca Batteries: A First-Principles Study. *Chem. Mater.* **2017**, *29*, 9308–9319. [[CrossRef](#)]
259. Udovic, T.J.; Matsuo, M.; Unemoto, A.; Verdal, N.; Stavila, V.; Skripov, A.V.; Rush, J.J.; Takamura, H.; Orimo, S.-I. Sodium superionic conduction in  $\text{Na}_2\text{B}_{12}\text{H}_{12}$ . *Chem. Commun.* **2014**, *50*, 3750–3752. [[CrossRef](#)]

260. Das, S.; Ngene, P.; Norby, P.; Vegge, T.; De Jongh, P.E.; Blanchard, D. All-Solid-State Lithium-Sulfur Battery Based on a Nanoconfined  $\text{LiBH}_4$  Electrolyte. *J. Electrochem. Soc.* **2016**, *163*, A2029–A2034. [[CrossRef](#)]
261. Unemoto, A.; Ikeshoji, T.; Yasaku, S.; Matsuo, M.; Stavila, V.; Udovic, T.J.; Orimo, S.-I. Stable Interface Formation between  $\text{TiS}_2$  and  $\text{LiBH}_4$  in Bulk-Type All-Solid-State Lithium Batteries. *Chem. Mater.* **2015**, *27*, 5407–5416. [[CrossRef](#)]
262. Matsuo, M.; Orimo, S. Lithium fast-ionic conduction in complex hydrides: Review and prospects. *Adv. Energy Mater.* **2011**, *1*, 161–172. [[CrossRef](#)]
263. Guzik, M.N.; Mohtadi, R.; Sartori, S. Lightweight complex metal hydrides for Li-, Na-, and Mg-based batteries. *J. Mater. Res.* **2019**, *34*, 877–904. [[CrossRef](#)]
264. Takano, A.; Oikawa, I.; Kamegawa, A.; Takamura, H. Enhancement of the lithium-ion conductivity of  $\text{LiBH}_4$  by hydration. *Solid State Ion.* **2016**, *285*, 47–50. [[CrossRef](#)]
265. Zhang, T.; Wang, Y.; Song, T.; Miyaoka, H.; Shinzato, K.; Miyaoka, H.; Ichikawa, T.; Shi, S.; Zhang, X.; Isobe, S.; et al. Ammonia, a switch for controlling high ionic conductivity in lithium borohydride ammoniates. *Joule* **2018**, *2*, 1522–1533. [[CrossRef](#)]
266. Yan, Y.; Grinderslev, J.B.; Lee, Y.-S.; Lee, M.; Cho, Y.W.; Černý, R.; Jensen, T.R. Ammonia-assisted fast Li-Ion conductivity in a new hemiammine lithium borohydride,  $\text{LiBH}_4 \cdot 1/2\text{NH}_3$ . *Chem. Commun.* **2020**, *56*, 3971–3974. [[CrossRef](#)]
267. Zhao, W.; Zhang, R.; Li, H.; Zhang, Y.; Wang, Y.; Wu, C.; Yan, Y.; Chen, Y. Li-Ion conductivity enhancement of  $\text{LiBH}_4 \cdot x\text{NH}_3$  with in situ formed  $\text{Li}_2\text{O}$  nanoparticles. *ACS Appl. Mater. Interfaces* **2021**, *13*, 31635–31641. [[CrossRef](#)]
268. Liu, H.; Ren, Z.; Zhang, X.; Hu, J.; Gao, M.; Pan, H.; Liu, Y. Incorporation of ammonia borane groups in the lithium borohydride structure enables ultrafast lithium ion conductivity at room temperature for solid-state batteries. *Chem. Mater.* **2020**, *32*, 671–678. [[CrossRef](#)]
269. Mohtadi, R.; Matsui, M.; Arthur, T.S.; Hwang, S.-J. Magnesium borohydride: From hydrogen storage to magnesium battery. *Angew. Chem. Int. Ed. Engl.* **2012**, *51*, 9780–9783. [[CrossRef](#)] [[PubMed](#)]
270. Higashi, S.; Miwa, K.; Aoki, M.; Takechi, K. A novel inorganic solid state ion conductor for rechargeable mg batteries. *Chem. Commun.* **2014**, *50*, 1320–1322. [[CrossRef](#)]
271. Le Ruyet, R.; Fleutot, B.; Berthelot, R.; Benabed, Y.; Hautier, G.; Filinchuk, Y.; Janot, R.  $\text{Mg}_3(\text{BH}_4)_4(\text{NH}_2)_2$  as inorganic solid electrolyte with high  $\text{Mg}^{2+}$  ionic conductivity. *ACS Appl. Energy Mater.* **2020**, *3*, 6093–6097. [[CrossRef](#)]
272. Roedern, E.; Kühnel, R.-S.; Remhof, A.; Battaglia, C. Magnesium ethylenediamine borohydride as solid-state electrolyte for magnesium batteries. *Sci. Rep.* **2017**, *7*, 46189. [[CrossRef](#)]
273. Burankova, T.; Roedern, E.; Maniadaki, A.E.; Hagemann, H.; Rentsch, D.; Lodziana, Z.; Battaglia, C.; Remhof, A.; Embs, J.P. Dynamics of the coordination complexes in a solid-state Mg electrolyte. *J. Phys. Chem. Lett.* **2018**, *9*, 6450–6455. [[CrossRef](#)] [[PubMed](#)]
274. Yan, Y.; Dononelli, W.; Jørgensen, M.; Grinderslev, J.B.; Lee, Y.-S.; Cho, Y.W.; Černý, R.; Hammer, B.; Jensen, T.R. The mechanism of  $\text{Mg}^{2+}$  conduction in ammine magnesium borohydride promoted by a neutral molecule. *Phys. Chem. Chem. Phys.* **2020**, *22*, 9204–9209. [[CrossRef](#)]
275. Yan, Y.; Grinderslev, J.B.; Jørgensen, M.; Skov, L.N.; Skibsted, J.; Jensen, T.R. Ammine magnesium borohydride nanocomposites for all-solid-state magnesium batteries. *ACS Appl. Energy Mater.* **2020**, *3*, 9264–9270. [[CrossRef](#)]
276. Kisu, K.; Kim, S.; Inukai, M.; Oguchi, H.; Takagi, S.; Orimo, S. Magnesium borohydride ammonia borane as a magnesium ionic conductor. *ACS Appl. Energy Mater.* **2020**, *3*, 3174–3179. [[CrossRef](#)]
277. Kisu, K.; Kim, S.; Shinohara, T.; Zhao, K.; Züttel, A.; Orimo, S. Monocarborane cluster as a stable fluorine-free calcium battery electrolyte. *Sci. Rep.* **2021**, *11*, 7563. [[CrossRef](#)]
278. Luo, X.X.; Rawal, A.; Salman, M.S.; Aguey-Zinsou, K.F. Core-Shell  $\text{NaBH}_4@ \text{Na}_2\text{B}_{12}\text{H}_{12}$  Nanoparticles as Fast Ionic Conductors for Sodium-Ion Batteries. *ACS Appl. Nano Mater.* **2022**, *5*, 373–379. [[CrossRef](#)]
279. Bao, K.; Pang, Y.; Yang, J.; Sun, D.L.; Fang, F.; Zheng, S.Y. Modulating composite polymer electrolyte by lithium closo-borohydride achieves highly stable solid-state battery at 25°C. *Sci. China Mater.* **2022**, *65*, 95–104. [[CrossRef](#)]
280. Tran, B.L.; Allen, T.N.; Bowden, M.E.; Autrey, T.; Jensen, C.M. Effects of Glymes on the Distribution of  $\text{Mg}(\text{B}_{10}\text{H}_{10})$  and  $\text{Mg}(\text{B}_{12}\text{H}_{12})$  from the Thermolysis of  $\text{Mg}(\text{BH}_4)_2$ . *Inorganics* **2021**, *9*, 41. [[CrossRef](#)]
281. Dobbins, T.A. Overview of the Structure-Dynamics-Function Relationships in Borohydrides for Use as Solid-State Electrolytes in Battery Applications. *Molecules* **2021**, *26*, 3239. [[CrossRef](#)] [[PubMed](#)]
282. Marks, S.; Heck, J.G.; Habicht, M.H.; Oña-Burgos, P.; Feldmann, C.; Roesky, P.W.  $[\text{Ln}(\text{BH}_4)_2(\text{THF})_2]$  (Ln = Eu, Yb)—A highly luminescent material. synthesis, properties, reactivity, and NMR studies. *J. Am. Chem. Soc.* **2012**, *134*, 16983–16986. [[CrossRef](#)] [[PubMed](#)]
283. Drozdov, A.P.; Eremets, M.I.; Troyan, I.A.; Ksenofontov, V.; Shylin, S.I. Conventional superconductivity at 203 kelvin at high pressures in the sulfur hydride system. *Nature* **2015**, *525*, 73–76. [[CrossRef](#)] [[PubMed](#)]
284. Somayazulu, M.; Ahart, M.; Mishra, A.K.; Geballe, Z.M.; Baldini, M.; Meng, Y.; Struzhkin, V.V.; Hemley, R.J. Evidence for superconductivity above 260 K in lanthanum superhydride at megabar pressures. *Phys. Rev. Lett.* **2019**, *122*, 027001. [[CrossRef](#)] [[PubMed](#)]
285. Drozdov, A.P.; Kong, P.P.; Minkov, V.S.; Besedin, S.P.; Kuzovnikov, M.A.; Mozaffari, S.; Balicas, L.; Balakirev, F.F.; Graf, D.E.; Prakapenka, V.B.; et al. Superconductivity at 250 K in lanthanum hydride under high pressures. *Nature* **2019**, *569*, 528–531. [[CrossRef](#)] [[PubMed](#)]
286. Dovgaliuk, I.; Hagemann, H.; Leyssens, T.; Devillers, M.; Filinchuk, Y.  $\text{CO}_2$ -promoted hydrolysis of  $\text{KBH}_4$  for efficient hydrogen co-generation. *Int. J. Hydrogen Energy* **2014**, *39*, 19603–19608. [[CrossRef](#)]

287. Lombardo, L.; Ko, Y.; Zhao, K.; Yang, H.; Züttel, A. Direct CO<sub>2</sub> capture and reduction to high-end chemicals with tetraalkylammonium borohydrides. *Angew. Chem.* **2021**, *133*, 9666–9675. [[CrossRef](#)]
288. Knopf, I.; Cummins, C.C. Revisiting CO<sub>2</sub> reduction with NaBH<sub>4</sub> under aprotic conditions: Synthesis and characterization of sodium trifluoroborohydride. *Organometallics* **2015**, *34*, 1601–1603. [[CrossRef](#)]
289. Grice, K.A.; Groenenboom, M.C.; Manuel, J.D.A.; Sovereign, M.A.; Keith, J.A. Examining the selectivity of borohydride for carbon dioxide and bicarbonate reduction in protic conditions. *Fuel* **2015**, *150*, 139–145. [[CrossRef](#)]
290. Zhu, W.; Zhao, J.; Wang, L.; Teng, Y.-L.; Dong, B.-X. Mechanochemical reactions of alkali borohydride with CO<sub>2</sub> under ambient temperature. *J. Solid State Chem.* **2019**, *277*, 828–832. [[CrossRef](#)]
291. Picasso, C.V.; Safin, D.A.; Dovgaliuk, I.; Devred, F.; Debecker, D.; Li, H.-W.; Proost, J.; Filinchuk, Y. Reduction of CO<sub>2</sub> with KBH<sub>4</sub> in solvent-free conditions. *Int. J. Hydrogen Energy* **2016**, *41*, 14377–14386. [[CrossRef](#)]
292. Laversenne, L.; Goutaudier, C.; Chiriach, R.; Sigala, C.; Bonnetot, B. Hydrogen storage in borohydrides comparison of hydrolysis conditions of LiBH<sub>4</sub>, NaBH<sub>4</sub> and KBH<sub>4</sub>. *J. Therm. Anal. Calorim.* **2008**, *94*, 785–790. [[CrossRef](#)]
293. Vitillo, J.G.; Groppo, E.; Bardají, E.G.; Baricco, M.; Bordiga, S. Fast carbon dioxide recycling by reaction with  $\gamma$ -Mg(BH<sub>4</sub>)<sub>2</sub>. *Phys. Chem. Chem. Phys.* **2014**, *16*, 22482–22486. [[CrossRef](#)] [[PubMed](#)]
294. Zuttel, A.; Rentsch, S.; Fischer, P.; Wenger, P.; Sudan, P.; Mauron, P.; Emmenegger, C. Hydrogen storage properties of LiBH<sub>4</sub>. *J. Alloys Compd.* **2003**, *356*, 515–520. [[CrossRef](#)]
295. Nakamori, Y.; Miwa, K.; Ninomiya, A.; Li, H.; Ohba, N.; Towata, S.-I.; Züttel, A.; Orimo, S.-I. Correlation between thermodynamical stabilities of metal borohydrides and cation electronegativities: First-principles calculations and experiments. *Phys. Rev. B* **2006**, *74*, 045126. [[CrossRef](#)]
296. Kharbachi, E.A.; Pinatel, E.; Nuta, I.; Baricco, M. A thermodynamic assessment of LiBH<sub>4</sub>. *Calphad Comput. Coupling Phase Diagrams Thermochem.* **2012**, *39*, 80–90. [[CrossRef](#)]
297. Dematteis, E.M.; Pinatel, E.R.; Corno, M.; Jensen, T.R.; Baricco, M. Phase diagrams of the LiBH<sub>4</sub>-NaBH<sub>4</sub>-KBH<sub>4</sub> system. *Phys. Chem. Chem. Phys.* **2017**, *19*, 25071–25079. [[CrossRef](#)] [[PubMed](#)]
298. Pinatel, E.R.; Albanese, E.; Civalleri, B.; Baricco, M. Thermodynamic modelling of Mg(BH<sub>4</sub>)<sub>2</sub>. *J. Alloys Compd.* **2015**, *645* (Suppl. 1), S64–S68. [[CrossRef](#)]
299. Błoński, P.; Łodziana, Z. Correlation between the ionic potential and thermal stability of metal borohydrides: First-principles investigations. *Phys. Rev. B* **2014**, *90*, 054114. [[CrossRef](#)]
300. Blanchard, D.; Zatti, M.; Vegge, T. Analysis of the decomposition gases from  $\alpha$  and  $\beta$ -Cd(BH<sub>4</sub>)<sub>2</sub> synthesized by temperature controlled mechanical milling. *J. Alloys Compd.* **2013**, *547*, 76–80. [[CrossRef](#)]
301. Mulliken, R.S. A new electroaffinity scale; together with data on valence states and on valence ionization potentials and electron affinities. *J. Chem. Phys.* **1934**, *2*, 782–793. [[CrossRef](#)]
302. Parr, R.G.; Pearson, R.G. Absolute hardness: Companion parameter to absolute electronegativity. *J. Am. Chem. Soc.* **1983**, *105*, 7512–7516. [[CrossRef](#)]
303. Kang, X.; Wang, P.; Cheng, H. Advantage of TiF<sub>3</sub> over TiCl<sub>3</sub> as a dopant precursor to improve the thermodynamic property of Na<sub>3</sub>AlH<sub>6</sub>. *Scr. Mater.* **2007**, *56*, 361–364. [[CrossRef](#)]
304. Yin, L.C.; Wang, P.; Fang, Z.; Cheng, H.M. Thermodynamically tuning LiBH<sub>4</sub> by fluorine anion doping for hydrogen storage: A density functional study. *Chem. Phys. Lett.* **2008**, *450*, 318–321. [[CrossRef](#)]
305. Sveinbjornsson, D.; Blanchard, D.; Myrdal, J.S.G.; Younesi, R.; Viskinde, R.; Riktor, M.D.; Norby, P.; Vegge, T. Ionic conductivity and the formation of cubic CaH<sub>2</sub> in the LiBH<sub>4</sub>-Ca(BH<sub>4</sub>)<sub>2</sub> composite. *J. Solid State Chem.* **2014**, *211*, 81–89. [[CrossRef](#)]
306. Ozolins, V.; Majzoub, E.H.; Wolverton, C. First-principles prediction of thermodynamically reversible hydrogen storage reactions in the Li-Mg-Ca-B-H system. *J. Am. Chem. Soc.* **2009**, *131*, 230–237. [[CrossRef](#)] [[PubMed](#)]
307. Xiong, Z.T.; Hu, J.J.; Wu, G.T.; Chen, P.; Luo, W.F.; Gross, K.; Wang, J. Thermodynamic and kinetic investigations of the hydrogen storage in the Li-Mg-N-H system. *J. Alloys Compd.* **2005**, *398*, 235–239. [[CrossRef](#)]
308. Gibb, B.C. The centenary (maybe) of the hydrogen bond. *Nat. Chem.* **2020**, *12*, 665–667. [[CrossRef](#)]
309. Chu, H.; Wu, G.; Zhang, Y.; Xiong, Z.; Guo, J.; He, T.; Chen, P. Improved dehydrogenation properties of calcium borohydride combined with alkaline-earth metal amides. *J. Phys. Chem. C* **2011**, *115*, 18035–18041. [[CrossRef](#)]
310. Chater, P.A.; David, W.I.F.; Anderson, P.A. Synthesis and structure of the new complex hydride Li<sub>2</sub>BH<sub>4</sub>NH<sub>2</sub>. *Chem. Commun.* **2007**, *45*, 4770–4772. [[CrossRef](#)]
311. Somer, M.; Acar, S.; Koz, C.; Kokal, I.; Hohn, P.; Cardoso-Gil, R.; Aydemir, U.; Akselrud, L.  $\alpha$ - and  $\beta$ -Na<sub>2</sub>[BH<sub>4</sub>][NH<sub>2</sub>]: Two modifications of a complex hydride in the system NaNH<sub>2</sub>-NaBH<sub>4</sub>; syntheses, crystal structures, thermal analyses, mass and vibrational spectra. *J. Alloys Compd.* **2010**, *491*, 98–105. [[CrossRef](#)]
312. Chu, H.L.; Xiong, Z.T.; Wu, G.T.; Guo, J.P.; Zheng, X.L.; He, T.; Wu, C.Z.; Chen, P. Hydrogen Storage Properties of Ca(BH<sub>4</sub>)<sub>2</sub>-LiNH<sub>2</sub> System. *Chem. Asian J.* **2010**, *5*, 1594–1599. [[CrossRef](#)] [[PubMed](#)]
313. Poonyayant, N.; Stavila, V.; Majzoub, E.H.; Klebanoff, L.E.; Behrens, R.; Angboonpong, N.; Ulutagay-Kartin, M.; Pakawatpanurut, P.; Hecht, E.S.; Breit, J.S. An investigation into the hydrogen storage characteristics of Ca(BH<sub>4</sub>)<sub>2</sub>/LiNH<sub>2</sub> and Ca(BH<sub>4</sub>)<sub>2</sub>/NaNH<sub>2</sub>: Evidence of intramolecular destabilization. *J. Phys. Chem. C* **2014**, *118*, 14759–14769. [[CrossRef](#)]
314. Aoki, M.; Miwa, K.; Noritake, T.; Kitahara, G.; Nakamori, Y.; Orimo, S.; Towata, S. Destabilization of LiBH<sub>4</sub> by mixing with LiNH<sub>2</sub>. *Appl. Phys. A Mater. Sci. Process.* **2005**, *80*, 1409–1412. [[CrossRef](#)]

315. Grube, E.; Jensen, S.R.H.; Nielsen, U.G.; Jensen, T.R. Reactivity of magnesium borohydride—Metal hydride composites,  $\gamma$ -Mg(BH<sub>4</sub>)<sub>2</sub>-MH<sub>x</sub>, M = Li, Na, Mg, Ca. *J. Alloys Compd.* **2019**, *770*, 1155–1163. [[CrossRef](#)]
316. Ibikunle, A.A.; Goudy, A.J. Kinetics and modeling study of a Mg(BH<sub>4</sub>)<sub>2</sub>/Ca(BH<sub>4</sub>)<sub>2</sub> destabilized system. *Int. J. Hydrogen Energy* **2012**, *37*, 12420–12424. [[CrossRef](#)]
317. Durojaiye, T.; Ibikunle, A.; Goudy, A.J. Hydrogen storage in destabilized borohydride materials. *Int. J. Hydrogen Energy* **2010**, *35*, 10329–10333. [[CrossRef](#)]
318. Dematteis, E.M.; Baricco, M. Hydrogen desorption in Mg(BH<sub>4</sub>)<sub>2</sub>-Ca(BH<sub>4</sub>)<sub>2</sub> system. *Energies* **2019**, *12*, 3230. [[CrossRef](#)]
319. Au, M.; Jurgensen, A. Modified lithium borohydrides for reversible hydrogen storage. *J. Phys. Chem. B* **2006**, *110*, 7062–7067. [[CrossRef](#)] [[PubMed](#)]
320. Au, M.; Jurgensen, A.; Zeigler, K. Modified lithium borohydrides for reversible hydrogen storage (2). *J. Phys. Chem. B* **2006**, *110*, 26482–26487. [[CrossRef](#)] [[PubMed](#)]
321. Muller, A.; Havre, L.; Mathey, F.; Petit, V.I.; Bensoam, J. Production of Hydrogen. U.S. Patent 4193978 A, 18 March 1980.
322. Mosegaard, L.; Møller, B.; Jørgensen, J.E.; Bosenberg, U.; Dornheim, M.; Hanson, J.C.; Cerenius, Y.; Walker, G.S.; Jakobsen, H.J.; Besenbacher, F.; et al. Intermediate phases observed during decomposition of LiBH<sub>4</sub>. *J. Alloys Compd.* **2007**, *446*, 301–305. [[CrossRef](#)]
323. Her, J.H.; Yousufuddin, M.; Zhou, W.; Jalisatgi, S.S.; Kulleck, J.G.; Zan, J.A.; Hwang, S.J.; Bowman, R.C., Jr.; Udovic, T.J. Crystal structure of Li<sub>2</sub>B<sub>12</sub>H<sub>12</sub>: A possible intermediate species in the decomposition of LiBH<sub>4</sub>. *Inorg. Chem.* **2008**, *47*, 9757–9759. [[CrossRef](#)] [[PubMed](#)]
324. Her, J.H.; Wu, H.; Verdal, N.; Zhou, W.; Stavila, V.; Udovic, T.J. Structures of the strontium and barium dodecahydro-closo-dodecaborates. *J. Alloys Compd.* **2012**, *514*, 71–75. [[CrossRef](#)]
325. Friedrichs, O.; Remhof, A.; Hwang, S.; Zuttel, A. Role of Li<sub>2</sub>B<sub>12</sub>H<sub>12</sub> for the formation and decomposition of LiBH<sub>4</sub>. *Chem. Mater.* **2010**, *22*, 3265–3268. [[CrossRef](#)]
326. Mauron, P.; Buchter, F.; Friedrichs, O.; Remhof, A.; Biemann, M.; Zwicky, C.N.; Zuttel, A. Stability and reversibility of LiBH<sub>4</sub>. *J. Phys. Chem. B* **2008**, *112*, 906–910. [[CrossRef](#)]
327. Orimo, S.I.; Nakamori, Y.; Kitahara, G.; Miwa, K.; Ohba, N.; Towata, S.; Zuttel, A. Dehydrogenating and rehydrogenating reactions of LiBH<sub>4</sub>. *J. Alloys Compd.* **2005**, *404*, 427–430. [[CrossRef](#)]
328. Orimo, S.; Nakamori, Y.; Ohba, N.; Miwa, K.; Aoki, M.; Towata, S.; Zuttel, A. Experimental studies on intermediate compound of LiBH<sub>4</sub>. *Appl. Phys. Lett.* **2006**, *89*, 021920. [[CrossRef](#)]
329. Hwang, S.J.; Bowman, R.C., Jr.; Reiter, J.W.; Rijssenbeck, J.; Soloveichik, G.L.; Zhao, J.C.; Kabbour, H.; Ahn, C.C. NMR confirmation for formation of [B<sub>12</sub>H<sub>12</sub>]<sup>2-</sup> complexes during hydrogen desorption from metal borohydrides. *J. Phys. Chem. C* **2008**, *112*, 3164–3169. [[CrossRef](#)]
330. Kato, S.; Biemann, M.; Borgschulte, A.; Zakaznova-Herzog, V.; Remhof, A.; Orimo, S.; Zuttel, A. Effect of the surface oxidation of LiBH<sub>4</sub> on the hydrogen desorption mechanism. *Phys. Chem. Chem. Phys.* **2010**, *12*, 10950–10955. [[CrossRef](#)] [[PubMed](#)]
331. Zuttel, A.; Borgschulte, A.; Orimo, S.I. Tetrahydroborates as new hydrogen storage materials. *Scr. Mater.* **2007**, *56*, 823–828. [[CrossRef](#)]
332. Schlapbach, L.; Zuttel, A. Hydrogen-storage materials for mobile applications. *Nature* **2001**, *414*, 353–358. [[CrossRef](#)] [[PubMed](#)]
333. Orimo, S.I.; Nakamori, Y.; Eliseo, J.R.; Zuttel, A.; Jensen, C.M. Complex hydrides for hydrogen storage. *Chem. Rev.* **2007**, *107*, 4111–4132. [[CrossRef](#)] [[PubMed](#)]
334. Palade, P.; Comanescu, C.; Mercioniu, I. Improvements of hydrogen desorption of lithium borohydride by impregnation onto MSH-H carbon replica. *J. Ovonic Res.* **2012**, *8*, 155–160.
335. Comanescu, C.; Guran, C.; Palade, P. Improvements of kinetic properties of LiBH<sub>4</sub> by supporting on MSU-H type mesoporous silica. *Optoelectron. Adv. Mater. Rapid Commun.* **2010**, *4*, 705–708.
336. Cahen, S.; Eymery, J.B.; Janot, R.; Tarascon, J.M. Improvement of the LiBH<sub>4</sub> hydrogen desorption by inclusion into mesoporous carbons. *J. Power Sources* **2009**, *189*, 902–908. [[CrossRef](#)]
337. Kruk, M.; Dufour, B.; Celer, E.B.; Kowalewski, T.; Jaroniec, M.; Matyjaszewski, K. Synthesis of mesoporous carbons using ordered and disordered mesoporous silica templates and polyacrylonitrile as carbon precursor. *J. Phys. Chem. B* **2005**, *109*, 9216–9225. [[CrossRef](#)]
338. Ryoo, R.; Joo, S.H.; Kruk, M.; Jaroniec, M. Ordered mesoporous carbons. *Adv. Mater.* **2001**, *13*, 677–681. [[CrossRef](#)]
339. Ngene, P.; Adelhelm, P.; Beale, A.M.; de Jong, K.P.; de Jongh, P.E. LiBH<sub>4</sub>/SBA-15 Nanocomposites prepared by melt infiltration under hydrogen pressure: Synthesis and hydrogen sorption properties. *J. Phys. Chem. C* **2010**, *114*, 6163–6168. [[CrossRef](#)]
340. Zhang, Y.; Zhang, W.Z.; Fan, M.Q.; Liu, S.S.; Chu, H.L.; Zhang, Y.H.; Gao, X.Y.; Sun, L.X. Enhanced hydrogen storage performance of LiBH<sub>4</sub>-SiO<sub>2</sub>-TiF<sub>3</sub> composite. *J. Phys. Chem. C* **2008**, *112*, 4005–4010. [[CrossRef](#)]
341. Gross, A.F.; Vajo, J.J.; Van Atta, S.L.; Olson, G.L. Enhanced hydrogen storage kinetics of LiBH<sub>4</sub> in nanoporous carbon scaffolds. *J. Phys. Chem. C* **2008**, *112*, 5651–5657. [[CrossRef](#)]
342. David, R.L. *Handbook of Chemistry and Physics*, 90th ed.; CRC Press: Boca Raton, FL, USA, 2009.
343. Fang, Z.Z.; Wang, P.; Rufford, T.E.; Kang, X.D.; Lu, G.Q.; Cheng, H.M. Kinetic- and thermodynamic-based improvements of lithium borohydride incorporated into activated carbon. *Acta Mater.* **2008**, *56*, 6257–6263. [[CrossRef](#)]
344. Ozawa, T. A New method of analyzing thermogravimetric data. *Bull. Chem. Soc. Jpn.* **1965**, *38*, 1881–1886. [[CrossRef](#)]
345. Ozawa, T. Kinetic analysis of derivative curves in thermal analysis. *J. Therm. Anal.* **1970**, *2*, 301–324. [[CrossRef](#)]
346. Nielsen, T.K.; Bosenberg, U.; Gosalawit, R.; Dornheim, M.; Cerenius, Y.; Besenbacher, F.; Jensen, T.R. A Reversible nanoconfined chemical reaction. *ACS Nano* **2010**, *4*, 3903–3908. [[CrossRef](#)]

347. Au, M.; Spencer, W.; Jurgensen, A.; Zeigler, C. Hydrogen storage properties of modified lithium borohydrides. *J. Alloys Compd.* **2008**, *462*, 1–2. [[CrossRef](#)]
348. Faivre, C.; Bellet, D.; Dolino, G. Phase transitions of fluids confined in porous silicon: A differential calorimetry investigation. *Eur. Phys. J. B* **1999**, *7*, 19–36. [[CrossRef](#)]
349. Petrov, O.; Furo, I. Curvature-dependent metastability of the solid phase and the freezing-melting hysteresis in pores. *Phys. Rev. E* **2006**, *73*, 011608. [[CrossRef](#)]
350. Verdal, N.; Udovic, T.J.; Rush, J.J.; Liu, X.; Majzoub, E.H.; Vajo, J.J.; Gross, A.F. Dynamical perturbations of tetrahydroborate anions in  $\text{LiBH}_4$  due to nanoconfinement in controlled-pore carbon scaffolds. *J. Phys. Chem. C* **2013**, *117*, 17983–17995. [[CrossRef](#)]
351. Ngene, P.; Nale, A.; Eggenhuisen, T.M.; Oschatz, M.; Embs, J.P.; Remhof, A.; de Jongh, P.E. Confinement effects for lithium borohydride: Comparing silica and carbon scaffolds. *J. Phys. Chem. C* **2017**, *121*, 4197–4205. [[CrossRef](#)]
352. Zhang, X.; Zhang, L.; Zhang, W.; Ren, Z.; Huang, Z.; Hu, J.; Gao, M.; Pan, H.; Liu, Y. Nano-synergy enables highly reversible storage of 9.2 wt% hydrogen at mild conditions with lithium borohydride. *Nano Energy* **2021**, *83*, 105839. [[CrossRef](#)]
353. Grochala, W.; Edwards, P.P. Thermal decomposition of the non-interstitial hydrides for the storage and production of hydrogen. *Chem. Rev.* **2004**, *104*, 1283–1316. [[CrossRef](#)] [[PubMed](#)]
354. Zaluska, A.; Zaluski, L.; Ström-Olsen, J.O. Structure, catalysis and atomic reactions on the nano-scale: A systematic approach to metal hydrides for hydrogen storage. *Appl. Phys. A* **2001**, *72*, 783. [[CrossRef](#)]
355. Imamura, H.; Masanari, K.; Kusuhashi, M.; Katsumoto, H.; Sumi, T.; Sakata, Y. High hydrogen storage capacity of nanosized magnesium synthesized by high energy ball-milling. *J. Alloys Compd.* **2005**, *386*, 211–216. [[CrossRef](#)]
356. Zaluski, L.; Zaluska, A.; Ström-Olsen, J.O. Nanocrystalline metal hydrides. *J. Alloys Compd.* **1997**, *253*, 70–79. [[CrossRef](#)]
357. Zhu, M.; Wang, H.; Ouyang, L.Z.; Zeng, M.Q. Composite structure and hydrogen storage properties in Mg-base alloys. *Int. J. Hydrogen Energy* **2006**, *31*, 251–257. [[CrossRef](#)]
358. Wiswall, R. Hydrogen Storage in Metals. In *Hydrogen Metals II*; Springer: Berlin, Germany, 1978; Volume 29, pp. 201–242. [[CrossRef](#)]
359. Fukai, Y. *The Metal–Hydrogen System, Basic Bulk Properties*; Springer Series in Materials Science; Springer: Berlin, Germany, 1993; ISBN 978-3-540-28883-1. [[CrossRef](#)]
360. Bogdanovic, B.; Bohmhamme, K.; Christ, B.; Reiser, A.; Schlichte, K.; Vehlen, R.; Wolf, U. Thermodynamic investigation of the magnesium–hydrogen system. *J. Alloys Compd.* **1999**, *282*, 84–92. [[CrossRef](#)]
361. Reule, H.; Hirscher, M.; Weißhardt, A.; Krönmüller, H. Hydrogen desorption properties of mechanically alloyed  $\text{MgH}_2$  composite materials. *J. Alloys Compd.* **2000**, *305*, 246–252. [[CrossRef](#)]
362. Vajo, J.J.; Skeith, S.L.; Mertens, F. Reversible storage of hydrogen in destabilized  $\text{LiBH}_4$ . *J. Phys. Chem. B* **2005**, *109*, 3719–3722. [[CrossRef](#)]
363. Bosenberg, U.; Doppiu, S.; Mosegaard, L.; Barkhordarian, G.; Eigen, N.; Borgschulte, A.; Jensen, T.R.; Cerenius, Y.; Gutfleisch, O.; Klassen, T.; et al. Hydrogen sorption properties of  $\text{MgH}_2$ – $\text{LiBH}_4$  composites. *Acta Mater.* **2007**, *55*, 3951–3958. [[CrossRef](#)]
364. Pinkerton, F.E.; Meyer, M.S.; Meisner, G.P.; Balogh, M.P.; Vajo, J.J. Phase boundaries and reversibility of  $\text{LiBH}_4$ / $\text{MgH}_2$  hydrogen storage material. *J. Phys. Chem. C* **2007**, *111*, 12881–12885. [[CrossRef](#)]
365. Walker, G.S.; Grant, D.M.; Price, T.C.; Yu, X.; Legrand, V. High capacity multicomponent hydrogen storage materials: Investigation of the effect of stoichiometry and decomposition conditions on the cycling behaviour of  $\text{LiBH}_4$ – $\text{MgH}_2$ . *J. Power Sources* **2009**, *194*, 1128–1134. [[CrossRef](#)]
366. Bosenberg, U.; Kim, J.W.; Gosslar, D.; Eigen, N.; Jensen, T.R.; von Colbe, J.M.B.; Zhou, Y.; Dahms, M.; Kim, D.H.; Gunther, R.; et al. Role of additives in  $\text{LiBH}_4$ – $\text{MgH}_2$  reactive hydride composites for sorption kinetics. *Acta Mater.* **2010**, *58*, 3381–3389. [[CrossRef](#)]
367. Wan, X.F.; Markmaitree, T.; Osborn, W.; Shaw, L.L. Nanoengineering-enabled solid-state hydrogen uptake and release in the  $\text{LiBH}_4$  Plus  $\text{MgH}_2$  System. *J. Phys. Chem. C* **2008**, *112*, 18232–18243. [[CrossRef](#)]
368. Bosenberg, U.; Ravnsbæk, D.B.; Hagemann, H.; D’Anna, V.; Minella, C.B.; Pistidda, C.; van Beek, W.; Jensen, T.R.; Bormann, R.; Dornheim, M. Pressure and temperature influence on the desorption pathway of the  $\text{LiBH}_4$ – $\text{MgH}_2$  composite system. *J. Phys. Chem. C* **2010**, *114*, 15212–15217. [[CrossRef](#)]
369. Price, T.E.C.; Grant, D.M.; Legrand, V.; Walker, G.S. Enhanced kinetics for the  $\text{LiBH}_4$ : $\text{MgH}_2$  multi-component hydrogen storage system—The effects of stoichiometry and decomposition environment on cycling behaviour. *Int. J. Hydrogen Energy* **2010**, *35*, 4154–4161. [[CrossRef](#)]
370. Martelli, P.; Caputo, R.; Remhof, A.; Mauron, P.; Borgschulte, A.; Zuttel, A. Stability and decomposition of  $\text{NaBH}_4$ . *J. Phys. Chem. C* **2010**, *114*, 7173–7177. [[CrossRef](#)]
371. Ugale, A.D.; Ghodke, N.P.; Kang, G.S.; Nam, K.B.; Bhoraskar, S.V.; Mathe, V.L.; Yoo, J.B. Cost-effective synthesis of carbon loaded  $\text{Co}_3\text{O}_4$  for controlled hydrogen generation via  $\text{NaBH}_4$  hydrolysis. *Int. J. Hydrogen Energy* **2022**, *47*, 16–29. [[CrossRef](#)]
372. Kaya, S.; Yilmaz, Y.; Er, O.F.; Alpaslan, D.; Ulas, B.; Dudu, T.E.; Kivrak, H. Highly Active RuPd Bimetallic Catalysts for Sodium Borohydride Electrooxidation and Hydrolysis. *J. Electron. Mater.* **2022**, *51*, 403–411. [[CrossRef](#)]
373. Yu, S.S.; Lee, T.H.; Oh, T.H. Ag-Ni nanoparticles supported on multiwalled carbon nanotubes as a cathode electrocatalyst for direct borohydride-hydrogen peroxide fuel cells. *Fuel* **2022**, *315*, 123151. [[CrossRef](#)]
374. Oh, T.H. Effect of cathode conditions on performance of direct borohydride-hydrogen peroxide fuel cell system for space exploration. *Renew. Energy* **2021**, *178*, 1156–1164. [[CrossRef](#)]

375. Schlesinger, H.J.; Brown, H.C.; Abraham, B.; Bond, A.C.; Davidson, N.; Finholt, A.E.; Gilbreath, J.R.; Hoekstra, H.; Horvitz, L.; Hyde, E.K.; et al. New Developments in the chemistry of diborane and the borohydrides. I. General Summary. *J. Am. Chem. Soc.* **1953**, *75*, 186–190. [[CrossRef](#)]
376. Broja, G.; Schlabacher, W. Process for the Production of Alkali Metal Borohydrides. DE Patent DE 000001108670 A, 15 June 1961.
377. Schubert, F.; Lang, K.; Schlabacher, W. Process for the Production of Borohydrides. DE Patent DE 000001067005 A, 15 October 1959.
378. Haga, T.; Kojima, Y. Method for Manufacturing Metal Borohydride. JP Patent P 2002-241109, 28 August 2002.
379. Kojima, Y.; Haga, T. Recycling process of sodium metaborate to sodium borohydride. *Int. J. Hydrogen Energy* **2003**, *28*, 989–993. [[CrossRef](#)]
380. Li, Z.P.; Morigazaki, N.; Liu, B.H.; Suda, S. Preparation of sodium borohydride by the reaction of  $MgH_2$  with dehydrated borax through ball milling at room temperature. *J. Alloys Compd.* **2003**, *349*, 232–236. [[CrossRef](#)]
381. Ozolins, V.; Majzoub, E.H.; Wolverson, C. First-principles prediction of a ground state crystal structure of magnesium borohydride. *Phys. Rev. Lett.* **2008**, *100*, 135501. [[CrossRef](#)] [[PubMed](#)]
382. Fichtner, M.; Zhao-Karger, Z.; Hu, J.; Roth, A.; Weidler, P. The kinetic properties of  $Mg(BH_4)_2$  infiltrated in activated carbon. *Nanotechnology* **2009**, *20*, 204029. [[CrossRef](#)]
383. Sartori, S.; Knudsen, K.D.; Zhao-Karger, Z.; Bardajii, E.G.; Fichtner, M.; Hauback, B.C. Small-angle scattering investigations of Mg-borohydride infiltrated in activated carbon. *Nanotechnology* **2009**, *20*, 505702. [[CrossRef](#)]
384. George, L.; Saxena, S.K. Structural stability of metal hydrides, alanates and borohydrides of alkali and alkali-earth elements: A review. *Int. J. Hydrogen Energy* **2010**, *35*, 5454–5470. [[CrossRef](#)]
385. Matsunaga, T.; Buchter, F.; Mauron, P.; Bielman, A.; Nakamori, Y.; Orimo, S.; Ohba, N.; Miwa, K.; Towata, S.; Zuttel, A. Hydrogen storage properties of  $Mg[BH_4]_2$ . *J. Alloys Compd.* **2008**, *459*, 583–588. [[CrossRef](#)]
386. Severa, G.; Ronnebro, E.; Jensen, C.M. Direct hydrogenation of magnesium boride to magnesium borohydride: Demonstration of >11 weight percent reversible hydrogen storage. *Chem. Commun.* **2010**, *46*, 421–423. [[CrossRef](#)] [[PubMed](#)]
387. Li, H.W.; Kikuchi, K.; Nakamori, Y.; Ohba, N.; Miwa, K.; Towata, S.; Orimo, S. Dehydrogenating and rehydrogenating processes of well-crystallized  $Mg(BH_4)_2$  accompanying with formation of intermediate compounds. *Acta Mater.* **2008**, *56*, 1342–1347. [[CrossRef](#)]
388. Van Setten, M.J.; de Wijs, G.A.; Fichtner, M.; Brocks, G. A Density Functional Study of  $\alpha$ - $Mg(BH_4)_2$ . *Chem. Mater.* **2008**, *20*, 4952–4956. [[CrossRef](#)]
389. Cansizoglu, M.F.; Karabacak, T. Enhanced hydrogen storage properties of magnesium nanotrees with nanoleaves. *Mat. Res. Soc. Symp. Proc.* **2009**, *1216*, 503. [[CrossRef](#)]
390. Bayca, S.U.; Cansizoglu, M.F.; Biris, A.S.; Watanabe, F.; Karabacak, T. Enhanced oxidation resistance of magnesium nanorods grown by glancing angle deposition. *Int. J. Hydrogen Energy* **2011**, *36*, 5998–6004. [[CrossRef](#)]
391. Zavorotynska, O.; Deledda, S.; Vitillo, J.; Saldan, I.; Guzik, M.; Baricco, M.; Walmsley, J.C.; Muller, J.; Hauback, B.C. Combined X-ray and raman studies on the effect of cobalt additives on the decomposition of magnesium borohydride. *Energies* **2015**, *8*, 9173–9190. [[CrossRef](#)]
392. Zavorotynska, O.; Saldan, I.; Hino, S.; Humphries, T.D.; Deledda, S.; Hauback, B.C. Hydrogen cycling in  $\gamma$ - $Mg(BH_4)_2$  with cobalt-based additives. *J. Mater. Chem. A* **2015**, *3*, 6592–6602. [[CrossRef](#)]
393. Liang, J.J. Theoretical insight on tailoring energetics of Mg hydrogen absorption/desorption through nano-engineering. *Appl. Phys. A Mater. Sci. Process.* **2005**, *80*, 173–178. [[CrossRef](#)]
394. Kim, J.-H.; Jin, S.-A.; Shim, J.-H.; Cho, Y.W. Reversible hydrogen storage in calcium borohydride  $Ca(BH_4)_2$ . *Scr. Mater.* **2008**, *58*, 481–483. [[CrossRef](#)]
395. Aoki, M.; Miwa, K.; Noritake, T.; Ohba, N.; Matsumoto, M.; Li, H.W.; Nakamori, Y.; Towata, S.; Orimo, S. Structural and dehydrogenating properties of  $Ca(BH_4)_2$ . *Appl. Phys. A* **2008**, *92*, 601–605. [[CrossRef](#)]
396. Kim, J.H.; Jin, S.A.; Shim, J.H.; Cho, Y.W. Thermal decomposition behavior of calcium borohydride  $Ca(BH_4)_2$ . *J. Alloys Compd.* **2008**, *461*, L20–L22. [[CrossRef](#)]
397. Kim, J.H.; Shim, J.H.; Cho, Y.W. On the reversibility of hydrogen storage in Ti- and Nb-catalyzed  $Ca(BH_4)_2$ . *J. Power Sources* **2008**, *181*, 140–143. [[CrossRef](#)]
398. Manchester, F.D.; San-Martin, A.; Pitre, J.M. The H-Pd (hydrogen-palladium) System. *J. Phase Equilibria JPE* **1994**, *15*, 62–83. [[CrossRef](#)]
399. Parry, R.W.; Schultz, D.R.; Girardot, P.R. The Preparation and properties of hexamminecobalt(III) borohydride, hexamminechromium(III) borohydride and ammonium borohydride. *J. Am. Chem. Soc.* **1958**, *80*, 1–3. [[CrossRef](#)]
400. Crabtree, R.H. A New Type of Hydrogen Bond. *Science* **1998**, *282*, 2000–2001. [[CrossRef](#)]
401. Sit, V.; Geanangel, R.A.; Wendlandt, W.W. The thermal dissociation of  $NH_3BH_3$ . *Thermochim. Acta* **1987**, *113*, 379–382. [[CrossRef](#)]
402. Li, L.; Yao, X.; Sun, C.; Du, A.; Cheng, L.; Zhu, Z.; Yu, C.; Zou, J.; Smith, S.C.; Wang, P.; et al. Lithium-catalyzed dehydrogenation of ammonia borane within mesoporous carbon framework for chemical hydrogen storage. *Adv. Funct. Mater.* **2009**, *19*, 265–271. [[CrossRef](#)]
403. Sephri, S.; Feaver, A.; Shaw, W.J.; Howard, C.J.; Zhang, Q.; Autrey, T.; Cao, G. Spectroscopic studies of dehydrogenation of ammonia borane in carbon cryogel. *J. Phys. Chem. B* **2007**, *111*, 14285–14289. [[CrossRef](#)] [[PubMed](#)]
404. Kim, H.; Karkamkar, A.; Autrey, T.; Chupas, P.; Proffen, T. Determination of structure and phase transition of light element nanocomposites in mesoporous silica: Case study of  $NH_3BH_3$  in MCM-41. *J. Am. Chem. Soc.* **2009**, *131*, 13749–13755. [[CrossRef](#)] [[PubMed](#)]

405. Paolone, A.; Palumbo, O.; Rispoli, P.; Cantelli, R.; Autrey, T.; Karkamkar, A. Absence of the structural phase transition in ammonia borane dispersed in mesoporous silica: Evidence of novel thermodynamic properties. *J. Phys. Chem. C* **2009**, *113*, 10319–10321. [[CrossRef](#)]
406. Wolf, G.; Baumann, J.; Baitalow, F.; Hoffmann, F.P. Calorimetric process monitoring of thermal decomposition of B–N–H compounds. *Thermochim. Acta* **2000**, *343*, 19–25. [[CrossRef](#)]
407. Lai, S.-W.; Lin, H.-L.; Yu, T.L.; Lee, L.-P.; Weng, B.-J. Hydrogen release from ammonia borane embedded in mesoporous silica scaffolds: SBA-15 and MCM-41. *Int. J. Hydrogen Energy* **2012**, *37*, 14393–14404. [[CrossRef](#)]
408. Feaver, A.; Sepehri, S.; Shamberger, P.; Stowe, A.; Autrey, T.; Cao, G. Coherent carbon cryogel–ammonia borane nanocomposites for H<sub>2</sub> storage. *J. Phys. Chem. B* **2007**, *111*, 7469–7472. [[CrossRef](#)] [[PubMed](#)]
409. Moussa, G.; Bernard, S.; Demirci, U.B.; Chiriach, R.; Miele, P. Room-temperature hydrogen release from activated carbon-confined ammonia borane. *Int. J. Hydrogen Energy* **2012**, *37*, 13437–13445. [[CrossRef](#)]
410. Srinivas, G.; Travis, W.; Ford, J.; Wu, H.; Guo, Z.-X.; Yildirim, T. Nanoconfined ammonia borane in a flexible metal–organic framework Fe–MIL-53: Clean hydrogen release with fast kinetics. *J. Mater. Chem. A* **2013**, *1*, 4167–4172. [[CrossRef](#)]
411. Chung, J.-Y.; Liao, C.-W.; Chang, Y.-W.; Chang, B.K.; Wang, H.; Li, J.; Wang, C.-Y. Influence of metal–organic framework porosity on hydrogen generation from nanoconfined ammonia borane. *J. Phys. Chem. C* **2017**, *121*, 27369–27378. [[CrossRef](#)]
412. Ramachandran, P.V.; Raju, B.C.; Gagare, P.D. One-pot synthesis of ammonia-borane and trialkylamine-boranes from trimethyl borate. *Org. Lett.* **2012**, *14*, 6119–6121. [[CrossRef](#)] [[PubMed](#)]